Biomolecular Applications of Interactive Molecular Dynamics in Virtual Reality

By

HELEN MARY DEEKS

Department of Chemistry
UNIVERSITY OF BRISTOL

A dissertation submitted to the University of Bristol in accordance with the requirements of the degree of DOCTOR OF PHILOSOPHY in the Faculty of Science.

SEPTEMBER 2020

Word count: Forty thousand six hundred and fifteen

Abstract

Recent advances in computational resources have allowed Molecular Dynamics (MD) to be run in real-time and displayed using Virtual Reality (VR), creating a fully interactive and immersive experience. Narupa is an open source program for performing Interactive Molecular Dynamics in Virtual Reality (iMD-VR), which is shown to have benefits for performing complex molecular manipulation tasks (in comparison to more conventional interfaces). Here, it is applied to the study of protein-ligand systems, starting with an initial exploration of three protein targets of varying complexity, and later expanded towards a target of high pharmacological relevance (SARS-CoV-2 Mpro). iMD-VR is demonstrated to be a useful tool for complexing proteins to both small, drug-like molecules and larger, more rotationally complex oligopeptides. Sound is also explored as a mechanism for providing feedback during iMD-VR about information relevant to ligand docking, where audio cues indicate the formation of key hydrogen bonding interactions to a user. Furthermore, the utility of iMD-VR is explored as a tool for enhancing the rate of sampling in a chemical system: the free energies of a series of distinct unbinding pathways, which were quickly generated using iMD-VR, are estimated using Umbrella Sampling. Chiefly, an iMD-VR unbinding pathway can be used to quickly describe a route in reduced dimensional space to bias sampling along. Overall, this thesis explores the utility of using iMD-VR for understanding protein-ligand systems, from recreating experimental (crystallographic) protein-ligand structures, to novel ways of conveying key simulation data, to quickly generating unbinding pathways which can be used to guide biased sampling methods. iMD-VR shows great promise as a tool for studying chemical systems of pharmacological interest.

Dedication and acknowledgements

Somehow, I have managed the incredible achievement of writing a PhD thesis. As nice as it would be to think of myself as a grassroots pull-herself-from-her-bootstraps kind of person, it would be highly remiss to imply there is nobody in this world whatsoever to thank; in truth, I am just one part of an ensemble cast of incredible people, each of whom have played their own role in making me who I am today.

The first acknowledgement very rightfully belongs to my two supervisors in Chemistry, Dr Dave Glowacki and Professor Adrian Mulholland. Neither of you had to offer me this opportunity to explore my potential, but I am immensely grateful for the journey I have taken over the past four years. A PhD is a very complex thing to navigate, so only with your extensive knowledge and expert guidance I have had the faintest idea which paths should be explored and which should be abandoned: if this work has any semblance of being cohesive, Dave and Adrian should be thanked first and foremost. Similarly, although their supervisory roles were more ancillary, Dr Anne Roudaut and Dr Oussama Metatla have given me highly valuable advice in any areas of this work related to Human Computer Interaction.

I have also fostered amazing relationships with a lot of people throughout this time, each of which I value as much as the next. Alas, as is the nature of the English language, they need to be thanked in turn. Before I start the official process of naming people "in no particular order" however, I need to make a very quick exception to this rule. Because she was a significant contributor to multiple chapters, I want to thank Rebecca Walters. You are someone who has always smiled and tried to make others laugh, even when things have been tough - that alone is a truly inspirational quality. A PhD is difficult at the best of times, but I know that your conscientious spirit and good nature will guide you the rest of the way through.

Writing up during a pandemic is not the easiest feat, but I have met (virtually!) most days with Alex Jamieson-Binnie. More than anyone else, you have made me laugh, knocked me down a much-needed peg or two, and kept my spirits up (no porkies, you have been the glue which helped hold a lot of people together through this). I would also like to thank my resident partner-in-crime Dr Robin Shannon: You are the living embodiment of the saying "when the pub closes the revolution begins" so, alongside a lot of highly valuable guidance and advice, I have enjoyed our heated discussions about how we are going to fix the world over a pint (or five, as the case may be). Alongside contributing to some of the work in this thesis, Alex Jones has been a pillar of support when things have been tough and always lent me a listening ear when I have needed to rant. Alex also shares my slightly offbeat sense of humour - a rare feat! Similarly, Dasha Shchepanovska is full of quiet, quirky insights that never cease to amuse me. I don't know where you are going from here, but I know it won't be boring.

Rhoslyn Roebuck-Williams is an extremely sunny person, but also one of the down-to-earth I have met; I am immensely grateful to know someone who is equal measures empathetic, thoughtful and cheerful. Shared values are the cornerstone of our friendship. Likewise, Harry Stroud has been my unconditional cheerleader, calling me an “absolute legend” at times when I have needed to hear that most (it is you, Harry, that is the legend). I also count myself extremely fortunate to have been graced with the meteoric light that is Dr Stephanie Hare, who will no doubt continue to reach greater and greater heights in her career. While I am gutted to lose out on working with such an awesome person, I wish you the best of luck in your new position.

Callum Bungey shares in my love of cheesy musical numbers and is someone who I have shared many libations with down the pub. Being able to meet with someone who consistently made me laugh and, equally so, commiserated with me throughout write up has massively helped. Dr Jonathan Barnoud’s rotating supply of comical t-shirts have brought myself and our colleagues much joy, however, he has also been the kind of person who would drop everything to give me advice or support without question or hesitation. Seriously, get a t-shirt which says “PhD student’s code whisperer”! Dr Simon Bennie has the rare accolade of being someone who I have worked with throughout the entirety of my PhD, so I have benefited greatly from his generous and thoughtful nature (I would also like to provide additional thanks to his dog Ripley - and all the other pets of the Centre for Computational Chemistry - for being so darn cute on zoom calls).

As well as sharing my nerdy interests, Dr Lars Bratholm has never failed to find the cavalcade of memes I produced over lockdown entertaining. Your quirky and offbeat perspective on life has always amused me so. Also, for being the one to introduce me to the Danish sweets Tyrkisk Peber (liquorice sweets with chilli and salmiak, honestly is better than it sounds), I will be eternally grateful. Jillisa Thompson knows her own mind, and is not afraid to speak it, which means I have had many enlightening and frank discussions with her. Joe Crossley-Lewis’ upbeat, happy-go-lucky nature has kept mine and others spirits up when we have needed it. Zack Williams is someone who I have had the immense pleasure of getting to know and I am particularly fond of his Batman impersonation. However, like other PhD candidates I have acknowledged here, he is already a hero for keeping at a challenging degree in a difficult and uncertain world.

Dr Mike O’Connor, who also contributed to several chapters, gave me a lot of advice and help throughout the years. Robert Arbon has been a much-valued ear of support during difficult times. Dr Silvia Amabilino started at the same time as me, therefore, she is the one I most closely experienced the trials and tribulations of doing a PhD with. In addition, I would also like to acknowledge Oliver Feighan, Mark Wonnacott, Dr Stephen Ingram, Dr Ella Gale, Ian Shepherd, Mike Connolly, Dr Fred Cascarini, Angus Voice, Rebecca Twidale, Dr Clem Stross, Dr Felix Vaughan, Dr Susannah Bourne-Worster, Dr Kara Ranaghan, Dr Victoria Taylor, Dr Matt Bain, Dr Balazs Hornung, Dr Natalie Fey, Professor Fred Manby, Professor Neil Allen, Dr Tom Oliver, and the countless others I have worked with during this time.

A star alone burns with a bright beauty, but it is only when you take a step back that you appreciate the night sky is made up of individuals all shining together. Alone, this manuscript represents four years of dedication and hard work from myself, but everyone I have worked with during that time are as much a part of this thesis as the words you are reading. However, the most important acknowledgement goes to my personal constellation, the stars that shine around me - my family. My sister and brother, Sarah and George Deeks, know me better than anyone else and have supported me unconditionally throughout this time. My mother, Mary Deeks, is an amazingly giving, kind and caring spirit who has been my main pillar throughout the years. Her support, above all, has made completing this PhD possible. I would like to finally acknowledge my late father, Henry Deeks, who I am deeply saddened to now be finishing this journey without. Although his star is furthest away, it shines no less brightly.

Dedicated to the memory of Henry Lorn Deeks

1958 - 2017

Author's declaration

I declare that the work in this dissertation was carried out in accordance with the requirements of the University's Regulations and Code of Practice for Research Degree Programmes and that it has not been submitted for any other academic award. Except where indicated by specific reference in the text, the work is the candidate's own work. Work done in collaboration with, or with the assistance of, others, is indicated as such. Any views expressed in the dissertation are those of the author.

SIGNED: ..... DATE: .....

TABLE OF CONTENTS

List of Tables

List of Figures

CHAPTER 1

INTRODUCTION

1.1 History of Molecular Representations

Crystallographic methods allow us to draw a three dimensional (3D) map of electron density - a blueprint for building a molecule. An early example of molecular modelling was a physical myogoblin sculpture built with rods and clips; although the backbone atoms were placed according to an electron density map, the overall shape was estimated by an "invisible integument of side chains". [1] Despite this simplified structure being the result of methodological limitations, future digital protein representations would only show the backbone because it emphasizes structural features [2], whereas other representations took advantage of advances in computational power to precisely detail the overall shape of a protein. [3] From these early - arguably rudimental - representations, molecular models evidently evolved and adapted to meet the needs of the end-user.

Scientific advances have allowed great flexibility in how atoms are both represented and how they can be interacted with. Some modern examples of physical molecular models include molymods [4], lasering chemical structures into glass [5], and 3D printing. [6] However, static models are contrary to the dynamical nature of chemistry, a snapshot of something performing incredible molecular choreography. Building accurate physical models was also noted as being "time-consuming and tedious" by early pioneers, largely as it relied on making many precise manual measurements. [7] However, physical models can be combined with computational methods. For example, humans can use their spatial judgement to build a molecular model over an electron density map (known as a Skinner box), however, more precise structural elements (e.g. bond angles) can then be computationally optimized. [8] Notably, these ‘computational Skinner boxes’ represent an early example of how the spatial intelligence of a human can be combined

with the mathematical precision of a computer to construct molecular models - a concept later heralded to great success with FoldIt. [9]

Early computational models were not dynamic in nature, however, they allowed detailed display of structural features in molecules, e.g. metal sites in proteins. [10, 11] The earliest computational models may have warranted dedicated workstations, which would have been a limitation against their use. [8, 12] Eventually however, molecular modelling, analysis and visualization software became independent and could be installed on personal computers [13], making them accessible to a wide-array of end users, therefore impetus existed for a suite of features to meet a broad range of applications. [14] Modern molecular visualization software is feature rich: as an example, using VMD [15], a computational drug designer can view a bound complex between a protein and a ligand, detect the presence of any hydrogen bonds, analyse the Root Mean Square Deviation (RMSD) of the ligand compared to a reference structure, and more. Additionally, these software packages often allow plug-ins, meaning users can create custom tools specific to their needs; such features allow an even greater level of insight into molecular data.

Computers have afforded increasingly sophisticated and varied means of representing molecules to end-users. However, computational visualization often necessitates that complex 3D structures are displayed on two dimensional (2D) displays. Some molecular graphics software is capable of stereoscopic output [15], however, this may require specialized hardware or equipment (which then may then need to be interfaced with the software). Given this, the expense, training, and equipment needs might not be accessible to a larger audience. Augmented Reality (AR) is a means of embodying molecules with a sense of 'realness' by making them an immersive aspect of the room they are being viewed in. A second option, Virtual Reality (VR), makes a bespoke world in which the user and molecule co-exist (although, admittedly, the distinction between AR and VR is rarely clear-cut). Both AR and VR are becoming increasingly available at a consumer level and, furthermore, developing software for them is accessible. Unity [16], a cross-platform engine for game development which has previous molecular applications [17, 18], can easily be interfaced with commercial VR headsets either natively or using toolkits, such as VRTK [19], and is programmable in C#. Additionally, software built in Unity can be exported as an executable which (i) can easily be saved between different machines and (ii) can interface with an existing VR setup, further bridging the gap to virtual representations.

Due to AR and VR becoming increasingly accessible, they are being applied to molecular applications as they afford the user a more 3D comprehension of atoms and chemical processes. The next section (1.2) provides an overview of how advances in computing technology has enabled molecular renderings to be tangible, 3D objects that a user can interact with.

1.2 Chemistry on the Augmented to Virtual Reality Spectrum

Presenting molecules as a part of an immersive, 3D environment can potentially benefit the user experience. [20–23] Although they may appear as separate entities, AR, VR, and other stereoscopic viewing methods, are thought to exist on the same reality-virtuality continuum. [24] Defining what these entail and how exactly a contribution to this field fits on this scale is beyond the scope of this discussion, however, for clarity, this section will be structured to move from one end of this spectrum to the other: starting with approaches which aim to build 3D objects in the 'real world' (defined broadly here as AR), towards those which immerse the user as part of a virtual molecular world (defined broadly here as VR). While it may not be possible to categorize these virtual representations with perfect consistency, this structure should help clarify where recent advances lie in relation to one another.

Molecules can be imparted with a sense of 3D 'realness' by overlaying them onto a camera display, making them appear as objects occupying the same room as the user. One way to bring molecular renderings into the real world is to export them to a 3D printing device [6, 25], meaning that they exist physically and can therefore be treated as tactile objects by the user. In theory, the same workflows to go from a molecular rendering to a 3D printed molecule can be applied to AR. First, the desired representation should be built using molecular visualization software, then exported to a generic 3D model file format (such as .obj or .stl). So long as these formats are compatible with computer graphics software (e.g. Blender [26]), these renders can be exported to other software or hardware, allowing a pipeline to exist between 2D and 3D molecular visualizations. Several examples of this process have been very recently documented in the literature. [27–30] Although the representation cannot be physically held like a 3D printed model, by exporting a 3D model onto an AR 'trigger image' and attaching it to an object, it can be indirectly picked up, rotated, and moved via interacting with this trigger, creating a tangible experience. [31, 32] As cameras and smartphones have become household items, online tools have been developed to easily automate this process [33], and furthermore, a potential application is integration into scientific posters and reports. [34] The recent advances discussed here mean that virtual molecules can be brought into the real world with consumer-level hardware (which the user likely already owns) and without the need for specialized training, therefore, the barrier to entry for these kinds of virtual representations is low.

Another approach to project virtual molecules into a room is with a Head Mounted Display (HMD), such as the Microsoft HoloLens which has previously been used to render proteins of varying size with good performance. [35–37] Although HMDs can often necessitate that the user has specialized hardware, a distinct experience is afforded in that the molecular rendering is directly overlaid onto the operator's field of view. A user looking at a molecule in AR via an external camera needs to focus their attention at a screen to see the effect, therefore, the atoms only appear to exist so long as the user is directing their attention to a 2D display. On the other hand, through the use of a HMD, users are free to move around the molecule and can easily

view it from a variety of angles, all whilst keeping the representation consistently positioned. Additionally, if a HMD has controllers or allows gesture control, users can directly interact with an atom or molecule with their hands in a responsive fashion, increasing both tangibility and immersion. [38]

Rather than imposing a molecule over the 'real world', an alternative approach is to build a bespoke physical environment which can host a rendered molecular world. For example, the Cave Automatic Virtual Environment, in which a VR environment is projected onto the walls of a room-sized cube, has been used to build immersive molecular virtual environments. [39–41] Once this world has been projected onto the space, the user can enter and then co-exist in the same environment as the molecule. [42] Alternatively, this world can be built onto a single surface and, using stereoscopic glasses to make the atoms appear 3D, it can be viewed and interacted with, where the surface itself acts as a 'portal' into the molecular world. [43] To increase the sense of immersion, molecular worlds can also be displayed using an HMD, meaning the user's entire field of view becomes the rendering space: rather than bringing the molecule to the user, they are instead transported into the representation itself. Recent technological advances have made VR-compatible HMDs widely commercially available, as such, they have been applied to multiple relevant scientific applications, including visualizations of RNA sequences [44], drawing simulated cellular environments [45], immersive exploration of chemical space [46], and as an visual interface to using a scanning probe microscope to directly manipulate molecules. [47] More pertinently, VR-compatible HMDs have been used as means of viewing - and manipulating - virtual molecular models.

As with previously discussed virtual representations, 3D models can be exported from molecular graphics software into Unity, which can then be interfaced with an HMD - for example, this pipeline has been applied to create a novel VR environment for inspecting structural differences between proteins. [48] Furthermore, as an alternative means of increasing accessibility, web applications - which are designed to easily interface with commercially available HMDs - have been developed. [49, 50] Novel interaction methods can also be used in tandem with an HMD, imparting the molecular object with both visual and physical tangibility. [51, 52] Users need not directly interact with the molecules in VR however, as many modern HMDs also incorporate a pair of controllers for interfacing with in-world menus: in practice, this means that users can adaptively customize how a molecule is rendered or what additional contextual information is displayed, according to their exact needs. [53, 54] As such, VR has also been developed for more specialized applications of molecular science. For pharmacological use cases, VR (or otherwise stereoscopic) interfaces can be connected to the output of molecular docking software and then used to visualize the results, allowing researchers to understand the 3D relationship between a protein and screening hit compound. [55, 56] Expanding on this concept, whilst viewing a protein-ligand complex, molecular editing tools can also be used to either (i) modify the structures of ligands to further improve a binding pose, or (ii) build new structures which fit into a binding

pocket. [18] Additionally, although most applications discussed here are biomolecular focused, these VR interfaces have also been developed to have applications in other areas of chemistry, for example, in materials science. [57]

1.3 Simulating Molecules in Interactive Molecular Dynamics

Improvements in both the Computational Processing Unit (CPU) and the Graphical Processing Unit (GPU) have also greatly enhanced how we can interact with virtual molecules, moving past static renderings and toward dynamic objects which model both the structure and behaviour of chemical systems. Early molecular simulations could take an extensive amount of computational resources to run [58], therefore, gaining an understanding of complex, high-dimensional systems, such as proteins, was difficult. However, recent advances in computational processing, Molecular Dynamics (MD) code optimization and theoretical methods for accelerating exploration of chemical systems have brought possible simulation timescales to the point where sampling is extensive enough to gain an understanding of the complex behaviour of biomolecules. [59] One result of these increases in MD efficiency is that an individual integration step can be calculated, and subsequently rendered, in real-time, meaning that users can watch molecular simulations unfold in front of their eyes. However, a limitation is that many biological processes of relevance occur on long timescales. For example, benzamidine unbinding from trypsin - arguably one of the simplest protein-ligand systems - is estimated to take milliseconds on average to spontaneously occur. [60] Assuming a dynamics rate of 75 fs per second during an interactive simulation [61], the user would have to wait 3.7 hours of real-time to observe a single nanosecond of dynamics. Obviously, this is highly impractical, therefore, there is impetus for the system or process of interest to be somehow accelerated, otherwise, these real-time simulations are arguably of limited use. While numerous methods to bias non-interactive simulations already exist [62–67], one solution to this problem is for the user to apply additional force into the system while observing it, allowing them to consciously drive a molecular process of interest to occur. Henceforth, this procedure shall be referred to as Interactive Molecular Dynamics (iMD).

An analogue to iMD is Steered Molecular Dynamics (sMD), where the user does not directly view the simulation as it runs, but instead predefines external forces to drive the process of interest. As sMD does not need to be rendered in real-time, there is no need to account for human patience when deciding what can be practically achieved. However, the drawback is that all interactions need to be set ahead of time; applied forces cannot be adjusted on-the-fly and there is a limit to the complexity of input. Nonetheless, sMD has been applied to accelerate a number of different biological processes. [68] Furthermore, by tracking the amount of force applied during sMD, theoretical methods can estimate a potential of mean force for the process under study. [69, 70] Successfully running sMD is a balance between having a high enough force that molecular processes are sufficiently accelerated, but also not so high that the system starts

to be pushed through an unfeasible pathway. One approach to balance these needs is to perform sMD semi-interactively, which can be achieved by running a short segment of steered dynamics, rendering the suspended simulation in molecular graphics software, and then having a researcher inspect the system and determine whether a new force should be applied. Interestingly, this process is one of the earliest examples of how 3D stereoscopic environments have found use in molecular science, as any applied force will need to be defined along three axes. [71]

Alternatively, with enough processing power for real-time integration, forces can be applied and adapted as a molecular simulation runs. Early examples of interactive simulations did not incorporate directly applying force to atoms, instead, the simulation parameters (such as temperature and velocity) could be tuned by the user. [72] Alternatively, instead of running dynamics, a parameterized protein structure can be iteratively minimized; forces can then be applied to this non-dynamic structure, allowing users to steer the system towards favourable interactions and away from steric clashes, thus guiding protein folding. [73] With the development of algorithms for optimizing interactions within a protein structure, this principle can be applied with increasing sophistication. FoldIt is an example of how human-directed computing can be used to solve problems in biochemistry. [9] In this case, human players try to minimize a protein structure by directing how these minimization algorithms should be applied and are scored on the energy acheived during this process, thus gamifying the problem. A player does not have the tactile ability to optimize these interactions with mathematical precision, however, human intelligence and spatial intuition can increase the breadth of both conformational space explored and search strategies tested, largely as we can choose the 'high-risk high-reward' strategies over high energy barriers that computational algorithms avoid making. Players can note their strategies for minimizing a protein structure as 'recipes', allowing easy communication of ideas between players [74] and, from this, new insights about protein structures can be achieved. [75, 76]

The study of protein-ligand complexes is one of the earliest examples of how (i) MD, (ii) VR, and (iii) haptic input devices can be combined to solve problems in molecular science. [77, 78] Henceforth, methods which combine Interactive Molecular Dynamics and Virtual Reality shall be known as Interactive Molecular Dynamics in Virtual Reality (iMD-VR). One of the pioneering examples of interactively steering a biochemical MD simulation used a haptic feedback device to pull a sodium ion through a bacterial gramicidin A channel structure. [79] Although this work utilized a standard 2D display, forces from the simulation were fed into the input device, therefore, users had both visual and force feedback for when they started to steer the system into an unfavourable state. Since then, iMD has been applied to understand even more sophisticated biomolecular processes. The E. coli glycerol uptake facilitator is responsible for drawing sugars into bacterial cells; iMD was combined with a VR interface to steer two sugars, arabitol and ribitol, through this structure. [80] In a similar vein to Stone et al., a haptic pen was used to give tactile feedback to users, therefore, this protocol could be used to detect at which points in the

channel were more or less stable for the sugar structures by how much resistance they could feel, allowing users to intuitively form stable complexes as they pulled the sugar through the channel. Additionally, glycerol was extracted from glycerol kinase using this protocol, where both an open and closed conformation of the enzyme was studied to understand how key structural differences can influence ligand unbinding. Future advances enabled even larger and more intricate systems to be studied using both iMD-VR and haptic devices, totalling up to 72,000 atoms. [81] Here, the mechanism of transporting an iron-enterobactin complex through a lipid bilayer protein, FepA, was interactively simulated. Through exploring a number of different pathways, two distinct routes where the complex could be pulled through with minimal disruption to the FepA structure were elucidated; although the high degree of force applied means it should not be taken at face value these pathways are realistic, they can be used as a starting point for more detailed analysis that might not otherwise be afforded due to the size of the system. Alternatively, rather than modelling extremely large systems with classical forcefields, smaller molecules can be modelled with quantum mechanical methods. Although this did not employ VR, pioneering work by several groups entered a new frontier by using a haptic device to make or break bonds during a simulation which modelled the quantum behaviour of atoms, allowing the user to rearrange molecules using iMD. [82, 83]

1.4 Narupa: An Open-Source Framework for Interactive Molecular Dynamics in Virtual Reality

A common limitation of the iMD methods discussed in this review is that they can necessitate specialized hardware, a dedicated space to host the VR, or access to specialized computing resources to run the dynamics engine at an interactive speed. However, the most recent advances in computational processing and VR has allowed iMD-VR to be performed with commodity hardware, extending to a range of molecular applications. [84] Narupa, an open-source framework for performing iMD-VR with commercially available HMDs, was initially extended to a small handful of use cases [20], however, potential applications have since expanded. An emergent use of iMD-VR is enhancing the rate at which molecular systems are sampled, ranging from a handful of small molecules to an expansive protein system. One recent application is quickly generating structures along a reaction coordinate defining a chemical process, which can subsequently be used to train a neural network to make predictions about the corresponding potential energy surface. As forming and breaking bonds can be simply achieved by bringing atoms closer together or further away, Narupa was used to accelerate hydrogen abstraction from a CN radical using isopentane. Points along the reaction coordinate were efficiently sampled, subsequently allowing a neural network for making predictions about the energy of this system to be trained with good accuracy - particularly where a conformation was near the Minimum Free Energy Path (MFEP) where sampling was most extensive. [85] As molecules get larger, and the number of degrees in

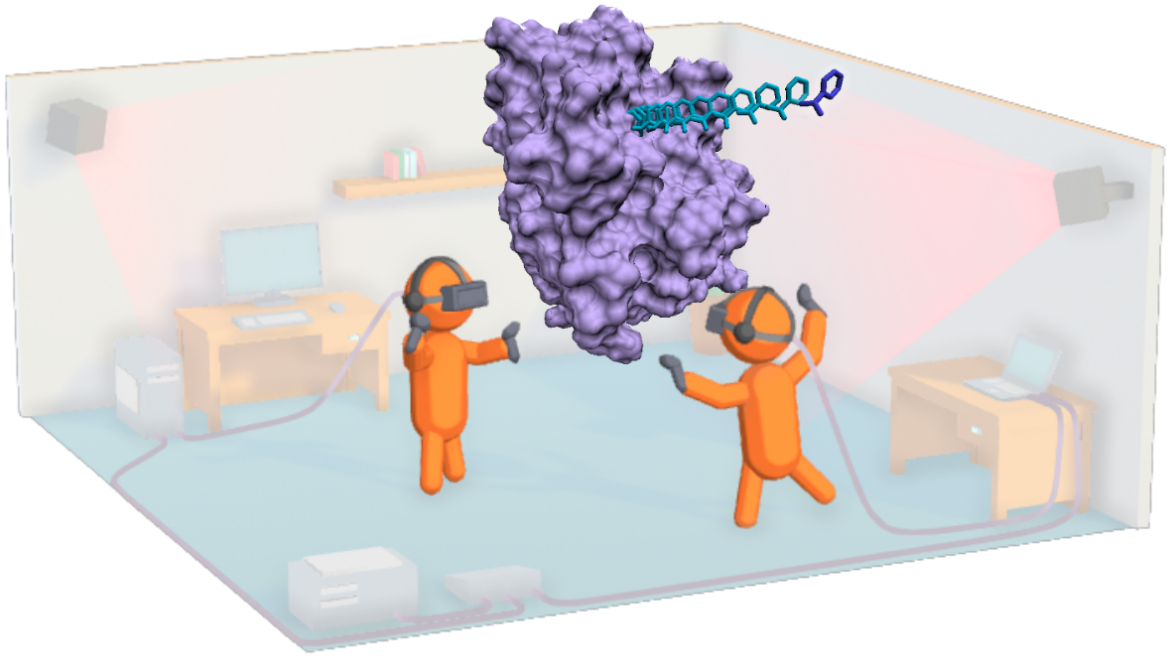

Figure 1.1: **Multi-user iMD-VR Protein Simulation**. Schematic showing two users interacting with a protein-ligand system (trypsin and benzamidine) in iMD-VR.

the system increases, it becomes harder to efficiently train neural networks on them. However, taking advantage of the versatility iMD-VR offers, a series of hydrocarbons of varying length were reacted with a cyano radical; six independent neural networks were then trained using this data. The models were then used in tandem to make energetic predictions about the reactivity of a larger molecule, squalene, subsequently only requiring 15,000 data points to obtain good accuracy. [85] Narupa has also been applied in an educational context, where it was used to teach undergraduate level students about chorismite mutase catalysed reactions: given the short scope of the study, it is admittedly harder to elicit longer-term learning benefits, however, an immediate improvement in student experience was reported. [21] Although moving outside the scope of molecular sciences, Narupa has also been used to develop and test new haptic devices [86], investigate how we perceive the flexibility of virtually simulated molecular objects [52], and has also been used to demonstrate that experiences in VR can induce 'mystical-type' experiences, i.e. subjective experiences that include a sense of connectedness, transcendence and ineffability. [87]

Recently Narupa has been applied to biomolecular applications: Fig. 1.1 shows two users interacting with a protein-ligand system (trypsin and benzamidine). Primarily, this thesis focuses on harnessing iMD-VR to solve problems in pharmacology and the following chapters detail the development and application of this tool for performing molecular docking tasks. Initially, this

work outlines the advantages of VR for performing complex 3D molecular manipulations over more traditional interfaces (i.e. mouse/keyboard and touchscreen). Building on this, protocols for accurately extracting a ligand from a protein binding pocket and re-establishing the starting complex using iMD-VR is described, using protein-ligand systems with increasing dynamical complexity. The apo structure of a target of high pharmacological importance (SARS-CoV-2 Main Protease) is docked with both a small ligand inhibitor and a reactive 11-mer oligopeptide, allowing new complexes to be generated using iMD-VR. Due to the added challenge of docking to non-cognate structures (potentially with a larger, more rotationally-complex molecule), this warranted a more extended exploration of how iMD-VR generated structures are assessed, where hydrogen bonding contacts were deemed significant. It is unsurprising that an component of successful iMD-VR ligand binding is the ability to form key contacts between the protein and the ligand; in light of this, sonification of non-bonded interactions is developed as a means of indicating to the iMD-VR user that favourable polar contacts have been formed. Finally, the iMD-VR interface is also developed as a means of deriving more quantitative information about the protein-ligand systems being studied. Chiefly, we use iMD-VR to sample complete unbinding pathways and use those coordinates to seed path-based biasing methods, allowing a free energy to be estimated along of a series of distinct routes along the protein surface (without the need to first sample them in non-interactive MD). Overall, this thesis provides a exploration of how an Interactive Molecular Dynamics in Virtual Reality can be developed for, and subsequently used to solve, questions in drug discovery.

CHAPTER 2

SAMPLING MOLECULAR CONFORMATIONS AND DYNAMICS IN A MULTI-USER VIRTUAL REALITY FRAMEWORK

In accordance with the University of Bristol guidelines on the integration of publications as chapters within a dissertation, this chapter was previously published in Science Advances. [20] My contribution was designing, carrying out and analyzing the results of the user studies described in this chapter, alongside producing mixed reality videos showcasing the three molecular tasks. Mike O'Connor, who is joint first author, developed the iMD software used in the studies. Edward Dawn, for his Masters dissertation project, jointly helped design and carry out the user studies. Oussama Metatla and Anne Roudaut contributed to the user study design through sharing their expertise in the field of Human Computer Interaction. Matthew Sutton collaborated with me in making mixed reality videos showing the three iMD-VR tasks. Lisa May Thomas, Becca Rose Glowacki, Rebecca Sage, Phillip Tew, Mark Wonnacott, Phil Bates, and Adrian J. Mulholland all contributed knowledge or software expertise towards this work. The manuscript was written jointly between myself, Mike O'Connor, and David R. Glowacki, however, David had a pivitol role in shaping the introduction, results and discussion (Sections 2.1. 2.2 and 2.3). Mike wrote Section 2.4.1. I wrote Sections 2.4.2 and 2.4.3.

2.1 Introduction

It is a fundamental human instinct to build both conceptual and tangible models that help to organize and make sense of our perceptions and experience in the natural world. The practice of building and manipulating models has a rich history and profound impacts across a range of domains, including the physical sciences, the social sciences, engineering, medicine, design, and architecture. Here, our primary focus is on modeling at the nanoscale. From a modeling

perspective, the nanoscale represents an interesting domain, because the objects of study (for example, molecules) are invisible to the naked eye, and their behavior is governed by physical forces and interactions significantly different from those forces and interactions that we encounter during our day-to-day phenomenological experience. In domains like this, which are imperceptible to the naked eye, effective models are vital to provide the insight required to make research progress.

In his visionary essay *The Ultimate Display*, Sutherland [88] highlighted the potential of immersive digital platforms to furnish an intuitive understanding of scientific and mathematical domains for which we otherwise lack intuition: "We live in a physical world whose properties we have come to know well through long familiarity. We sense an involvement with this physical world which gives us the ability to predict its properties well. For example, we can predict where objects will fall, how well-known shapes look from other angles, and how much force is required to push objects against friction... We lack corresponding familiarity with the forces on charged particles, forces in nonuniform fields, the effects of non-projective geometric transformations, and high-inertia, low friction motion..."

The fundamental forces that govern the physical mechanics of nanoscale molecular objects are relatively well characterized, owing to decades of experimental, theoretical, and computational study. The nanoscale represents a domain that is full of the sorts of "nonintuitive" physics highlighted by Sutherland: Forces acting on charged particles in nonuniform fields are the norm, and high-inertia, low-friction regimes are common in a range of applications. Moreover, molecular systems typically have thousands of degrees of freedom. As a result, their motion is characterized by a complicated, highly correlated, and elegant manybody dynamical choreography, which is nonintuitive compared to the more familiar mechanics of objects that we encounter in the everyday physical world. Their combined complexity, unfamiliarity, and importance make molecules particularly interesting candidates for investigating the potential of new digital modeling paradigms.

Tangible physical models have an important place in the history of chemistry and biochemistry. 3D molecular models have been used as conceptual and educational tools dating back to at least von Hofmann in the 1860s. More recent examples include Dorothy Hodgkin's crystallographic model of penicillin's structure [89] demonstrating the presence of a β-lactam ring, Pauling et al.'s [90] use of (originally paper!) models to identify the structure of α helices, and Crick and Watson's [91] famous DNA model. Large room-sized models, made from, for example, wire, plastic, brass, balsawood, and plasticine, were used to refine and represent protein crystal structures by pioneers such as Kendrew et al. [1] and Perutz et al. [92] For example, Levitt [93] (in the 2013 Nobel lecture) recounted building a so-called Kendrew model of hen egg white lysozyme: "... slow work but at the end you really know the molecule."

Physical models like these provide structural insight but cannot represent the often non-intuitive mechanics that determine how molecules move and flex. Going back to pioneers like

Bernal [94], whose attempts to understand liquid structure involved mechanical simulation of assemblies of macroscopic spheres, molecular scientists have since made heroic efforts to include the fourth dimension (time) into their models. In the 1970s, pioneers like Levitt and Warshel [95] and McCammon, Gelin, and Karplus [96] were able to simulate the motion of complex molecules such as proteins. The year 1979 saw the first movie of a time-dependent Molecular Dynamics (MD) simulation (bovine pancreatic trypsin inhibitor), one of several developments that heralded the eventual replacement of tangible mechanical models by screen-based graphics. These rose to prominence in the 1980s and are now ubiquitous for the purpose of understanding and teaching molecular structure and dynamics.

Advances in computer power, and decreasing cost, have transformed many domains of computational science, including molecular visualization and simulation. For example, GPUs, designed to facilitate fast rendering in video games, not only have benefited scientific visualization but also have been adapted to accelerate a range of molecular physics algorithms [97], now allowing routine simulation of systems with hundreds of thousands of atoms at time scales ranging from hundreds of nanoseconds to microseconds, with applications to areas including protein folding [98], enzymology [99], and drug discovery. [100] Beyond GPUs, application-specific integrated circuits (ASICs) [101], cloud computing platforms [102], distributed computing networks [103], and new architectures enable simulation of large systems at millisecond time scales. [101, 102]

Nevertheless, computational simulation of chemical transformation in molecular systems is characterized by considerable complexity, partly because it arises from spontaneous rare events that occur during the course of a molecule's hyperdimensional dynamical choreography. There is good evidence that mapping such transformations belongs to a class of "NP-hard" problems, for which no obviously optimal computational solution exists. [104] For the foreseeable future, many important molecular-level transformations occur on time scales that will remain beyond even the most sophisticated simulation architectures. "Chemical intuition" (an oft-invoked concept that broadly refers to the chemist's ability to efficiently navigate hyperdimensional molecular space) is therefore likely to play an important role in (bio)chemistry and synthetic biology for a long time to come. Tools accelerating the rate at which chemical intuition can be brought to bear on structurally and physically detailed models will facilitate creative teams making progress on challenging problems.

Like many domains of scientific computing, the basic workflow for molecular simulation has remained largely unchanged for the past 30 to 40 years, that is, iterative cycles of job submission to High-Performance Computing (HPC) resources, followed by visualization on a 2D display. Pioneers with interests spanning molecular simulation and human computer interaction, led by Fred Brooks [105] and Kent Wilson [106], were among the first to imagine improvements to this workflow using interactive computational technologies: Following on from the ideas outlined by Sutherland [88], they speculated that Interactive Molecular Simulation (iMS) frameworks would lead to models that would be as intuitive to manipulate as the old tangible models, but which

followed rigorous physical laws, and could be used to tackle hard rare event sampling problems. Brooks and co-workers [73, 105] designed an immersive six–degree of freedom force-feedback haptic system, which users could manipulate to carry out molecular docking tasks. Inspired by this work, Schulten and co-workers subsequently miniaturized Brooks' setup: By manipulating a desktop-mounted haptic pointer, users could steer the real-time dynamics of molecules rendered on a stereographic screen [107], a setup that has since been extended by others to interactively steer real-time molecular mechanics [81] and quantum chemistry simulations. [82, 83]

These interactive setups face a well-known limitation in their ability to achieve 3D "co-location," that is, aligning the interaction sites in 3D physical space and 3D virtual space. [108] Touchscreens solve the problem of 2D co-location because the interaction site in physical space is identical to the virtual interaction site. For iMS, 3D co-location is an important design problem, given that molecules are 3D objects that move in 3D. Despite these difficulties, the utility of the iMS idea has been demonstrated by tools like Foldit. [9] Using a keyboard-mouse interface, Foldit enables users to apply their intuition to explore protein conformational space and predict protein structures. Cooper et al. [9] highlighted cases where Foldit users made better predictions (that is, located deeper energetic minima, which correspond to more stable structures) than automated algorithms, owing to users' willingness to explore high-energy ("high risk") pathways that automated strategies avoided. Khatib et al. [109] analyzed user search strategies to construct new algorithms.

Driven mostly by the consumer gaming market, recent advances in VR hardware provide commodity-priced solutions to the problem of 3D co-location. Combining infrared optical tracking, inertial movement units, and ASICs, high-end commodity VR technology such as the HTC Vive tracks a user's real-time 3D position with errors of less than a centimeter, allowing users to reach out and touch simulated objects within the virtual world, as shown in Fig. 2.1 and movie S1. [110, 111] VR pioneers like Lanier [112] have emphasized the fact that several so-called VR frameworks do not allow this type of interaction, enabling little more than "just looking around in a spherical video." Lanier [112] has made a point to distinguish those technologies that do afford this sort of interaction: "If you can't reach out and touch the virtual world and do something to it, you are a second class citizen within it... a subordinate ghost that cannot even haunt".

In the medical field, VR technologies that enable surgeons to "reach out and touch the virtual world" have an established track record: Several studies have shown that VR-trained surgeons complete surgical procedures faster, with significantly lower error rates. [113] However, the use of VR in surgical contexts, where it is intended to simulate a surgeon's experience of manipulating human tissue, is rather distinct from the use of VR to manipulate molecular structure and dynamics. Whereas surgical applications have a well-defined and measurable design reference (that is, how does the VR simulation "feel" compared to an experience involving human tissue?), molecular applications have no similarly well-defined design reference (that is, what does a molecular system feel like?) This lack of reference is what makes developing

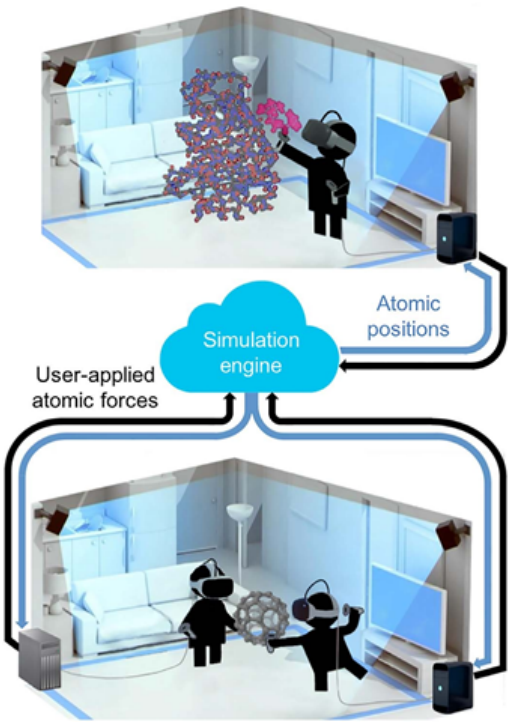

Figure 2.1: **Technical schematic of the HTC Vive VR setup designed to carry out iMD-VR studies**. Bottom: Two users within the multiperson VR framework passing a simulated C_{60} molecule back and forth. Each user's position is determined using a real-time optical tracking system composed of synchronized infrared light sources. Each user's VR HMD is rendered locally on a computer fitted with a suitable GPU; MD calculations and maintenance of global user position data take place on a separate server, which can be cloud-mounted. As long as the network connecting the client and server enables sufficiently fast data transfer, system latency is imperceptible to the human senses. Top: Single-person setup, where the user is chaperoning a real-time GPU-accelerated MD simulation to generate an association pathway that docks a benzylpenicillin ligand (magenta) into a binding pose on the TEM-1 β-lactamase enzyme.

a real-time molecular simulation and manipulation framework such a fascinating challenge, which must necessarily consider aesthetics, design, and user psychology to be effective. The lack of design reference also highlights the arbitrariness of tangible (for example, plastic or metal) molecular models.

2.2 Results

Building on our previous work using optical tracking technologies to interactively steer real-time molecular simulations [114], Fig. 2.1 (bottom) shows the framework that we have developed to interface the HTC Vive with rigorous real-time molecular simulation algorithms, which we henceforth refer to as the "iMD-VR app". Two optically tracked researchers are shown [each wearing a VR-enabled HMD and holding two small wireless controllers that function as atomic "tweezers"] manipulating the real-time MD of a C_{60} molecule. As shown in movie S1 [110, 111],

the researchers can easily "grab" individual C_{60} atoms and manipulate their real-time dynamics to pass the C_{60} back and forth between each other. This is possible and immediately intuitive because the real-time C_{60} simulation and its associated ball-and-stick visual representation are perfectly co-located—that is, the interaction site in 3D physical space is exactly the interaction site in 3D simulation space. The cloud architecture provides further benefits: Because each VR client has access to global position data of all other users, any user can see through his/her headset a co-located visual representation of all other users at the same time. To date, our available resources have allowed us to simultaneously co-locate six users in the same room within the same simulation. The interaction shown in movie S1 [110, 111], in which multiple users in the same room are able to easily pass a simulated molecule between themselves (or, for example, collaboratively tie a knot in a protein) as if it were a tangible object, represents a class of simulated virtual experience which is not possible within the large-scale immersive stereoscopic CAVE environments that have become popular within academic and industrial research institutions around the world. [115] The cloud mounted framework shown in Fig. 2.1 also makes it straightforward to enable remotely located workers to occupy the same virtual space.

While a real-time MD simulation of C_{60} is relatively cheap, the cloud architecture enables access to more powerful computational servers as needed. For example, Fig. 2.1 (top) and movie S2 [110, 116] show a researcher taking hold of a fully solvated benzylpenicillin ligand and interactively guiding it to dock it within the active site of the TEM-1 β-lactamase enzyme (with both molecules fully flexible and dynamic) and generate the correct binding mode [117], a process that is important to our understanding of antimicrobial resistance. The β-lactamase example [which benefits from a plug-in that communicates with the GPU-accelerated molecular simulation package OpenMM [118] via PLUMED [119]] illustrates that our framework is sufficiently intuitive and easy to control to enable a researcher to quickly formulate and evaluate dynamical hypotheses in large molecular systems. Generating a benzylpenicillin docking pathway involves a nonlinear sequence of complex molecular manipulations that would be difficult to formulate algorithmically. Thus, the framework has potential as an effective tool for understanding molecular docking and binding kinetics (standard tasks in structure-based drug design) and may prove particularly effective as a complement to enhanced sampling techniques for challenges such as identifying allosteric and cryptic binding sites that are not present in crystal structures. [120]

An essential question is whether co-located interaction of the sort enabled by VR affords any real advantage in accelerating complex 3D manipulation tasks compared to more conventional interaction technologies. The application of interest in this case is molecular modeling. To tackle this question, we exploited the fact that the Fig. 2.1 framework runs on a wide range of different client interaction hardware, including mice (connected to personal computers/laptops) and tablets. Both are extremely familiar interfaces: the former offering non-co-located interaction, and the latter offering co-located interaction in 2D. We designed three specific tasks (Fig. 2.2 and movie S1)

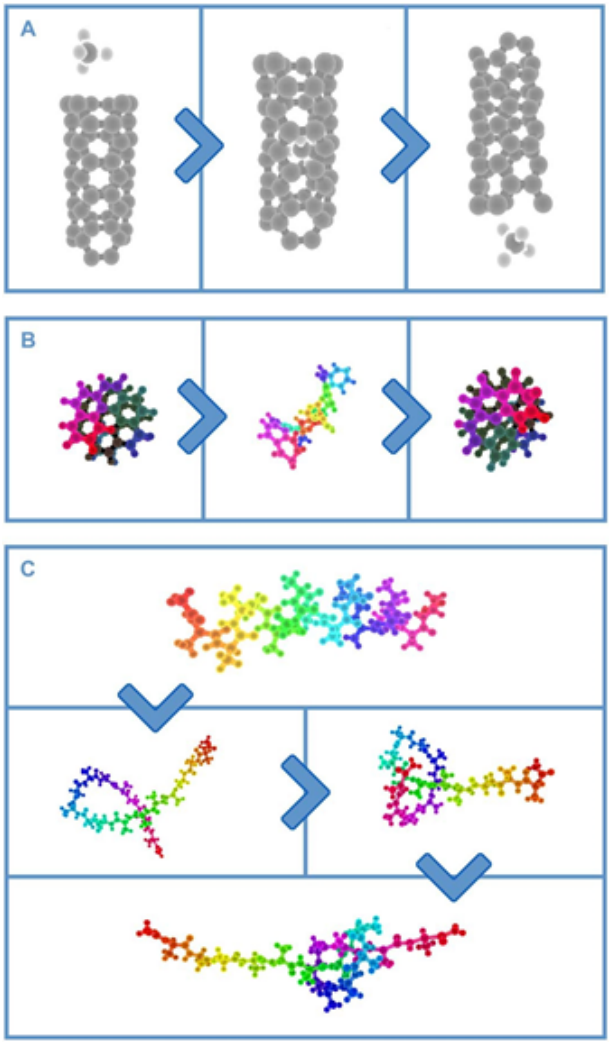

Figure 2.2: **Experimental iMS tasks**. Experimental iMS user studies featured the following tasks: (i) threading CH_4 through a nanotube, (ii) changing the screw sense of a helicene molecule, and (iii) tying a knot in a polypeptide (17-ALA). Colors selected in this figure are chosen for the sake of clarity.

[110, 111] for users to carry out and compared the rates of task accomplishment across different interaction hardware. Each task involves an increasingly complicated choreography: (i) guiding a methane molecule (CH4) through a carbon nanotube, (ii) changing the screw sense of an organic helicene molecule, and (iii) tying a knot in a small polypeptide [17-alanine (17-ALA)]. Each task represents a class of dynamics that is important across natural and engineered nanosystems. For example, nanopores are ubiquitous across bio/materials chemistry [121], induced changes in molecular helicity offer a strategy for synthetic biologists to transmit chemical messages [122], and protein knots are associated with neurodegenerative diseases. [123] To control for variations in the graphics and computational capabilities of different interaction hardware, each interaction platform used the same renderer and the same back-end MD simulation engine. The

Supplementary Materials [110] include details on the simulation setups, along with instructions enabling readers to use the executables at isci.itch.io/nsb-imd to initialize a cloud-based interactive simulation instance so that they can attempt the Fig. 2.2 tasks on any of the three interaction platforms.

Fig. 2.3 shows the rates at which cohorts of 32 users (who reported little or no previous VR experience) accomplished each of the three tasks in Fig. 2.2 on different hardware platforms. Before their participation, study candidates were warned of the potential for VR sickness and instructed to inform the demonstrators if they wanted to exit at any point. We recorded zero such instances, suggesting that our design produces little user discomfort. Reported errors in the measured rates were obtained using Poisson statistics, a common strategy in chemical kinetics. Rare event (or "task accomplishment") rates are said to be statistically distinguishable if their corresponding Poisson error bars do not overlap.

2.3 Discussion

A significant fraction of study participants were able to use the real-time VR simulation framework to accomplish (in a relatively short time) the molecular rearrangement tasks that we set for them (shown in Fig. 2.2). Specifically, 97% were able to thread methane through the nanotube, 47% were able to change the helicene screw sense, and 72% were able to tie a protein knot. This indicates that our preset simulation parameters (outlined in further detail below) enabled most of the participants to accomplish the Fig. 2.2 tasks. For tasks A and C, Fig. 2.3 indicates that VR provides a clear acceleration benefit compared to the other platforms. The more inherently 3D the task, the greater the benefit. Thus the knot-tying results (Fig. 2.3C) are the most dramatic, showing that this task is very difficult to accomplish using a mouse or a touchscreen. To ascertain whether the knot-tying results were reproducible, we carried out another set of tests with a different cohort; reassuringly, the results were the same within Poisson error limits (see the Supplementary Materials). [110]. For the nanotube task (Figs. 2.2A and 2.3A), the accomplishment rates, mean time, and median time in VR are approximately a factor of 2 times faster than on other platforms.

At first glance, the helicene task (Fig. 2.3B) is a case in which VR appears to provide little significant rate enhancement compared to other platforms. Observation suggests that this is because changes in helicene screw sense are most efficiently accomplished using a simple 2D circular motion, as shown in movie S1. [110, 111] Essentially, the 2D limitations of the mouse and touchscreen constrain the user to carrying out a motion that is well suited to inducing changes in molecular screw sense. However, closer inspection of the helicene time distributions suggests that VR does afford some advantage: The median time required to change molecular screw sense in VR is 30 to 40% less than the median time required on a touchscreen. Significantly, every task considered in Figs. 2.2 and 2.3 shows a median VR time that (i) is always faster than the

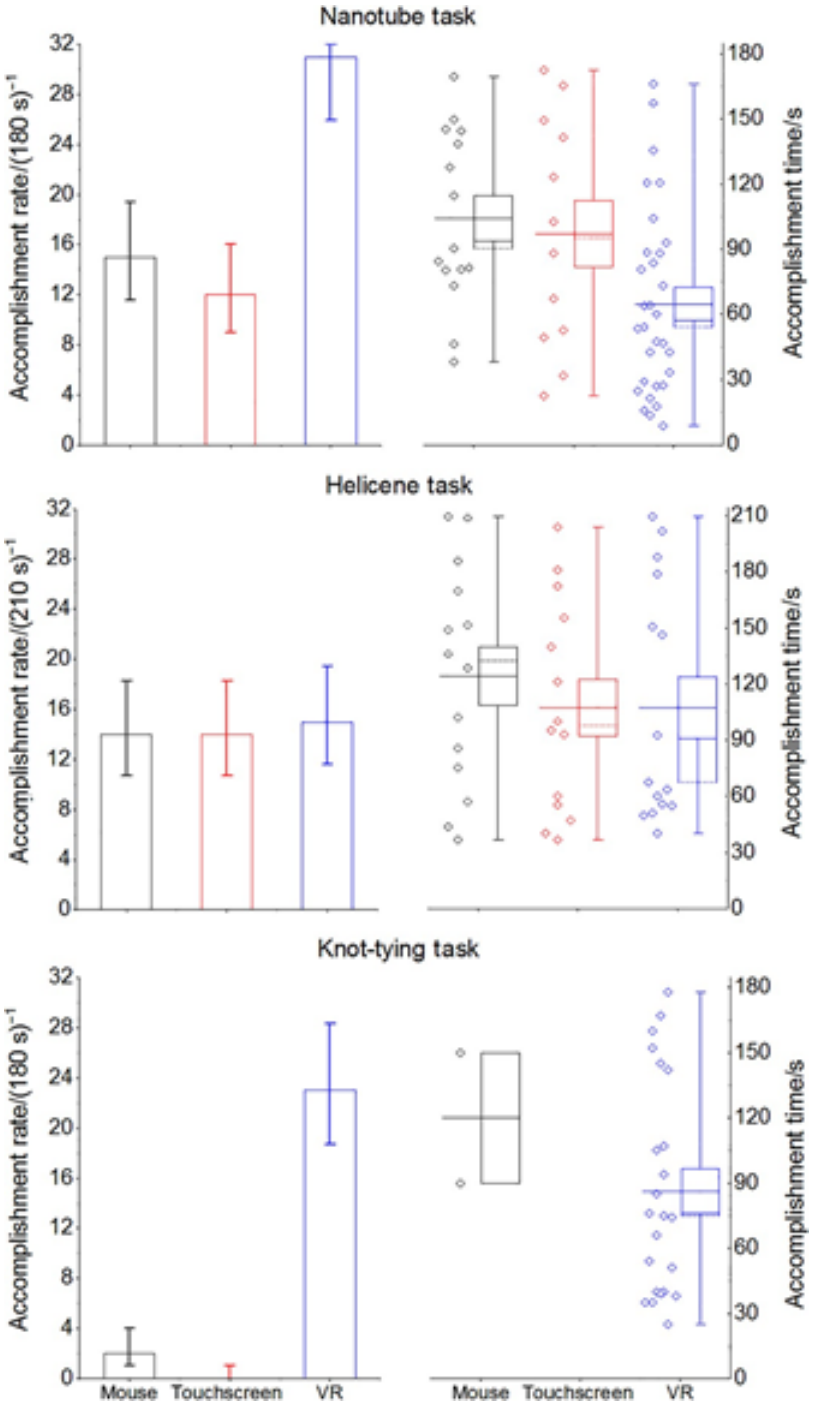

Figure 2.3: **User study results for the three experimental iMS tasks**. Left-hand panel shows user accomplishment rates for the tasks outlined in Fig. 2.2 (n = 32 for all tasks), with Poisson error estimates. Right-hand panel shows the corresponding distribution of task accomplishment times, along with box-and-whisker plots. Whiskers indicate the data range, and box limits indicate the standard error of the distribution. The mean is shown as a solid line, and the median is shown as a dashed line.

mean and (ii) lies outside the standard error limits. This distribution of waiting times is clearly not Gaussian; rather, it resembles the waiting time distribution that characterizes first-order kinetics, suggesting a cluster of VR users who accomplish tasks quickly with a longer tail of slow users.

Fig. 2.3 shows that our VR platform provides a clear advantage over conventional visualization/interaction platforms, and this advantage appears to increase as the complexity of the problem increases. To better understand the results, we carried out further evaluation in the form of participant questionnaires and interviews (detailed in the Supplementary Materials) [110]. Despite the fact that very few of the study participants had previous VR experience, participants indicated an overwhelming preference for VR in carrying out the Fig. 2.3 tasks (compared to a mouse or touchscreen) for three reasons: (i) quick perception of depth, (ii) the ability to inspect the molecule by walking around it, and (iii) the use of both hands to accomplish the tasks.

The results presented here represent a first attempt to quantify the acceleration that can be achieved by carrying out 3D molecular sampling, modeling, and manipulation tasks in VR. Our exclusive focus in this article has been on interactive dynamics with molecular mechanics force fields, rather than quantum mechanical force fields. There are two main reasons for this: Quantum mechanical (electronic structure) methods are only feasible for small molecules because they require greater processing resources, and quantum mechanical methods are generally less stable than molecular mechanics force fields, owing to difficulties that arise as one attempts to numerically converge quantum mechanical self-consistent field equations on-the-fly. Because molecular mechanics force fields are more robust than their quantum mechanical equivalents, they afforded better control during user studies reported here. However, we have recently undertaken work to interface our VR framework with the quantum mechanical force field engine described by Mühlbach et al. [124] This enables us to perform real-time simulations of chemical reactivity in a fully co-located multiperson VR environmental and to carry out a range of studies that we will report on in the near future.

For biomolecular conformational problems like dynamical path sampling or drug docking, where computational search spaces are too large for brute force approaches, our results suggest that VR frameworks, like those that we have outlined here, may offer a powerful tool enabling research experts (for example, structural biologists, molecular modelers, and medicinal chemists) to occupy the same virtual environment and efficiently express their 3D biomolecular intuition to test hypotheses for collaboratively tackling important microscopic questions linked to molecular mechanism and design. For example, using VR technologies to generate seeds for subsequent automated searches could represent a powerful strategy for obtaining molecular insight, which is likely to save on valuable computational clock cycles. It may even be possible to imagine a scenario where machines “learn” efficient strategies for navigating hyperdimensional biomolecular search spaces by accumulating observational data on how human experts navigate hyperdimensional biomolecular spaces in VR.

Recent advances in HPC, the cloud, data science, robotics, and machine learning have led many workers across academia and industry to begin speculating about the future of scientific practice, asking important questions as to the sort of scientific future that we should be consciously working to design over the next few decades. [112, 125] In an increasingly automated future that is reliant on machines, it is extremely important to think carefully about and discuss the role that human creative expression will play. Many scientists and engineers express a philosophical sentiment that automation is often desirable because it eliminates mistakes and unpredictability; however, these are staple features that are inevitably entangled with creative expression. So long as human creativity continues to play an important role in the process of scientific discovery and design, then we believe that VR frameworks like that outlined here may play a crucial role in our emerging scientific future. In our view, advanced visualization and interaction frameworks are complementary to research activities aimed at increasing the automation of research tasks and scientific discovery, because they provide an efficient means for humans to express high-level creative scientific and design insight, leaving automated frameworks to subsequently sort out the computational and mechanistic details. Another practical role for VR frameworks in an era of increasing automation pertains to quality assurance: As robotic automation becomes more prevalent (for example, in molecular simulation workflows), we are going to need efficient new visualization tools that enable us to continually review and evaluate robot performance to understand the actions and decisions they are taking, determine whether those actions and decisions make sense, and decide whether the robots need additional training.

Moving forward, there are a range of related domains that we intend to explore. For example, we aim to better understand how changes in simulation parameters (for example, force strength, MD timestep, simulation temperature, holonomic constraints, and rendering options) affect the ability of users to intuitively accomplish molecular tasks and furnish meaningful microscopic insight. We are interested in designing analytical methods that can be combined within interactive sampling strategies so that mechanistic observables (for example, free energies, barrier heights, and conformational probabilities) can be extracted from VR simulations. We are also exploring the extent to which other sensory modalities (for example, sound) might be engaged to provide additional information within a real-time immersive simulation environment. [126] As we explore the potential of VR across both molecular mechanics–based and quantum mechanics–based simulations and study its ability to enable specialists and nonspecialists alike to better understand and more efficiently manipulate complex data, we look forward to understanding how it may be used to advance molecular science in a range of research, communication, and educational contexts.

2.4 Materials and Methods

2.4.1 MD simulation setup

The broad strategies that we have previously used to carry out iMD were outlined by Glowacki et al. [114] and briefly summarized here for the sake of completeness. In classical mechanics, the time-dependent dynamics of molecular systems are solved by numerically integrating Newton's equations of motion. The vector of forces acting on a set of atoms $\boldsymbol{F(t)}$ can be written in terms of the system's potential energy V, that is:

$$\boldsymbol{F}(t) = -\frac{dV}{d\boldsymbol{q}} \tag{2.1}$$

where $\boldsymbol{q}$ is a vector containing the position of each atom in the ensemble. Our system effectively allows users to interactively chaperone a realtime MD simulation by splitting V into two different components:

$$V = V_{int} + V_{ext} \tag{2.2}$$

where V_{int} corresponds to the system internal potential energy, and V_{ext} corresponds to the additional potential energy added when a user exerts a force on a specific atom (or group of atoms) when he/she grabs it using the handheld wireless controller shown in Fig. 2.1. Substituting Eq. 2.1 into Eq. 2.2 then gives:

$$\boldsymbol{F}(t) = -\frac{dV_{int}}{d\boldsymbol{q}} - \frac{dV_{ext}}{d\boldsymbol{q}} \tag{2.3}$$

The external forces were implemented by projecting a spherical Gaussian field into the system at the point specified by the user and applying the field to the nearest atom j through the following formula:

$$\frac{dV_{ext}}{d\boldsymbol{q}} = \frac{m_j c}{\sigma^2}(\boldsymbol{q}_j - \boldsymbol{g}_i)e^{\frac{-\|\boldsymbol{q}_j - \boldsymbol{g}_i\|^2}{2\sigma^2}} \tag{2.4}$$

where m_j is the atomic mass of the atom, c is a scale factor that tunes the strength of the interaction, $\boldsymbol{q}_j$ is the position of atom j, $\boldsymbol{g}_i$ is the position of the interaction site, and σ controls the width of the interactive fields. For all tasks on all the platforms, c was set to 2000 (kJ·mol^{-1})/(atomic mass unit), a value that achieves responsive interaction while preserving dynamical stability, and σ was set to the default value of 1 nm. While an interaction is active, it is always applied to the same atom (or group of atoms), which means that a user can dynamically adjust the course and strength of the interaction by repositioning their field with respect to the

atoms with which they are interacting, until he/she decides to "let go". As discussed in the main text, the position of the interaction field in VR is co-located to precisely where the user's controller is; for the mouse and touchscreen interfaces, the field is attached to the nearest atom (measured in the 2D plane of the screen). Movements of the field are only possible in 2D, so 3D motions must be built up from successive 2D motions followed by repositioning of the camera.

Simulating the dynamics of a particular molecular system requires specifying an engine to calculate the internal forces. Here, we benefit from the fact that our framework has been designed to flexibly communicate with a wide range of force engines via a defined application programming interface. For the hydrocarbon systems in the nanotube and helicene task, we used our own "in-house" implementation of the MM3 force field. [127] The 17-ALA protein knot task used the GPU-accelerated Amber99SBILDN force field provided within the OpenMM MD package. [118] For the simulation of larger biomolecular systems such as β-lactamase, we used a custom build of PLUMED [119] to communicate with simulations running within OpenMM on a workstation consisting of four NVIDIA 1080 Ti GPUs. This workstation enables us to simulate proteins using the Amber99SBILDN force field and optionally include either implicit (for example, continuum) or explicit (for example, TIP3P water) solvent models. In cases where we modeled an explicit solvent, we did not typically visualize the solvent molecules to maintain clarity and high-quality rendering. To integrate the forces, all tasks used a Velocity Verlet integrator, with a Berendsen thermostat [128] set to a target temperature of 200 K. For the nanotube and helicene tasks, a time step of 1 fs was used, while the protein knot task used a time step of 2 fs along with the RATTLE holonomic constraint, owing to the fact that the conformational change occurs over a longer time scale.

To carry out the user studies (detailed further in what follows), the simulations were hosted on separate machines within our own local area network. We used one machine for each task to avoid any latency that might arise from excessive computational load on a single machine. The three machines that we used as simulation servers during user studies included the following: (i) a mid-range gaming desktop with a 3.5 GHz quad-core Intel i5-6600K processor and an NVIDIA GTX 970 graphics card, (ii) a high-end Alienware13 R3 gaming laptop with a 2.6 GHz quad-core Intel Core i7-6700HQ processor and an NVIDIA 1060 dedicated VR graphics card, and (iii) a high-end Alienware15 R3 gaming laptop with a 2.6 GHz quad-core Intel Core i7-6700HQ and an NVIDIA 1070 GTX dedicated VR graphics card. The user tests involving mouse input (described in the "User study one" section) were run at two different sites: (i) our laboratory at the University of Bristol, using the mid-range gaming desktop along with an external USB mouse and a 21-inch external monitor and (ii) the CCPBioSim (Collaborative Computational Project for Biomolecular Simulation) 2017 conference using the screen on the Alienware15 along with an external USB mouse. During all user studies, we throttled the performance on all platforms that achieves responsive interaction while preserving dynamical stability to guarantee that (despite differences in each machine's specifications) they were capable of running at 30 frames per second. This

ensured that the latency across all test platforms gave an equally fluid user experience. For the touchscreen version of the tasks, we used a Samsung Galaxy S3 tablet, connected to the simulation over an 802.11ac Dual Band Gigabit WiFi connection.

2.4.2 Controlled user studies

2.4.2.1 User study one

A total of 32 participants were recruited for this study. To mitigate any learning or fatigue effect, the platform on which any given participant started was randomly selected. 12 participants began with the mouse platform, 9 participants started with the touchscreen platform, and 11 participants started with the VR platform. Participants were rotated using a Latin square in the order of VR, mouse, and touchscreen.

Before starting on a platform, participants were given the buckminsterfullerene task (see the “Buckminsterfullerene task” section for details) to familiarize themselves with the feel of the molecular interaction on a given platform. Once participants indicated to the study facilitators that they had a sufficient level of familiarity, they were moved onto the nanotube/methane task (see the “Nanotube/methane task” section for details). Study facilitators moved a participant onto the helicene task if they either managed to accomplish the nanotube task or time expired (see the “Helicene task” section for details). Once the user had attempted both tasks, the process was repeated on the next platform until the participant had tried the task on all three platforms. Once participants had attempted both tasks on all three platforms, they were given a short questionnaire to fill out, details of which are discussed in further detail below.

In total, 32 participants were recruited through email to staff and students at the UoB and offered a £10 Amazon gift voucher for their time. For reproducibility, such that a comparable group can be recruited, demographic information was collected about the participants. Seventeen (53.125%) of the participants were ages 18 to 24, 10 (31.25%) were ages 25 to 34, 4 (12.5%) were ages 35 to 44, and 1 (3.125%) was ages 45 to 54. Twenty-two (68.75%) of the participants were male, and 10 (31.25%) were female. Participants reported a range of education levels. Eleven (34.375%) of the participants were undergraduate students, 16 (50%) were postgraduate students, 3 (9.375%) were postdoctoral researchers, and 2 (6.25%) were researchers.

Participants were given a Likert scale question to complete to indicate their familiarity with using VR and tablets, where 1 represents having no experience and 5 represents being very experienced. A breakdown of responses can be found in table S1. Altogether, self-reported VR experience was found to be low, where tablet use was more prevalent. Given the education level of the group, and the fact that they were drawn from a university chemistry department, we assumed that mouse familiarity was high.

2.4.2.2 User study two

Here, 12 people were recruited and interviewed afterward. We used a smaller sample size, because our emphasis during these studies was on gaining qualitative user feedback on attitudes to the three platforms, achieved via interview. Task accomplishment rates for this study are presented in Fig. S2. [110] In addition to administering questionnaires used during the first user study, qualitative analysis of participants' subjective feedback [129] was performed on the recorded interview transcripts, a summary of which is presented below.

Participants were recruited in group sizes varying between one and three. To mitigate any learning or fatigue effect, the platform on which participants started was randomized. Specifically, four people started with the mouse platform, four started with touchscreen platform, and four started with the VR platform. Participants were rotated using a Latin square in the order of VR, mouse, and touchscreen. Again, participants were first given the buckminsterfullerene task so that they could familiarize themselves with the interactive feel. Before starting on a platform, participants were first shown a short, instructional video of the specific trefoil knot that they were being asked to tie. Once they grasped what they were being asked to do, participants were moved onto the knot-tying task. A more detailed description of what both tasks entailed can be found below. Once the task was completed (or once time had elapsed), the process was repeated on the next platform until the participant had tried the task on all three platforms.

After each group had attempted the knot-tying task on each of the three platforms, they were interviewed about their experience using each of the platforms. During this interview stage, the following points were covered: (i) How had the participants found the task in general? (ii) Was there a preferred platform (or platforms) for completing the task? (iii) Why did participants prefer a given platform over others? (iv) Was there a least preferred platform (or platforms) for completing the task? (v) Are there any suggestions for how the platforms can be improved? (vi) Any further points?

Once again, the participants for this study were recruited by email to staff and students at the UoB and offered a £10 Amazon gift voucher for their time. For reproducibility, such that a comparable group can be recruited, demographic information was collected about the participants. Six (50%) of the participants were ages 18 to 24, five (41.7%) were ages 25 to 34, and one (8.3%) was age 35 to 44. Seven (58.3%) participants were male, and five were female (41.7%). Participants reported a range of education levels. Four (33.3%) reported themselves as being undergraduate students, three (25%) reported themselves as being postgraduate students, four (33.3%) reported themselves as being postdoctoral researchers, and one (8.3%) reported themselves as being a research technician.

Participants were given a Likert scale question to complete to clarify their familiarity with using VR and tablets, where 1 represents having no experience and 5 represents being very experienced. A breakdown of responses can be found in table S1. Together, self-reported VR experience was found to be low, where tablet use was more prevalent among the cohort. Given

the education level of the group, mouse familiarity was again assumed to be high.

2.4.2.3 User study three

We decided to repeat the methodology from the second user study with a larger sample size of 32 participants, identical to the sample sizes selected for the nanotube and helicene talks in the first user study. The primary aim of this leg was to obtain better statistics on knot task completion; therefore, no questionnaire or interview was given afterward.

Participants were recruited in group sizes varying between one and three. To mitigate any learning or fatigue effect, the platform on which participants started was randomly selected. Specifically, 10 participants started with the mouse platform, 11 participants started with the touchscreen platform, and 11 participants started with the VR platform. Participants were rotated using a Latin square in the order of VR, mouse, and touchscreen.

Participants were recruited during the fifth annual UK CCPBioSim conference (13 to 14 September 2017), held at the University of Southampton (www.ccpbiosim.ac.uk). The chance to participate in the user study was advertised by email, flyers, and word of mouth. For reproducibility, such that a comparable group can be recruited, demographic information was collected about the participants. Six (18.75%) of the participants were ages 18 to 24, 20 (62.5%) were ages 25 to 34, four (12.5%) were ages 35 to 44, one (3.125%) was ages 45 to 54, and one (3.125%) was over the age of 65. Twenty-four (75%) of the participants were male, and 7 (22%) were female. One (3%) participant chose not to state their gender. Participants reported a range of education levels. Nineteen (59.375%) of the participants were postgraduate students, 11 (34.375%) were postdoctoral researchers, and 2 (6.25%) reported themselves as researchers.

Participants were given a Likert scale question to complete to ascertain their familiarity with using VR and tablets, where 1 represents having no experience and 5 represents being very experienced. A breakdown of responses can be found in table S1. Self-reported VR experience was low; tablet use was far more prevalent. Given the education level of the group, mouse familiarity was again assumed to be high.

2.4.3 Molecular simulation tasks

2.4.3.1 Buckminsterfullerene task

Two buckminsterfullerene molecules were loaded into the iMD-VR app. Users were then instructed to grab the molecule and experiment with moving it around within the virtual space, and also to familiarize themselves with resizing and rotating the virtual space, thus giving them an understanding of the platform controls and the feel of the molecular interaction. There was no time limit to this task, nor did it have any specific end goal. The simulation details are included in section S1.

2.4.3.2 Nanotube/methane task

One C_{60} nanotube and one methane molecule were loaded into the iMD-VR app. Users were instructed to grab the methane molecule and lead it through the center of the nanotube, from one end to the other. The task had a time limit of 180 s, and completion was marked as the point that the user had successfully pulled the methane molecule through the entire nanotube, that is, leaving the opposite side from which it entered. The simulation details are included in section S1.

2.4.3.3 Helicene task

One 12-helicene molecule was loaded into the iMD-VR app. Users were instructed to manipulate the helicene molecule so that the screw sense of the helix was reversed. The task had a time limit of 210 s, and completion was marked as the point at which the screw sense of the helicene molecule had gone from its clockwise initial conditions to being completely anticlockwise. The simulation details are included in section S1.

2.4.3.4 Knot-tying task

One 17-ALA molecule was loaded into the iMD-VR app. Before starting the task on each of the platforms, users were shown a brief instructional video on the task. Users were then instructed to tie a 3_1 or trefoil knot in 17-ALA. The task had a time limit of 180 s, and completion was marked as the point at which a stable trefoil knot was formed in 17-ALA. The simulation details are included in section S1.

2.5 Supplementary Materials

Supplementary material for this chapter is available at `http://advances.sciencemag.org/cgi/content/full/4/6/eaat2731/DC1`

CHAPTER 3

iMD-VR FOR ACCURATE FLEXIBLE PROTEIN-LIGAND DOCKING

In accordance with the University of Bristol guidelines on the integration of publications as chapters within a dissertation, this chapter was previously published in PLoS One. [61] My contribution was designing, carrying out the expert user tests where trypsin and HIV-1 protease are the protein targets, and analyzing the results of the user studies described in this chapter, alongside producing a mixed reality video and three animations showcasing the protein-ligand docking tasks. I also modified the Narupa source code to enable trace atoms to be overlaid on the simulation. Rebecca K. Walters performed the expert user tests where neuraminidase was the protein target (and wrote any relevant background on the protein system and observations during iMD-VR), as described in Sections 3.2.1 and 3.3.1. Rebecca also aided in carrying out the novice user studies. Stephanie R. Hare carried out the PCA on the iMD-VR generated ligand undocking and redocking paths with PathReducer [130], including any relevant analysis discussed in the text. Mike O'Connor contributed software expertise. Adrian J. Mulholland and David R. Glowacki contributed both their knowledge and expertise towards this work.

3.1 Introduction

Computational researchers across a wide range of fields are becoming increasingly aware of their responsibility to explore low-cost simulation methodologies whose energy and hardware demands are environmentally sustainable. [131] Whilst the MD approach to biomolecular simulation [96, 132–134] and protein ligand-binding [135–140] has exploded in recent years, [141] the computational cost of MD-based approaches remains significant–a result of the fact that proteins are high-dimensional systems characterized by many local energy minima separated by a rugged

landscape.

Building on previous work constructing interactive simulation frameworks (e.g., led by Brooks [73, 105, 142], Wilson [106], Schulten [79, 80], and others [81–83]), we have been exploring iMD-VR as a low-cost strategy for investigating biomolecular problems like protein-ligand binding. Part of the attraction of an MD-based approach is the fact that it can capture movement and flexibility of both the protein and the ligand. Our open-source iMD-VR framework Narupa [84] allows users to interactively visualise and manipulate the molecular dynamics of real-time simulations within a virtual environment with atomic-level precision. The iMD-VR approach recognizes that the neural nets of the human brain, trained over several aeons, offer extremely sophisticated machinery for efficiently undertaking tasks linked to 3D insight, spatial navigation, and manipulation, with energy demands that are a fraction of those required by sophisticated hardware-accelerated machine-learning frameworks. Narupa enables humans to utilize their 3D spatial awareness skills, and their ability to undertake 'on-the-fly' reasoning, to perform sophisticated operations on complex 3D molecular structures, giving them the ability to move molecular systems between different regions of configuration space. In previous work, we have demonstrated that iMD-VR has acceleration benefits for various 3D molecular tasks compared to 2D interfaces. [20, 84] The ability to physically reach out and manipulate simulated systems as if they were tangible objects gives users the opportunity to explore molecular transformations, mechanisms, and rare events that may otherwise be inaccessible using conventional HPC MD simulations. While we have previously demonstrated the potential of iMD-VR to generate dynamical pathways in small systems, it remains to be seen whether iMD-VR is sufficiently intuitive and enables enough control for researchers to undertake more complex tasks.

In this article, we focus on applying Narupa to unbinding and rebinding small molecules to proteins, as illustrated in Fig. 3.1. Applying iMD-VR to protein-ligand systems requires moving a simulation between thermodynamically and kinetically distinct states (i.e., bound and unbound). This requires sophisticated 3D spatial reasoning: the protein binding pocket needs to be located, and the ligand orientated such that key contacts to specific residues are properly recreated. We evaluate the utility of iMD-VR to facilitate such manipulations through applications to three protein-ligand systems of increasing complexity, and investigate the extent to which iMD-VR 'experts' and 'novices' were able to reversibly generate protein unbinding and rebinding pathways and recover crystallographic ligand poses for the systems shown in Fig. 3.1. The results of the experimental protocol outlined herein show that iMD-VR users can quickly unbind and rebind ligands to proteins and recover experimental protein-ligand structures. For example, we show that an hour-long training session with an expert user enables novice iMD-VR users to recover the original binding poses for several different protein-ligand systems. We have established that the pathways generated by iMD-VR users are reproducible, and that the binding poses they recover are stable when used to initiate MD simulations over longer simulation timescales.

iMD-VR represents a relatively new approach to simulating drug binding, since it involves a

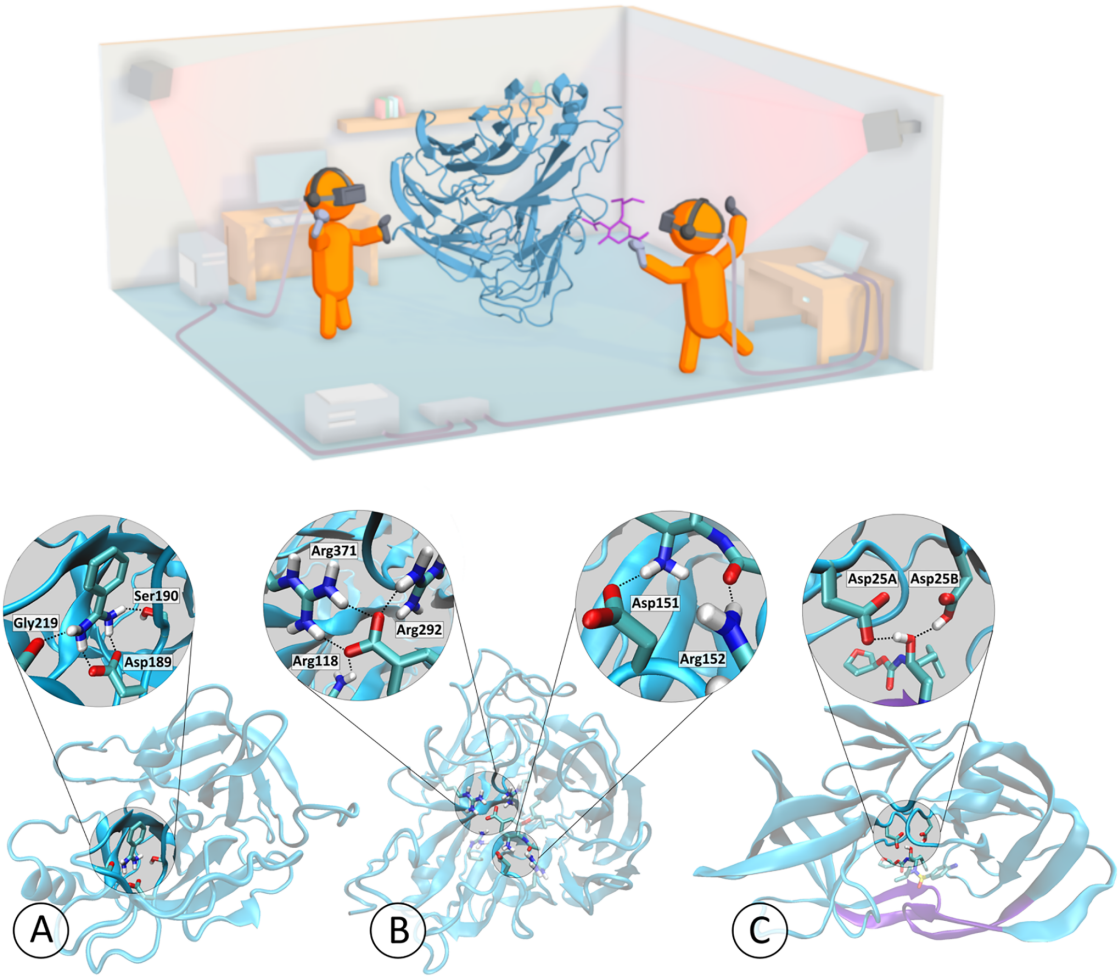

Figure 3.1: **Interactive protein-ligand rebinding using iMD-VR**. The top panel shows a schematic of Narupa, the open-source multiperson iMD-VR framework used to carry out the studies described herein, showing two participants using handheld wireless controllers to manipulate a real-time MD simulation of neuraminidase and oseltamivir. More information on the Narupa setup is available in Ref. [84]. The bottom panel shows a 3D representation of the binding pockets of each of the three protein systems interactively undocked and redocked, each bound to a ligand. The trypsin graphic (A) highlights the network of hydrogen bond interactions from Asp189, Ser190, and Gly219 to benzamidine (based off PDB code 1S0R). The neuraminidase graphic (B) highlights the hydrogen bonds between oseltamivir and both the 150-loop and a positively-charged trio of arginine residues of neuraminidase (based off a mutated neuraminidase structure derived from PDB code 2QWK). The HIV-1 protease graphic (C) highlights the hydrogen bonds between the hydroxyl group of amprenavir with both Asp25A and the protonated form of Asp25B (based off PDB code 1HPV). For HIV-1 protease, the protein 'flaps' have been highlighted in purple.

fully (or predominantly) flexible dynamic system and also does not require predefining a Collective Variable (CV) along which to carry out biased molecular dynamics simulations. [85] Instead, the researcher simply 'draws' the desired pathway by manipulating a complex system between different states. This approach has the potential to accelerate the exploration of pathways through high-dimensional configuration space. Overall, our tests show that a well-designed iMD-VR setup enables expert and novice users alike to accelerate complex 3D state changes of biomolecular systems. Our results suggest that iMD-VR tools are sufficiently intuitive and provide adequate control to enable users to recover experimentally derived bound complexes. Moreover, the fact that the sampled pathways are reproducible suggests that they are not too far from the equilibrium ensemble.

3.2 Methods

3.2.1 System selection

The systems selected for the studies outlined herein include, at one extreme, those that have well-characterized binding modes, where a user with prior knowledge of the system can use iMD-VR to sample binding and unbinding pathways. At the other extreme, we sought to push the limits of the iMD-VR tools and examine more complex protein-ligand systems. The three systems we chose are shown in Figs. 3.1 and 3.2 and are described below in order of increasing complexity.

3.2.1.1 Trypsin

The first protein-ligand system is the enzyme trypsin with a benzamidine ligand. Trypsin is a well-studied serine protease hallmarked by a catalytic triad consisting of histidine, serine and aspartic acid. As shown in Fig. 3.1A, a secondary motif of the trypsin binding pocket is an additional aspartic acid residue (at position 189) that stabilises the positively charged amino acids, binding a peptide chain in a pose that allows for specific cleavage of the carboxyl-side chain in which these amino acids are present. [148] Asp189 is charged, partially-buried, and is surrounded by a water network that favours desolvation. [149–151] Trypsin inhibitors can exploit this by mimicking positively-charged residues and forming an electrostatic contact with Asp189, an interaction further stabilized by a network of hydrogen bonds to Ser190 and Gly216 (Fig. 3.1A). [152] The binding mode between trypsin and one of its inhibitors, benzamidine, has relatively fast kinetics and is therefore often applied as an initial use case for theoretical methods. [60, 153–155] From an iMD-VR perspective, the trypsin-benzamidine system represents a binding mode where users do not need to induce significant conformational changes in the protein, and the ligand has only one rotatable bond. In effect, a user need only move the benzamidine out of the binding pocket before placing it back, making trypsin a relatively simple test case for iMD-VR.

Fig. 3.1A shows a 3D binding mode of benzamidine in the secondary binding pocket of trypsin, illustrating how residues Asp189, Ser190, and Gly216 bind to ligands (based off PDB code 1S0R).

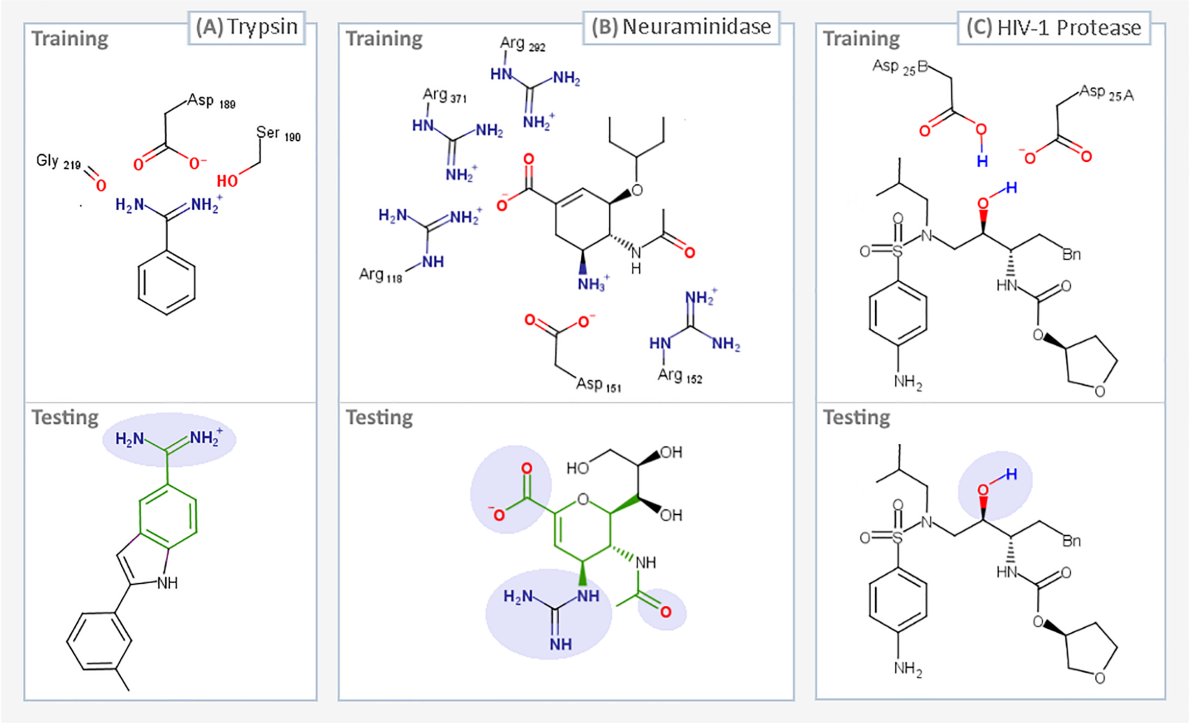

Figure 3.2: **Summary of iMD-VR docking tasks**. The ligands that were interactively unbound and rebound in a series of user tests, two for each of the three systems: Trypsin (A), Neuraminidase (B), and HIV-1 Protease (C). For each protein system, we devised two docking tasks, a training phase (where a trace representation of the ligand in the bound pose was present to guide users as shown in supplementary videos A–C in S1 File [143–147]), and a testing phase, where no trace atoms were shown. For the testing tasks, parts of the ligand which interact with key residues have been highlighted in lilac. For proteins A and B, where the testing task ligand differs from training, the shared scaffold between the two ligands is highlighted in green.

Fig. 3.2A shows the 2D binding mode of two ligands, benzamidine and indole-amidine, into trypsin. Supplementary video A.1 in S1 File [143, 144] shows an example of an expert iMD-VR user unbinding and rebinding benzamidine from trypsin in iMD-VR.

3.2.1.2 Neuraminidase

H7N9 neuraminidase is a glycoside enzyme found on the surface of influenza virions that catalyzes the hydrolysis of sialic acid residues, a process integral to influenza virus mutation. [156, 157] This strain was found in the influenza virus responsible for the 2013 bird flu pandemic. [158] The process of influenza virus replication begins with the virus attaching itself to the cell via the binding of hemagglutinin (a viral cell surface protein) to sialic acid, found on the end of glycoproteins attached to the cell membrane. Once anchored, the virus can enter the cell and hijack its machinery in order to replicate itself. After new viruses have been manufactured, neuraminidase proteins cleave sialic acid groups from cellular glycoproteins, breaking the anchor between the virus and the host cell, freeing the new viruses to infect other cells. In recent years,

there has been extensive research on the discovery of inhibitors that mimic sialic acid, thereby preventing the cleavage of sialic acid residues by neuraminidase and obstructing the release of new viruses. [159, 160] Oseltamivir (Tamiflu) is a transition state analogue of sialic acid and licensed therapy for influenza that binds to a triad of arginine residues in the neuraminidase active site (Arg118, Arg292, and Arg371) via its carboxylate group. [161] In addition to this, a crucial loop opening and closing mechanism, known as the 150-loop motion, is involved in the unbinding and rebinding of oseltamivir (Fig. 3.1B). [162, 163] From an iMD-VR perspective, the binding of oseltamivir to neuraminidase represents a more complex task than the trypsin-benzamidine system for two reasons: (1) Given that 150-loop movement is imperative to binding, this backbone motion needs to be carried out by the iMD-VR user; (2) with eight rotatable bonds, oseltamivir has considerably more conformational flexibility than benzamidine, making it more of a challenge to re-establish the correct bound configuration.

Fig. 3.1B shows a 3D binding mode of oseltamivir in the active site of neuraminidase, illustrating how the 150-loop and arginine trio binds to ligands (based off a mutated neuraminidase structure derived from PDB code 2QWK; details for how this was done can be found in ref [158]). Fig. 3.2B shows the 2D binding mode of two ligands, oseltamivir and zanamivir, into neuraminidase. Supplementary video B in S1 File [143, 146] shows an example of an expert iMD-VR user unbinding and rebinding oseltamivir from neuraminidase in Narupa.

3.2.1.3 HIV-1 Protease

HIV-1 protease is a viral aspartyl protease essential to the life cycle of HIV, responsible for cleaving precursor polypeptides into functional proteins, making it an attractive drug target for preventing HIV maturation. Structurally, HIV-1 protease is a homodimer that shares a single active site between two protein subunits, each of which contributes a catalytic aspartic acid. Mechanisms for HIV-1 protease cleavage of precursor proteins have been proposed [164]; however, it is broadly understood that the two aspartic acid residues each act as an acid or base respectively, activating a water molecule that then goes on to break peptide carbonyl bonds via nucleophilic attack. Sulfonamides are a class of drug licensed for the treatment of HIV that hydrogen bond to the catalytic aspartic residues and thus block protease activity [165], an example of which is amprenavir. Functionally, the two aspartic acids are thought to primarily exist in a monoprotonated state, especially when in the presence of an inhibitor [166], although it has been debated which tautomer favours amprenavir binding. [167–171] The HIV-1 protease active site is gated by two beta-hairpin flaps that shift through a series of different conformational states before ligand binding. [172] Therefore, this task requires iMD-VR users to move these flaps into an open position to guide amprenavir out, and then carefully place the loops back without disrupting their secondary structure. From an iMD-VR perspective, the motion of these flaps, combined with the higher rotational flexibility of amprenavir, makes this a particularly challenging binding task. Fig. 3.1C shows a 3D binding mode of amprenavir in the active site

of HIV-1 protease, illustrating how Asp25A and Asp25B bind amprenavir (based off PDB code 1HPV). The active site flaps are coloured in purple. Fig. 3.2C shows the 2D binding mode of amprenavir into HIV-1 protease. Supplementary video C in S1 File [143, 147] shows an example of an expert iMD-VR user unbinding and rebinding amprenavir from HIV-1 protease in Narupa.

3.2.2 Overview of binding and rebinding tasks

Using these candidate protein-ligand systems, we carried out iMD-VR tests. Users were split into expert and novice cohorts. Expert users had extensive experience using iMD-VR to interact with molecules and had some degree of familiarity with the protein-ligand systems described in this paper. The experts first tested the viability of using iMD-VR to generate ligand unbinding and rebinding pathways. Expert iMD-VR studies were carried out to establish whether the original crystallographic structure could be re-established for each task. Then, a cohort of novice users were asked to carry out a series of unbinding and rebinding tasks, in order to control for the experts' familiarity with iMD-VR tools and the selected systems. Novice users had little experience using iMD-VR but did have a scientific background in biomolecular simulations.

3.2.2.1 Expert user tests

Expert iMD-VR users were tasked with unbinding and rebinding three ligands from the binding pockets of three proteins: trypsin, neuraminidase, and HIV-1 protease, detailed in Section 3.2.1. Fig. 3.1 shows a 3D representation of each of the three experimentally derived poses that expert users were asked to recreate. In these tasks, experts were initially given a faint trace of the ligand atoms in the correct pose, providing a visual indication of where the ligand sits in the crystallographic binding pose. Experts could freely switch between interacting with either a single atom at a time or a group of atoms together (e.g., moving one atom of the ligand or the center of mass of the entire ligand at once). Experts could also add or remove positional restraints to atoms, such as when manipulating the active site flaps during the HIV-1 protease task. Supplementary videos A-C in the S1 File [143–147] show experts unbinding and rebinding small molecules from trypsin, neuraminidase and HIV-1 protease, and also show the guide trace for the position of the ligand atoms. [84]

3.2.2.2 Novice user tests

Once the iMD-VR unbinding and rebinding pathways in Narupa had been established by the expert users, novice users were recruited to complete unbinding and rebinding tasks with each of the three protein systems. Novice users interacted with each system until they felt they had correctly established a binding pose, spending approximately five minutes on each task. The protein-ligand systems were given in order of increasingly complexity. Fig. 3.2 gives a summary of tasks novice participants were asked to complete. We recruited a total of ten novice participants

in two cohorts of five ('cohort one' and 'cohort two'). Cohort one completed tasks described in Sections 3.2.3.1–3.2.3.4. Cohort two completed tasks described in Sections 3.2.3.1–3.2.3.4 and 3.2.3.6. More detailed demographic and task information can be found in the S1 File. [143]

To ensure there was a comparable level of proficiency with the Narupa iMD-VR interface prior to attempting protein-ligand binding, novice participants were first placed in a simulation of C_{60} molecules and given an opportunity to familiarize themselves with the controls and the interaction, as was done in previous studies. [20] Additionally, before interacting with each of the three protein systems described in Section 3.2.1, we took advantage of the multiplayer feature of Narupa: novice users were placed in the same iMD-VR simulation as the expert user (as shown in the Fig. 3.1 schematic), where they could see a fully 3D representation of the bound poses shown in Fig. 3.1. To ensure the novices had a comparable level of knowledge of each system, while co-habiting the simulation space, the iMD-VR expert gave a brief background on the system and highlighted the interactions shown in Fig. 3.1.

Once the system had been introduced, participants were asked to complete a 'training' ligand unbinding-rebinding task. During the training phase, novices had a trace of the ligand atoms in the bound pose to help guide them. Next, participants were given a 'testing' ligand unbinding and rebinding task. A summary of the training and testing tasks for each of the three protein systems is shown in Fig. 3.2. In these experiments, no trace atoms of the ligand were present, meaning that participants had to rely more on their chemical insight to find the correct binding pose. To control for learning effects during the testing phase of trypsin and neuraminidase binding, novices were asked to bind different ligands from those used during training. The alternative ligands were chosen on the basis of key interactions remaining between the ligand and protein in the training portion of the study (highlighted in lilac in Fig. 3.2A and 3.2B) and sharing structural similarities (highlighted in green in Fig. 3.2A and 3.2B). Due to a lack of availability of an appropriate alternative ligand to amprenavir, and because of the heightened complexity of the task owing to the number of rotatable bonds amprenavir contains, amprenavir was used for both the training and testing phases of the HIV-1 protease system. Novice users also had a more limited user interface, where they only had the option of interacting with a single atom at a time and could not apply or remove positional restraints.

3.2.3 iMD-VR simulation set up

The Narupa selection utility, shown in supplementary videos A–C in S1 File [143–147], allows users to select and apply visualization and interaction settings to a subset of atoms in a system. For all systems, the following selections were created: (a) protein backbone atoms, (b) key active site residues, (c) ligand atoms. Each system had some specific features, detailed below. Further simulation-specific details can be found in the S1 File. [143]

3.2.3.1 Trypsin and benzamidine (expert task and novice training task)

This task (Fig. 3.2A, 'Training') was completed by both experts and novices. Given the relatively simple binding mode between benzamidine and trypsin, where the protein does not need to be manipulated by the user, the entire protein backbone was held in place with a positional restraint (details can be found in the S1 File). [143] To enable the user to visually identify the location of the active site in the protein, residues Asp189 and Ser190 were fully rendered and the backbone oxygen of Gly219 was shown, similar to the representation shown in Fig. 3.1A. Additionally, supplementary video A.1 in the S1 File [143, 144] shows the rendering scheme used for trypsin and benzamidine. For the remaining residues, only the protein backbone was rendered. A trace of benzamidine in the crystallographic pose was used as a visual indication of where the ligand binds, encouraging the user to re-establish the original bound pose as closely as possible.

3.2.3.2 Trypsin and indole-amidine (novice testing task)

Following the training phase, novices were asked to bind indole-amidine into trypsin (Fig. 3.2A 'Testing'). Indole-amidine was selected as an alternate ligand for novices to bind as it contains the benzamidine moiety and adopts the same binding mode to Asp189, Ser190 and Gly219. However, unlike benzamidine, indole-amidine has a non-symmetrical extended scaffold that needs to be correctly orientated. This testing task used the same protein restraints and rendering scheme as the training task with trypsin and benzamidine. However, no trace atoms were shown.

3.2.3.3 Neuraminidase and oseltamivir (expert and novice training task)

This task was completed by both experts and novices. Binding oseltamivir requires a small amount of manipulation of the protein, as the positions of the 150-loop residues over the ligand need to be carefully maintained. However, as no significant shift in the tertiary structure of neuraminidase is required, all backbone atoms were held with a positional restraint (details can be found in the S1 File). [143] To aid in ensuring the 150-loop was correctly placed, two strategies were adopted. First, residues Asp151 and Arg152 of the 150-loop were fully rendered so the user could see their position. Second, a trace representation of the position of the 150-loop residues in the closed position was rendered so the user could see where they should be placed. Additionally, to show if a hydrogen bond between the carboxylic acid of oseltamivir and the arginine trio of the neuraminidase binding pocket had been established, Arg118, Arg292, and Arg371 were also fully rendered. For the remaining residues, only the backbone atoms were shown. A trace of the oseltamivir atoms in the correct position was used as a visual indication of where the ligand binds, ensuring that the original binding pose could be closely replicated. Supplementary video B in S1 File [143, 146] shows the rendering scheme used in Narupa for neuraminidase and oseltamivir.

3.2.3.4 Neuraminidase and zanamivir (novice testing task)

Following the training phase, novice users were asked to bind zanamivir to neuraminidase. Zanamavir was selected as the second binding task as it is a chemical analogue to oseltamivir, sharing the same ring scaffold, carboxylic acid group, and hydrogen-bonding contacts to the 150-loop. However, zanamivir does exhibit some structural differences from oseltamivir; therefore, this task requires the user to recognize the similarity in binding modes between the two drugs. As discussed below, we used this particular task to examine the results obtained if we removed backbone restraints entirely. The same protein rendering scheme as neuraminidase and oseltamivir was used, however, no trace atoms were present.

3.2.3.5 HIV-1 protease and amprenavir (expert task)

Binding small molecules to HIV-1 protease requires a significant shift in the backbone atom positions, altering the structure from closed to open. During the simulation, the user could toggle a positional restraint force on the active site flaps, allowing them to be held in place once an open or closed conformation had been established. An additional strategy to aid in the opening and closing of HIV-1 protease was to render trace atoms of the protein backbone in the position of the active site flaps in both the closed position and the open position, giving the expert user a visual indication of the range of motion the loop has between the two states, as well as allowing the user to closely re-establish the original closed conformation once amprenavir had been redocked; details on how this was done can be found in the S1 File. [143] Aside from the active site beta-hairpin flaps, which were manipulated by the expert user during the simulation, the protein backbone atoms were held by backbone restraints. Details on the positional restraints can be found in the S1 File. [143] Key contact residues Asp25A and Asp25B were fully rendered; the remaining amino acids only had their backbone atoms shown. A trace atom representation of amprenavir was used as a visual indication of where the ligand binds, ensuring the original bound conformation could be re-established.

3.2.3.6 HIV-1 protease and amprenavir (novice testing and training tasks; cohort two only)

Novice users from cohort two, totalling five participants, were asked to unbind and rebind amprenavir twice, once with the aid of trace atoms and once without. All other backbone atoms in the protein were positionally restrained. To streamline the task, novices were not required to open and close the HIV-1 protease flaps prior to and after binding amprenavir, instead starting from an HIV-1 protease conformation that had been pre-opened by an expert using iMD-VR and held with a positional restraint. Details of this can be found in the S1 File. [143] Both the testing and training binding tasks used the same rendering scheme as the expert user tests – the only difference between the two tasks was the presence of trace atoms.

3.2.3.7 Backbone restraints

During iMD-VR, users can apply force to any atom in the system–including those integral to the protein tertiary or quaternary structure. In order to ensure that the protein tertiary structure required for binding was not distorted, a positional restraint was applied to the backbone atoms in the proteins. To evaluate the impact of these restraints, we removed the backbone restraints for cohort two during the neuraminidase and zanamivir testing phase. A comparison of task completion between cohort one and cohort two for undocking and redocking zanamivir from neuraminidase can be found in Fig. S3 in S1 File. [143] These results, discussed in further detail in the S1 File, show that careful iMD-VR users (expert and novice alike) were able to carry out binding and unbinding tasks without positional restraints. For analysis of iMD-VR trajectories, we observed that Principal Component Analysis (PCA) carried out on iMD-VR trajectories which utilized positional restraints produced better results for the binding/unbinding pathways of interest, owing to diminished noise from the backbone fluctuations.

3.2.4 Analysis of iMD-VR results

For both the expert and novice interactive unbinding and rebinding tasks, trajectories of the protein-ligand system were recorded, taking a snapshot of the system every 0.25 ps. iMD-VR trajectories were analysed using an RMSD calculation protocol (described in the S1 File). [143] The RMSD was used to: (1) analyse the expert trajectories to see how the system is changed from a bound to unbound and back to bound state; (2) analyse novice trajectories to identify how close a user got to recreating the starting pose; and (3) analyse whether the recovered binding poses were stable. Specifically, we selected an iMD-VR frame with an RMSD close to the starting coordinates and used it to initialize a longer timescale (200 nanoseconds) MD trajectory. Further details can be found in the S1 File. [143]

To qualitatively assess the reproducibility of the binding pathways users explored using iMD-VR, we utilized a PCA tool called PathReducer, [130] which takes as input an .xyz file containing a series of molecular structures (in this case, an iMD-VR-generated trajectory) and outputs the set of principle coordinates which captures the most structural variance in the fewest coordinates. In effect, PathReducer collapses a 3N-dimensional (where N = number of atoms) trajectory into a visualisable path which spans two or three dimensions. Further details of this can be found in the S1 File. [143]

3.3 Results and Discussion

3.3.1 Expert unbinding and rebinding tasks

3.3.1.1 Trypsin

Fig. 3.3A shows the RMSD of the expert user-generated trajectory of benzamidine unbinding and rebinding to trypsin, alongside the top two and top three Principal Components (PC) along the trajectory path. The RMSD plot of benzamidine shows that the original binding pose was recovered by the expert user, as the RMSD between the ligand at the end of the trajectory and the beginning is very low. The PCA results for this system showed that the direction of PC1 (the PC that captures the most structural variance along the trajectory) corresponds predominantly to motion of the ligand away from the protein. The value of PC1 at the end of the trajectory is very similar to that at the beginning, which is more evidence that this user was able to replicate the original bound pose of the drug. PC2 and PC3 correspond to fluctuations of the backbone and side chains not in the active site of the protein, hence the trajectory not returning precisely to its initial value of these PCs. Supplementary animation A in S1 File [143, 173] shows the trajectory generated by an expert user (31 picoseconds of simulation in total). Fig. 3.4A shows the RMSD of an expert-generated rebound trypsin-benzamidine complex over 200 nanoseconds of production MD, after solvation, minimization and equilibration as described in the S1 File [143], establishing that the iMD-VR produces stable poses for this system.

Expert study subjects were able to unbind benzamidine in under 5 picoseconds and obtain the rebound pose within another 5 picoseconds (Fig. 3.3A). Using our computing architecture, as described in the S1 File [143], we were able to achieve MD simulation rates of 4.45 picoseconds per minute of real time, meaning that benzamidine could be unbound and rebound on the scale of minutes. As such, this demonstrates the efficiency with simulations can be interactively pushed between two distinct states. Trypsin-benzamidine binding events have previously been observed to take nanoseconds of simulation time [153], and theoretical calculations of trypsin-benzamidine unbinding rate constants, k_{off}, predict millisecond dissociation times [60, 154]. To unbind or rebind benzamidine, the user does not need to make any major conformational changes to the binding site of trypsin, so completing this task was a matter of applying sufficient force to break the relatively weak electrostatic contacts between benzamidine and Asp189 and continuing to apply this force until the ligand had fully dissociated from the protein (supplementary video A.1 in S1 File). [143, 144] On rebinding, the user had to take care to keep the orientation of benzamidine such that the charged amidine group is pointing towards the bottom of the pocket. If the user attempted to bind benzamidine with the benzyl group directed towards the positively-charged Asp189 residue the ligand would be repelled out of the binding pocket, demonstrating the real-time responsiveness of iMD-VR to energetically unfavourable input, as shown in Supplementary video A.2 in S1 File. [143, 145] The video shows how, after being guided out of the binding pocket and replaced in an incorrect orientation, the N1 and N2 of benzamidine fail to form electrostatic

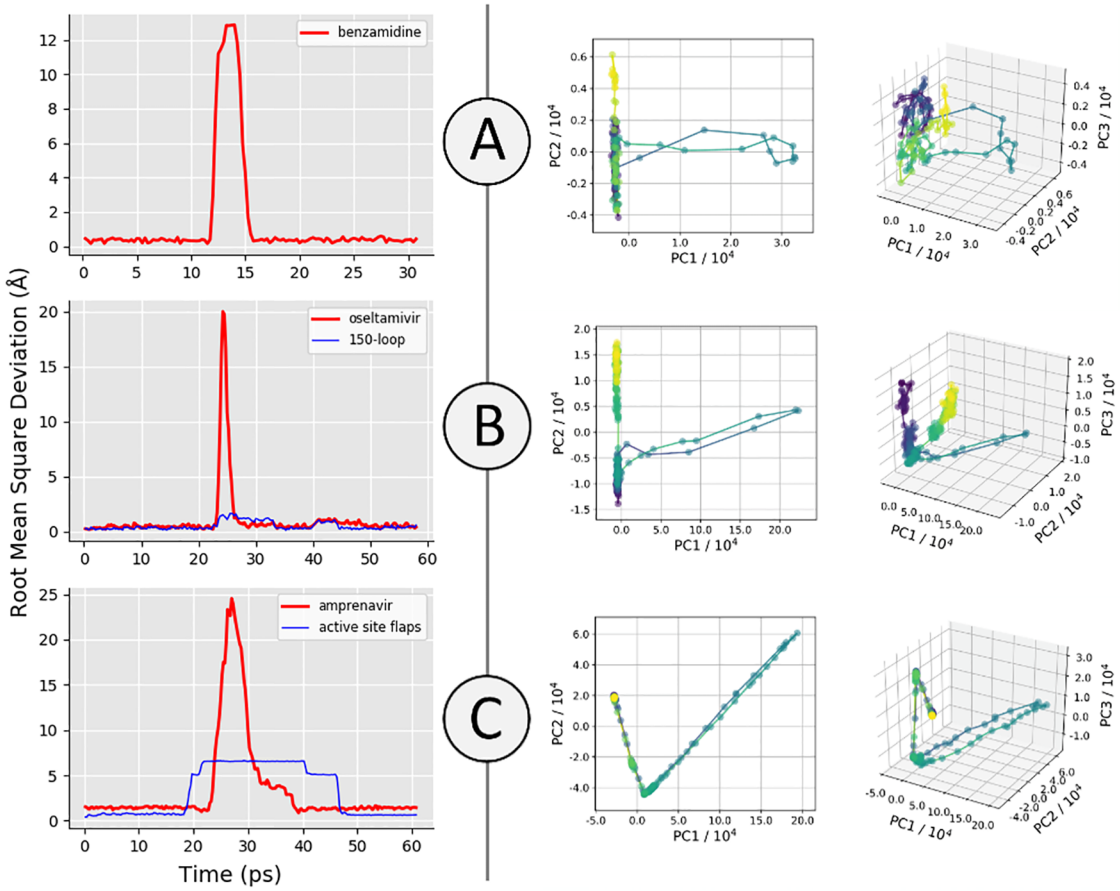

Figure 3.3: **Recovering binding poses of three protein-ligand systems using iMD-VR**. Left: Ligand RMSD of iMD-VR generated trajectories by experts (compared to starting coordinates): (A) trypsin and benzamidine, (B) neuraminidase and oseltamivir, and (C) HIV-1 protease and amprenavir. For neuraminidase, the RMSD of the 150-loop residues is shown in blue. For HIV-1 protease, the RMSD of the active site flaps backbone atoms is shown in blue. Right: The top two (left plots) and top three (right plots) PCs (PC1-3) for representative trajectories of the three protein-ligand systems. Time is represented for each trajectory by the colour of the plot, starting at purple for the beginning of the trajectory and yellow for the end, passing through blue and green in between.

contacts to Asp189, and is subsequently repelled out of the binding pocket, moving towards the HE1 of His57 in Trypsin, where it remains in a transiently stable pose over at least 200 ps, as shown in Fig. S2-A1 in S1 File. [143] Supplementary video A.2 in S1 File [143, 145] shows the expert utilizing the 3D interface of Narupa to identify those amino acids with which the amidine group interacts with. This alternate binding mode, in which benzamidine favours the catalytic triad and polar residues surrounding the binding pocket is similar to previous observations by Buch et al. [153] Fig. S2-A2 in S1 File [143] shows how it was possible for the expert user to apply continuous force to the benzamidine when rebinding, guiding it past the cluster of hydrophilic groups and into the protein core and moving it out of the protein via an alternate opening. Whilst the kinetic barriers for these pathways are likely to be very large they nevertheless show the ability of iMD-VR to quickly enable exploration of new dynamical pathways.

3.3.1.2 Neuraminidase

Fig. 3.3B shows the RMSD of the expert-generated trajectory, alongside PathReducer-generated PC plots, establishing that the original binding pose was recovered by the expert user. Similar to the trypsin system, PC1 is dominated by distances between atoms in the ligand and atoms in the protein, and so the variation along PC1 that can be seen along the trajectory path can be directly attributed to the removal of oseltamivir from the active site. PC2 and PC3 are again predominantly defined by distances between atoms in residues of the protein far from the active site, and thus fluctuations of the associated side chains lead to an offset in the pathway start and endpoints. Supplementary animation B in S1 File [143, 174] shows the trajectory generated by an expert user (58 picoseconds of simulation time in total). Fig. 3.4B shows the RMSD of an expert-generated rebound oseltamivir-neuraminidase complex over 200 nanoseconds of production MD, after solvation, minimization and equilibration as described in the S1 File [143], establishing that the iMD-VR can produce stable poses for this system.

Using our computing architecture, as described in the S1 File [143], we were able to achieve MD simulation rates of 4.51 picoseconds per minute of simulation time, meaning that oseltamivir could be unbound and rebound on the scale of minutes of real time. Unbinding oseltamivir requires applying enough force to break any charged contacts or hydrogen bonds formed between the triad of positively charged arginine residues in the active site and the negatively charged carboxylate group of oseltamivir. Upon unbinding, the interactions from the amine group and carbonyl group of the drug and the two residues which comprise the 150-loop (Asp151 and Arg152 – see Fig. 3.1B) were also broken, causing the loop residues to dynamically open as the drug leaves the active site as shown in supplementary video B in S1 File. [143, 146] The backbone of the 150-loop did not dynamically open when the drug exited the active site as the backbone was held in place with restraints. When removing oseltamivir from the binding site, the molecule would occasionally flip itself over, losing the bound orientation. As such, when attempting to re-establish the correct binding pose, the user needed to be extremely careful to ensure that

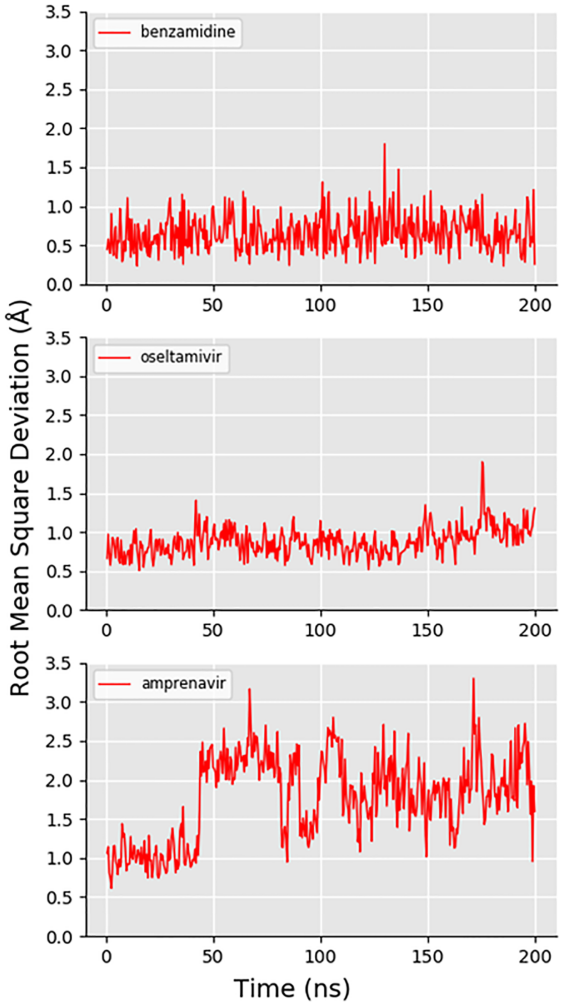

Figure 3.4: **Ligand RMSDs over 200 nanoseconds of molecular dynamics**. Showing the RMSD of each of the three ligands (compared to the initial solvated, minimized and equilibrated bound coordinates) during 200 nanoseconds of molecular dynamics simulation. From top to bottom: (A) benzamidine (in trypsin), (B) oseltamivir (in neuraminidase), and (C) amprenavir (in HIV-1 protease).

binding interactions between the drug and the 150-loop residues were successfully recreated, allowing the drug to flip itself back into the correct pose; if the user was too forceful, the drug would enter the active site in the incorrect orientation. A representation of oseltamivir 'flipping' as it is being removed from the neuraminidase binding pocket can be found in Fig. S2-B1 the S1 File. [143] We observed that when oseltamivir is back into the correct bound conformation, the two 150-loop residues will also move back into the original configuration without any input from the user, demonstrating how iMD-VR can dynamically reform energetically-favourable contacts.

3.3.1.3 HIV-1 Protease

Fig. 3.3C shows the RMSD of the expert-generated trajectory, alongside generated PC plots, establishing that the original binding pose was recovered by the expert-user. The PCA results in this case are unique, as the user had to move two flaps capping the active site prior to removal of the bound amprenavir (discussed in more detail below, see Fig. 3.5). Each approximately linear segment of the PC plots corresponds to a conformational change event: First, one flap is moved away from the active site. Then the second flap is moved away from the active site. Finally, the ligand is removed from the active site. This process is then reversed to rebind the ligand. The plots show strikingly similar pathways for unbinding and rebinding, likely as the principal coordinates are each capturing a significant movement of the protein backbone and thus ignoring smaller residue fluctuations; comparatively, PC2 and PC3 in the trypsin and neuraminidase systems do not have the same starting and end points as they are 'picking up' protein fluctuations along the trajectory. Intuitively, PC1 is dominated by changes in distances corresponding to movement of the ligand out of the protein, PC2 corresponds predominantly to distances between the first 'flap' and other parts of the protein, and PC3 corresponds predominantly to distances between the second 'flap' and other parts of the protein. Supplementary animation C in S1 File [143, 175] shows the trajectory generated by an expert user (61 picoseconds simulation time in total). Fig. 3.4A shows the RMSD of an expert-generated rebound HIV-1 protease-amprenavir complex over 200 nanoseconds of production MD, after solvation, minimization and equilibration as described in the S1 File. [143] Some fluctuations to the RMSD value are observable. Inspection of the 200 nanosecond trajectory shows that the hydroxyl group 'flips' its orientation relative to the two catalytic aspartic acid residues, resulting in amprenavir adopting a slightly different binding pose throughout the simulation, albeit still remaining in the binding pocket of HIV-1 protease. Fig. 3.5 shows a step-by-step breakdown of the process of unbinding and rebinding amprenavir from HIV-1 protease, establishing that the iMD-VR can produce stable poses for this system. In the apo form, the active site flaps of HIV-1 protease are thought to dynamically switch between various open and closed conformations. [172] Upon binding, the once-open flaps have a stabilizing effect by closing over the ligand. [176, 177] Experimental estimates of k_{off} for amprenavir binding to wild-type HIV-1 protease correspond to an average binding residence time on the scale of seconds [178, 179], making it a difficult transition to simulate without some form of biasing. Using our computing architecture, as described in the S1 File [143], we were able to achieve MD simulation rates of 4.45 picoseconds per minute of simulation time, meaning that amprenavir could be unbound and rebound–including opening and closing the active site flaps—on the scale of minutes of real time.

Additionally, the Narupa selection language enabled the expert user to remove positional backbone restraints and move the flaps into an open position, before replacing the restraints and extracting amprenavir away from the binding pocket. To rebind amprenavir, the hydrogen bonding to Asp25A and Asp25B was reformed and, once the stable binding configuration had

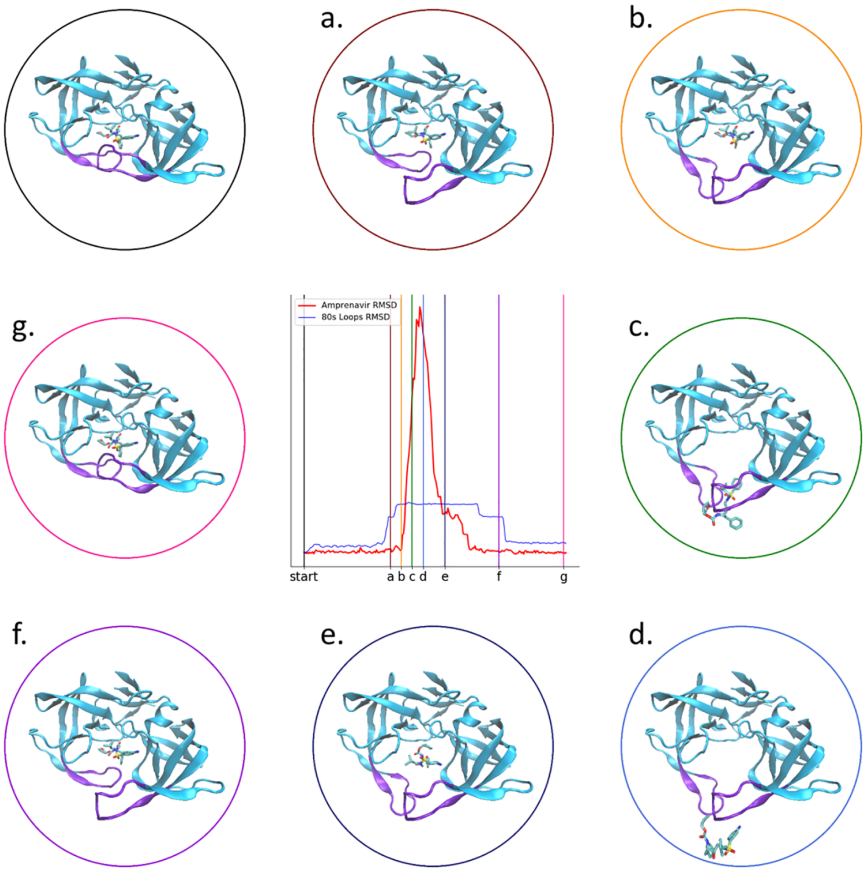

Figure 3.5: **Snapshots along the interactive unbinding and rebinding of amprenavir into HIV-1 protease**. The image in the upper left shows the bound "start" pose. (a)–(c) shown snapshots as the user unbinds amprenavir; (d) shows the unbound pose; and (e)–(g) shows snapshots as the user rebinds amprenavir. The corresponding RMSD time traces are shown in the middle plot, identical to that shown in Fig. 3.3c.

been found, the user moved the beta-hairpin flaps back into the closed conformation, again replacing the restraints. We note that we initially performed this task with a tautomer of HIV-1 protease where neither Asp25 residues were protonated; in this state, amprenavir seemed to favour a slightly different binding pose as its hydroxyl group no longer acts as a hydrogen bond acceptor. To further investigate the difference in binding mode between the two tautomers of HIV-1 protease, both were placed in Narupa with all positional backbone restraints removed. The expert user observed both binding poses without interacting with the system over 125 picoseconds of simulation time. In the monoprotonated HIV-1 protease system, the hydroxyl group of amprenavir rigidly points towards the deprotonated aspartic acid residue. Conversely, when both catalytic residues are deprotonated, the hydroxyl group frequently flips between pointing at either aspartic acid, causing amprenavir to 'sag' in the active site (see Fig. S2-C1 in S1 File). [143] The positively charged hydrogen on the protonated aspartic acid appears to have a stabilising effect on the orientation of the hydroxyl group, whereas removing the hydrogen causes

the hydroxyl group to more easily flip as one orientation is no longer electrostatically 'penalized' by the protonated residue. Nonetheless, it is worth highlighting that Narupa enables qualitative observation of such binding dynamics in real time, demonstrating that iMD-VR enables both manipulation of molecular dynamics and easy comprehension of distinct dynamical behaviour in systems that have only small structural differences.

3.3.2 Novice unbinding and rebinding tasks

Fig. 3.6 shows the minimum achieved RMSD of each small ligand novices tried to dock in both 'training' and 'testing' phases. For fully flexible simulations like these, which explore a range of conformational space as a result of thermal fluctuations, there is an open question how to assess whether a particular simulation has successfully recovered the binding pose seen in the crystal structure. For example, in a recent review by Pagadala et al. [180] which evaluated several different docking software programs, they used a cutoff of 2 Å to determine whether or not a fully flexible docking program managed to find the 'correct' pose. This strategy makes sense for cases where the proteins unbiased fluctuations span a range less than 2 Å. The solid boxes in the left hand panel of Fig. 3.6 show the RMSD range (mean $\pm 2\sigma$) spanned by a non-interactive Narupa simulation run for 50 picoseconds initialized in the bound pose at 298 K. Fig. 3.6 shows that the $\pm 2\sigma$ range is less than 2 Å for all but the trypsin + indole-aminidine testing system. During user 'training' phases, the results from Fig. 3.6 show that all of the user generated poses are either within $\pm 2\ \sigma$ of the mean RMSD, or else have an RMSD which is within 2 Å of the crystal structure. During user 'testing' phases, where the binding guide was switched off and the ligand identity was different for trypsin and neuraminidase, the results show more scatter, exactly as we would expect. Nevertheless the results are encouraging. For trypsin, all of the novice-generated testing poses lie within $\pm 2\sigma$ of the mean RMSD. For neuraminidase and HIV-1 protease, which are considerably more complicated tasks, the results are similarly encouraging: 4/5 of the neuraminidase testing poses are within 2.08 Å RMSD of the crystal structure; and 3/5 of the HIV-1 protease testing poses are within 2.15 Å RMSD of the crystal structure. Below we discuss the results for each system in further detail.

3.3.2.1 Trypsin

Directly comparing the trypsin training and testing tasks for the same participant shows that task accomplishment was better for all participants (ranging between 1.0Å and 1.9Å lower) during the training task. Benzamidine, used during the training task, is a small ligand and users had the benefit of trace atoms (Fig. 3.6A), explaining the good performance on the task. During the testing task, Fig. 3.6A shows that participants were all able to recreate the amidine contact to Asp189, correctly aligning the indole-amidine benzamidine moiety. The variation in RMSD can be attributed to the rest of the molecule, where users had no prior guidance; variation in the extended scaffold between users can be seen in Fig. 3.2A. Therefore, task accomplishment for

binding indole-amidine into trypsin could likely be improved by providing additional feedback to indicate poses that are energetically favourable.

3.3.2.2 Neuraminidase

Fig. 3.6B shows the minimum achieved RMSD for the neuraminidase training and testing tasks. All participants were able to recreate the original bound pose of oseltamivir in neuraminidase, getting within 1 Å RMSD of the starting coordinates. The training results gave better minimum ligand RMSDs compared to the testing task, which were between 0.3 Å and 3.2 Å higher when the results between the training and testing task are compared for the same participant (Fig. 3.6B). For the testing task, four out of five participants were able to place zanamivir in the correct orientation, indicating that users recognized the shared scaffold between oseltamivir and zanamavir (highlighted in green in Fig. 3.2B). In particular, there was very good alignment of polar moieties (e.g. the carboxylate group, the ring ether) between participants (Fig. 3.6B). However, variation arose from the flexible nature of zanamivir (whereas oseltamivir was very consistently aligned throughout the molecule when participants completed the task with the aid of trace atoms). This would suggest that an interface for completing drug binding tasks using iMD-VR could benefit from being able to give ligand-centric feedback, indicating whether functional groups are in an optimal geometry.

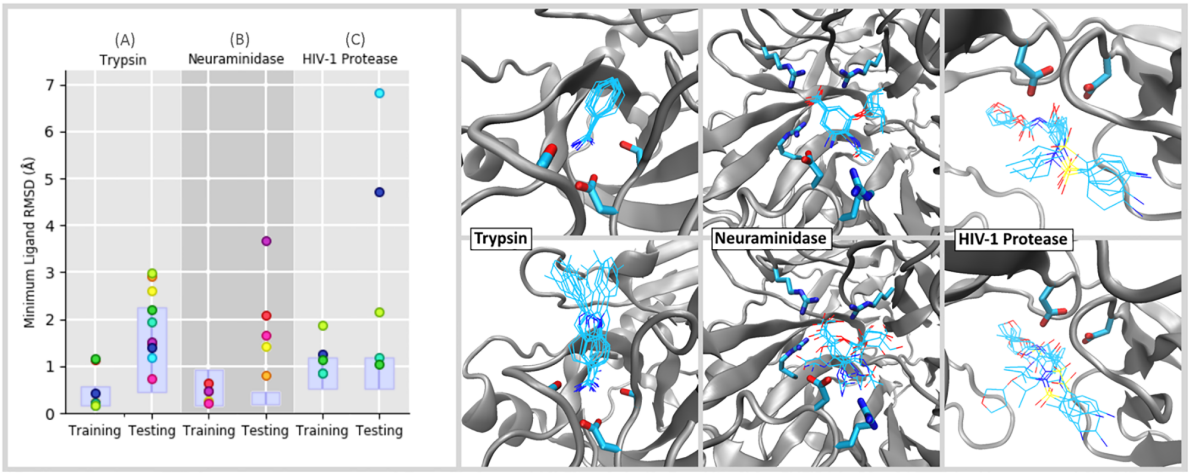

Figure 3.6: **Minimum RMSD values for novice tasks**. (Left) Showing the minimum achieved RMSD of each small ligand novices tried to dock, where each participant is assigned a unique colour. Two ligands were docked for each system, in both 'training' and 'testing' phases; each ligand is denoted in Fig. 3.2. To determine the extent to which user-identified poses aligned with the native RMSD, a non-interactive Narupa simulation was run for 50 picoseconds in the bound pose and the average RMSD (plus or minus two standard deviations) was calculated, shown as the purple box. (Right) The pose corresponding to the minimum RMSD value shown is on the left for each participant, overlaid on top of one another. Testing tasks for the three are shown in the top row, training tasks are shown on the bottom.

3.3.2.3 HIV-1 Protease

Fig. 3.6C shows the minimum achieved RMSD for the HIV-1 protease training and testing tasks. Likely owing to the increased size of amprenavir and the number of rotatable bonds it has, both the training and test tasks for HIV-1 protease had a higher degree of variation in minimum RMSD achieved when directly comparing results between the two tasks for the same participant. Interestingly however, when rebinding amprenavir a second time without trace atoms to guide them (testing task), three participants were able to get an RMSD close to the training task, one of which was lower by 0.08Å. This may be a result of users remembering the correct binding pose but it is nonetheless encouraging that iMD-VR can be used to recreate poses of larger, torsionally complex molecules with limited iMD-VR training. In particular, recreation of the contact between the amprenavir hydroxyl group and Asp25B was generally good between both tasks (Fig. S4-C in S1 File). [143] For the training task, Baker-Hubbard hydrogen bond analysis [181] on the minimum RMSD pose confirms this as all participants were able to establish this contact. In the testing task, 4/5 participants were able to orientate the hydroxyl group and subsequently form a hydrogen bond to the catalytic Asp25A/Asp25B catalytic residues. However, the HIV-1 protease 'testing' task still had the highest variation in minimum RMSD, as some participants had a poorer performance without having a trace of the correct binding pose in the active site (the highest difference in RMSD between training and testing tasks was 5.9Å). In the testing task, four participants were able to orientate the hydroxyl group and subsequently form a hydrogen bond to the catalytic Asp25A/Asp25B catalytic residues. However, when inspecting the two outliers, the overall scaffold of amprenavir is incorrectly orientated–regardless of whether the user had established the hydrogen bonding contact to Asp25A and Asp25B.

3.4 Conclusions and Future Directions

In this paper, we have outlined an experimental protocol for setting up an iMD-VR simulation for the purposes of interactively manipulating protein-ligand systems to recover experimentally derived bound poses using iMD-VR. Utilizing this protocol, we have carried out studies exploring iMD-VR as a strategy for interactively sampling the unbinding and rebinding of ligands from proteins. The iMD-VR strategy enables this process to be accelerated compared to the much larger timescales required in unbiased MD simulations. To the best of our knowledge, this study represents the first time that iMD-VR has been extended to studies of complex protein-ligand binding and unbinding dynamics.

Our results show that expert iMD-VR users are able to manipulate protein-ligand systems to sample bound and unbound states. We also assessed the extent to which novice iMD-VR uses were able to sample binding and unbinding pathways using a training phase followed by a testing phase. Overall, the training phase showed slightly better task accomplishment; however, binding was still generally successful for many of the users during the testing phase, with the

majority of users able to get within 2.15 Å RMSD of the experimental crystal structure, which is a comparable level of accuracy to other fully flexible docking programs. [180] So as not to overwhelm participants with having to learn a new VR-rendering interface during training, we took the decision to simplify the protein representations as shown in Supplementary videos A–C in S1 File [143–147], showing a backbone representation along with a subset of those amino acids which are known to have key interactions with the ligands, and which make a large contribution to the overall binding free energy. Encouragingly, even though only a limited set of binding interactions were shown, participants were still able to accurately rebind the ligands studied herein, including amprenavir, whose size and flexibility makes the binding task particularly complicated. This raises an interesting question: Is it the quantity of rendered interactions (i.e., showing all possible interactions) or the quality of rendered interactions (i.e., showing a few of the most important interactions) which enable better results to be obtained during interactive docking tasks? At this stage, because we have not carried out the appropriate control experiment, our results do not conclusively show that focusing on a few key interactions enables better results, but this is an interesting avenue of future research which we intend to explore in future work. Nonetheless, these results are especially encouraging given that our cohort of novice users had a very limited time (less than 60 minutes) to be trained in both the interface and each of the three protein-ligand systems. The results suggest that the iMD-VR paradigm is sufficiently intuitive and affords adequate control to enable the sorts of detailed manipulations required to carry out VR-enabled atomistic docking in a fully flexible MD environment. Our 'expert' results show that iMD-VR users benefit from further training, given their familiarity with the interface and the specific protein systems.

Beyond the quantitative analysis described herein, these studies also show that iMD-VR can be used to reveal interesting qualitative features of protein-ligand unbinding, such as benzamidine not forming electrostatic contacts to Asp189 if it is incorrectly orientated and subsequently being repelled out of the trypsin binding pocket (Supplementary video A.2 in S1 File) [143, 145], or changes in the binding of amprenavir to tautomers of HIV-1 protease. In particular, the 3D interface aided in the identification of key interactions between the protein and the ligand, as well as allowing the user to directly observe dynamical behaviours in real time.

Our iMD-VR framework enables users to quickly apply restraints to arbitrary subsets of atoms, which can be turned on and off 'on-the-fly'. The flexible application of restraints enables the user to rapidly identify those regions where they would like to either explore or dampen conformational flexibility–e.g., in loop domains. As a training strategy, we have found that restraints enable less experienced iMD-VR users to familiarize themselves with a system without the risk of inadvertently damaging the tertiary structure. For expert iMD-VR users, restraints permit the sampling of sophisticated docking strategies that involve complex conformational changes, like that in HIV-1 protease. In future work, we intend to carry out more detailed studies on how to apply restraints so as to enable users to efficiently and accurately carry out binding

tasks.

We also intend to develop additional strategies to help iMD-VR users quickly formulate and test binding hypotheses. For example, checkpoints will enable users to return the system to previous states visited earlier in the simulation, along with additional audio and visual feedback to indicate to the user how structural manipulation influences the overall energy of the system, and allowing the user to pause the simulation and carry out energy minimizations 'on-the-fly'. For the purposes of streamlining these particular studies and not overwhelming novice users, we limited the studies described herein to a 'backbone and key residue' visualization scheme for the proteins. While such a representation aims to facilitate locating the active site and identifying key interactions, it makes it difficult to see unfavourable van der Waals interactions between the ligand and protein. In future work, we will examine the extent to which different rendering strategies influence task accomplishment. Such methods will help inform binding hypotheses in cases where the bound pose is unknown.

Unbiased simulation of protein ligand-binding typically occur on timescales of milliseconds or seconds [178, 179], and is therefore inaccessible to even the most sophisticated simulation architectures without recourse to a biasing or acceleration method. There is evidence that finding minimum energy pathways in hyperdimensional systems such as these is an "NP-hard" problem (for which no optimal method exists). [104] Having established herein that iMD-VR offers a reliable tool for experts and novices alike to generate accurate protein-ligand binding poses, we intend to carry out studies aimed at analysing the user-generated iMD-VR pathways. Specifically, we plan to analyse: (i) how closely user-generated iMD-VR pathways follow the system MFEP; and (ii) methods where iMD-VR pathways may be used to recover free energies for association and dissociation. For example, the configurations and pathways generated from iMD-VR (shown in Fig. 3.3) could serve as initial guesses for adaptive path-based free energy sampling algorithms like transition path sampling [62], umbrella sampling [63], path-based metadynamics [64], forward flux sampling [65], string methods [66], or boxed molecular dynamics. [67] In addition, the configurations generated during an iMD-VR run could be used to produce Markov state models for ligand binding systems [136], by seeding the model with initial conditions which are not trapped within metastable energy minima. [155, 182] Whilst there are a number of details which require further investigation in order to establish a reliable and integrated workflow for recovering free energies along user-generated iMD-VR pathways, such a framework will enable us to explore the differences in kinetics and thermodynamics between different ligands binding to the same protein target, or the free energy landscape of the same drug binding to different protein mutants, with potential applications to areas like antimicrobial resistance. More broadly, the 3D iMD-VR interface can be used to explore and sample cryptic binding configurations which may not be indicated in the crystal structure, offering exciting new opportunities for interactive drug design.

3.5 Supplementary Materials

Supplementary material for this chapter is available at https://doi.org/10.1371/journal.pone.0228461.s001

CHAPTER 4

iMD-VR is an Effective Tool for Flexible Substrate and Inhibitor Docking to the SARS-CoV-2 Main Protease

In accordance with the University of Bristol guidelines on the integration of publications as chapters within a dissertation, this chapter was recently accepted for publication in the Journal of Chemical Information and Modelling. [183] This online version contains revisions and is therefore more up-to-date. My contribution was performing the small inhibitor (X77) iMD-VR docking experiments and analyzing the results (Sections 4.2.2 and 4.3.1) Rebecca K. Walters performed the 11-mer oligopeptide iMD-VR docking experiments and analyzed the results (Sections 4.2.3 and 4.3.2). The introduction and conclusions (Sections 4.1 and 4.4) were written jointly between us. Jonathan Barnoud provided invaluable expertise to this work and is currently working on porting the simulations to be hosted on (and therefore accessible via) the cloud. David R. Glowacki and Adrian J. Mulholland contributed both their knowledge and expertise towards this work.

4.1 Introduction

COVID-19 has rapidly spread across the world, rising to the level of a global pandemic within only a few months. This potentially lethal disease is caused by the SARS-CoV-2 Coronavirus. Coronaviruses of this type can be pernicious as they can spread between numerous different organisms [184, 185] and lethally infect the respiratory, gastrointestinal, and central nervous systems. [186] There has been a rapid and widespread response to the COVID-19 pandemic from the global biomedical research community to understand the disease and attempt to identify potential vaccines and treatments. Antiviral drugs may have a useful role to play, particularly in the absence of an effective vaccine [187], for this and for potential future coronavirus pandemics.

One promising drug target is the SARS-CoV-2 main protease (Mpro), also known as 3-chymotrypsin-like protease (3CLpro). As a result of the original SARS (severe acute respiratory syndrome) epidemic in 2003, the structure of the original SARS-CoV Mpro (which shares 96% sequence identity with SARS-CoV-2 Mpro) [188] was determined and has been used for structure-based drug discovery efforts, including computational 'docking'. [189–191] The Mpro of both the original SARS-CoV and SARS-CoV-2 is a homodimeric protein [192] responsible for the cleavage of polypeptides translated from viral RNA into smaller non-structural proteins, using a catalytic Cys145/His41 dyad present in each subunit of the dimer. [191] Both the SARS-CoV and SARS-CoV-2 Mpro are believed to operate on 11 different cleavage sites of the large overlapping polyprotein PP1ab (replicase 1ab, 790 kDa) and PP1a (replicase 1a). [193–195] It has been reported that substrate specificity of the Mpro is determined by amino acids at positions -P2-P1↓P1'- of PP1ab [196] (with a preference for residues Leu-Gln↓(Ser,Ala,Gly) [187, 197], where ↓ marks the cleavage site). The non-structural proteins generated from proteolytic cleavage play a vital role in viral transcription and replication [198, 199], making the Mpro an essential component for the viral lifecycle. [190, 200–202]

There are currently many efforts globally aimed at identifying promising drug targets for COVID-19. [201, 202] Molecular simulation and modelling methods have the potential to contribute to the discovery and development of SARS-CoV-2 Mpro inhibitors, e.g. in structure-based ligand discovery and drug repurposing efforts for this and other COVID-19 targets. [203, 204] Recent crystallographic determination of the structure of the enzyme complexed with inhibitors [205, 206] allows structure-based drug discovery methods to be used; at the time of writing, there are currently 179 SARS-CoV-2 Mpro structures on the protein data bank. A standard initial approach in structure-based ligand discovery is computational molecular 'docking' of approved drugs and other small molecules from docking libraries, such as the ZINC database [207], that can identify 'hit' molecules that may bind to and inhibit the enzyme. Several docking studies on SARS-CoV-2 targets have already appeared, including for the Mpro. [187, 203, 206, 208, 209] Such automated docking methods are typically highly approximate to allow rapid, high throughput screening of large numbers of compounds. For example, automated docking methods, usually by necessity, can have a very limited treatment of protein dynamics and structural changes and use simplified descriptions of molecular interactions. Poses obtained with these high throughput methods often require further refinement. Recognised limitations of automated docking methods include the approximate nature of energy functions used, limited treatment of solvation, and little or no modelling of protein and ligand conformational variability, particularly for large, flexible ligands. These simple methods mean that automated docking can test millions of compounds in a relatively short time but also that the results are prone to error and may identify many false positives.

More sophisticated biomolecular simulation methods, such as MD, can be used to filter out false positives from docking. [210] MD simulations can also be used to account for protein

flexibility, e.g. by generating ensembles of structures to dock ligands. [139] Human intuition and expertise play an essential role in drug discovery, e.g. in refining structures in crystallographic studies or for predicting binding modes of ligands. Emerging tools based on VR can provide a useful addition to the armoury of computational methods for drug discovery and development. Furthermore, VR potentially allows for sharing structural information in an intuitive and accessible form, and for distributed, virtual collaboration, e.g. when supported by cloud-based resources. [20] VR frameworks for protein visualisation, such as ProteinVR, are being used for the SARS-CoV-2 Mpro. [211] While VR is undoubtedly a useful tool for visualising complex structures in 3D, many such representations are static and do not include protein dynamics. Narupa, an open-source software framework, allows users to manipulate rigorous, physics-based atomistic MD simulations within a VR environment, can be used to perform a method which we call 'interactive molecular dynamics in virtual reality' (iMD-VR). [61]

Recently, we have shown that iMD-VR using Narupa provides an effective and accurate approach for recreating known protein-ligand complexes. [61] It allows fully flexible docking through the inclusion of molecular motion in a physically rigorous MD simulation. iMD-VR allows interactive, dynamic, and flexible manipulation of structures, enabling the user to discover favourable binding modes. We applied this framework to several systems: pertinently, two of the three proteins studied were viral enzymes (HIV-1 protease and influenza neuraminidase) with clinically approved drugs. We showed that non-expert iMD-VR users could accurately recreate experimentally observed structures of protein-ligand complexes, with a comparable level of accuracy to standard docking methods (within 2.15 Å RMSD of the crystallographic binding pose). [180] In VR, users share a 3D virtual space with proteins and drug molecules (and can also share the space with each other, enabling multiple users to interact with the same system).

Here, we apply iMD-VR to dock both a small ligand and an oligopeptide substrate to variants of Mpro (both structures are shown in Fig. 4.1), testing different protocols. As in previous work on other enzymes, we compare results from iMD-VR with the crystal structure. We use iMD-VR to dock the inhibitor into an apo SARS-CoV-2 Mpro structure. We also dock an 11-mer oligopeptide into the original SARS-CoV Mpro with H41A mutant, giving structures in good agreement with the crystal structure. Finally, we created substrate complexes for SARS-CoV-2 Mpro for which, at the time of writing, no crystal structure exists (and of course capturing active substrate structures crystallographically is generally not possible). MD simulation was performed on each docked structure from iMD-VR to test the stability of the predicted binding poses. We make these models available for the wider community to use.

This iMD-VR framework is open source, uses commodity hardware, and so is easily applicable. These tools are freely available to the global research community and we believe that they should find wide application. This will be useful in structure-based drug discovery and development efforts targeting the SARS-CoV-2 Mpro and may help in developing inhibitors, complementing other computational and experimental methods. It will also be useful for education on viral

enzyme structure and function (as we have shown in other contexts) [21] and testing hypotheses e.g. on substrate binding and Mpro mechanism, complementing other types of simulations. [212]

4.2 Methodology

4.2.1 Simulation parameters and setup

The AMBER ff14sb forcefield [213] was used for protein and peptide structures. X77 was parameterised with GAFF. [214] All simulations used the OBC2 implicit water model [215] and used OpenMM as the force engine. Prior to iMD-VR, crystallographic water molecules were removed and the structures were minimised and equilibrated: details given in the ESI. [216] To prevent unrealistic perturbation of the protein structure during iMD-VR (e.g. protein unfolding), a harmonic positional restraint of 50 $kJ{\cdot}mol^{-1}$ was applied to the protein backbone atoms in most of the protocols (except one in which the protease is fully flexible), as in previous work. [61] Each iMD-VR docking experiment was repeated a total of five times, generating a total of five final structures per run.

To evaluate the stability of enzyme complexes generated by iMD-VR, all five final structures were subjected to energy minimization and re-equilibrated using the protocol described in the ESI. [216] After energy minimization, an additional 10 ns of MD simulation was run and the resulting trajectories were analysed to evaluate each structure. Details of these MD runs, and analysis, are given in the ESI. [216]

To guide iMD-VR docking, a trace representation of the docked ligand or oligopeptide in the crystallographic position in the binding pocket was superimposed onto the simulation space and used as a 3D visual guide to where X77 or the oligopeptide should be placed; these are referred to here as 'trace atoms'. Further details can be found in the ESI. [216]

4.2.2 iMD-VR docking of a small ligand (X77) to Mpro

4.2.2.1 Docking X77 into ligand-complexed SARS-CoV-2 Mpro

We first tested the iMD-VR framework using the protocol from our previous work [61] based on a known SARS-CoV-2 Mpro protein-ligand complex (PDB: 6W63). The ligand started in the bound position, as observed in the crystal structure. The operator interactively applied force on the ligand to move it out of the pocket to a position where it was clearly not bound to the protein. Then, they moved the ligand back to its initial pose. Trace atoms were placed at the initial position of the ligand to guide the user, taking the form of a fixed and translucent representation of the molecule. Trace atoms are only visual clues and do not take part in the equation of motion. As noted in the Methods, we used an implicit solvent model (as in our previous work) to simplify and speed docking, and also applied positional restraints on the protein backbone to avoid large deformations (see ESI). [216]

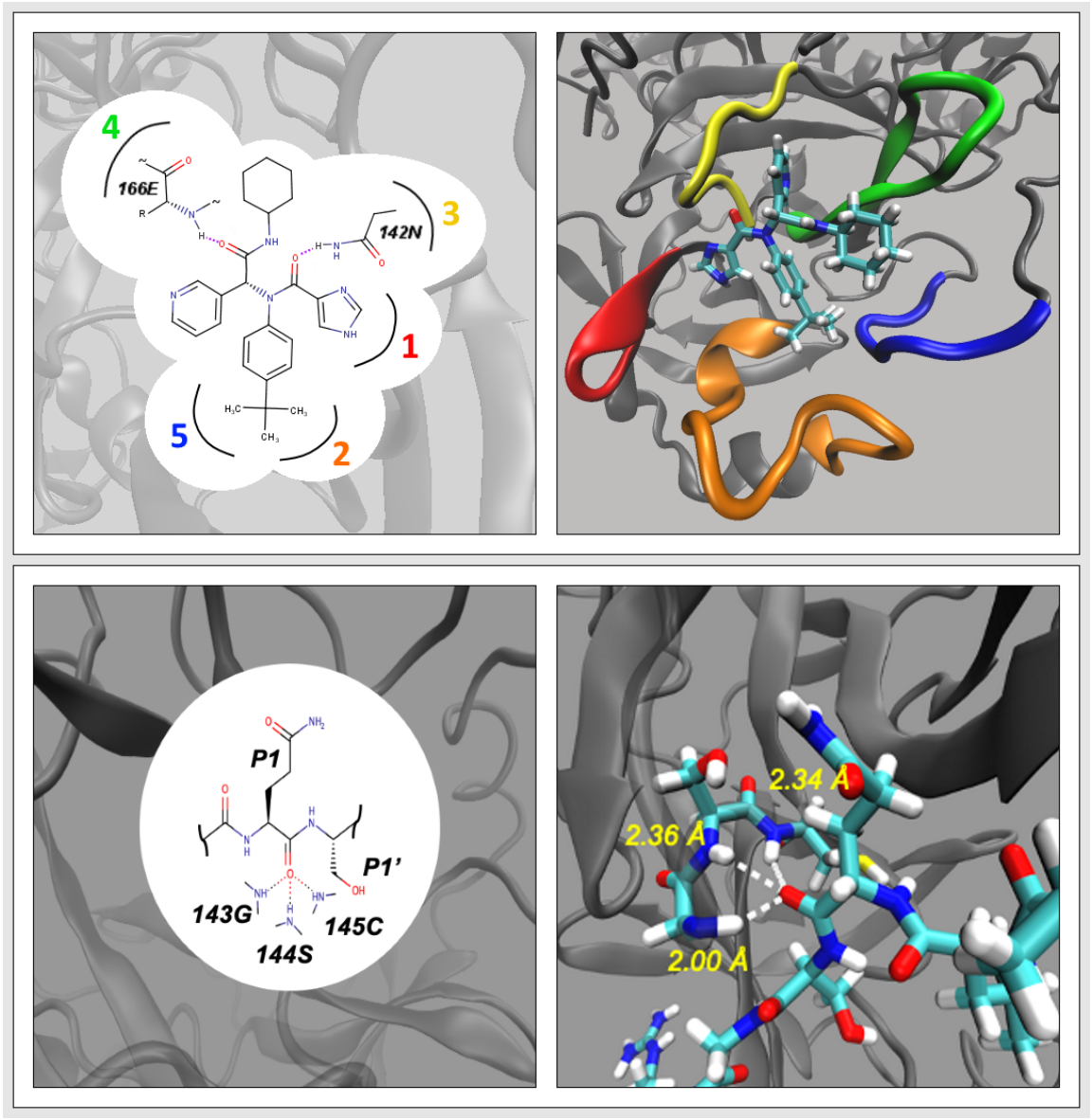

Figure 4.1: **Binding modes for X77 and the oligopeptide into the SARS-CoV-2 Mpro binding pocket**. Binding modes for X77 and the oligopeptide into the SARS-CoV-2 Mpro binding pocket. Top: Details of the binding of the X77 inhibitor revealed by crystallography (Top left) The X77 inhibitor forms two hydrogen bonds with the SARS-CoV-2 Mpro; five active site loops around the ligand are also indicated schematically. (Top right) X77 bound covalently in the active site of SARS-CoV-2 Mpro (PDB: 6W63). The five active site loops are coloured as follows: (1) residues 22 to 27 is leftmost in red, (2) residues 41 to 54 is at the bottom in orange, (3) residues 140 to 145 is at the top left in yellow, (4) residues 163 to 173 is at the top right in green, and (5) residues 186 to 191 is rightmost in blue. Bottom: substrate complex models created in this work: (Bottom left) Oxyanion hole interactions between the 11-mer oligopeptide substrate (observed both for the for the SARS-CoV and SARS-CoV-2 Mpros). (Bottom right) Oxyanion hole interactions in a structure from iMD-VR docking to an apo SARS-CoV Mpro structure (PDB: 6M03).

The small inhibitor, X77, was selected because it does not covalently bind to the protein and is similar in size and number of rotatable bonds to compounds that we docked using iMD-VR in previous work (Ref. [61] or see Chapter 3). Fig. 4.1 shows the structure and binding mode of X77 in SARS-CoV-2 Mpro. There is uncertainty about the protonation state of the SARS-CoV-2 Mpro catalytic His41-Cys145 dyad, and it has been suggested that ligand binding to the active site promotes formation of the zwitterionic state. [217] Previous work has shown differential docking behaviour between different protein tautomers [61], so we tested SARS-CoV-2 Mpro with neutral and zwitterionic forms of the dyad. We interactively unbound and docked X77 from both using iMD-VR. After iMD-VR docking, a representative structure was selected based on having the lowest ligand heavy atom RMSD compared to the ligand coordinates in the minimized and equilibriated structure (i.e. compared to the starting bound pose).

4.2.2.2 Docking X77 into apo SARS-CoV-2 Mpro

We also tested iMD-VR docking of X77 into the apo form of SARS-CoV-2 Mpro (PDB: 6M03). In this case, only the neutral tautomer was modelled, because the complexes were generally more stable than the zwitterionic form (Fig. S1). [216] The same trace atoms from the iMD-VR docking experiments on the complexed protein (Section 4.2.2.1) were superimposed onto the apo protein structure and used as a visual guide. We tested two iMD-VR protocols. In one protocol, the user tries to superimpose X77 over the trace atoms as closely as possible. A representative frame from this iMD-VR docking run was chosen based on having the lowest X77 heavy atom RMSD compared to the crystal structure of the complex. In the other protocol, the user uses trace atoms to orientate the ligand, but instead primarily focuses on reforming the two hydrogen bonds shown in Fig. 4.1. A representative structure was chosen based on the two interactions being present. Henceforth, these two protocols are referred to as “apo X77 docking protocol 1” and “apo X77 docking protocol 2”, respectively.

4.2.3 iMD-VR docking of an oligopeptide to Mpro

4.2.3.1 Docking a substrate into H41A mutant SARS-CoV Mpro

The 11-mer oligopeptide (derived from one of the 11 cleavage sites of PP1ab [191], sequence TSAVLQSGFRK) was interactively removed from, and then docked into the active site of the SARS-CoV Mpro with an inactivating H41A mutant (PDB: 2Q6G). [200] The aim was to test iMD-VR docking of long, flexible molecules. We chose this substrate because it is processed by both the SARS-CoV and SARS-CoV-2 Mpro. [218] A SARS-CoV Mpro crystal structure is available for comparison. As with the small ligand docking described above, a trace representation of the substrate heavy atoms in the bound position from the crystal structure was superimposed onto the protein as a visual guide (trace atoms). Based on our results with the X77 ligand, we only modelled the neutral dyad for all substrate docking tasks with the substrate here.

Before beginning iMD-VR docking, 10 ns of MD in implicit solvent was performed on the crystal structure. This MD simulation removes any initial strain in the structure and relaxes it in the solvent environment. It also provides a benchmark of how a substrate complex behaves in the same implicit solvent as in iMD-VR. The set-up of this MD simulation followed the same protocol as all the other MD simulations and is described in the ESI. [216] This simulation will henceforth be referred to as the substrate reference simulation.

We tested two protocols for iMD-VR docking. In both protocols, the docked oligopeptide trace atoms were rendered as a visual guide and the focus of docking was on reforming 14 key hydrogen bonds observed in the crystal structure. A representative docked structure was extracted in which the oxyanion hole interactions are present (Fig. 4.1). In the first protocol, we applied positional restraints to the backbone of the protease, like those used for X77 (see above), and in our previous work. [61] In the second protocol, the protease is fully flexible. These protocols will henceforth be called “protocol 2” and “protocol 3”, respectively. Another protocol, “protocol 1”, was also tested. This protocol is similar to protocol 2, but the focus lies on superimposing the substrate atoms directly on top of the trace atoms. For this protocol, we extracted the structure with the lowest substrate RMSD compared to the crystal structure. However, the resulting structures lacked important interactions observed in the crystal structure, and so protocol 1 was not used for further oligopeptide docking. These findings emphasise the limitations of RMSD alone as a metric for measuring quality of docking solutions. Formation of binding interactions, such as hydrogen bonds, is crucial. iMD-VR allows the user to find such interactions intuitively and correctly (within the limitations of the forcefield). Results of the docking experiment with protocol 1 are detailed in the ESI. [216]

4.2.3.2 Docking the oligopeptide into apo and complexed structures of SARS-CoV-2 Mpro

To the best of our knowledge, there is no crystal structure available of a substrate bound to the SARS-CoV-2 Mpro. iMD-VR was employed here to dock a substrate into two different structures of the SARS-CoV-2 Mpro: an apo structure (PDB: 6M03), and the structure of the X77 inhibitor complex (PDB: 6W63), which will henceforth be described as the ‘inhibitor-complexed’ structure. These two structures were chosen to test the effect of starting structure on the docking solution.

Protocols 2 and 3 were tested for iMD-VR docking to both SARS-CoV-2 Mpro structures, using trace atoms taken from the crystal structure of the substrate bound to the H41A mutant SARS-CoV. These trace atoms were used as a visual guide to indicate the position and orientation of the binding pocket.

4.3 Results and Discussion

4.3.1 iMD-VR docking of a small ligand (X77) to Mpro

4.3.1.1 Docking X77 into complexed SARS-CoV-2 Mpro

We used iMD-VR to dock a known inhibitor (X77) into both its cognate protein complex (PDB: 6W63) and the apo (PDB: 6M03) form of the SARS-CoV-2 Mpro. For the ligand-complexed structure, we applied our tested iMD-VR ligand docking protocol [61] to recreate the ligand-protein complex: the user interactively pulled X77 out of Mpro and then manually reintroduced it into the binding site using iMD-VR. The user was able to recreate the X77 bound structure within a similar RMSD range as for previous protein-ligand systems, i.e. less than 2.5 Å. [61] Five structures from iMD-VR docking attempts were then subject to 10 ns of unrestrained MD simulation, to test their stability. The complexes were stable: the heavy atom RMSD of X77 remained within 2.5 Å of the equilibrated and minimized structure used to initiate iMD-VR (Fig. 4.2a). The trajectory with the lowest RMSD had an average value of 1.6 Å. Combining the data from all five runs, the structures also showed little variation in position, with a total average RMSD of 1.8 Å and standard deviation of 0.3 Å. These results show that iMD-VR docking is an effective tool for (re)creating stable binding poses of ligands of the SARS-CoV-2 Mpro and should be useful in predicting binding poses of novel ligands.

4.3.1.2 Docking X77 into apo SARS-CoV-2 Mpro

Crystal structures of apo enzymes (i.e. structures with no ligand bound) are sometimes not suitable for predicting structures of protein-ligand complexes (e.g. if the protein is in a different conformation, or the binding site is occluded). We tested the use of an apo structure for predicting X77 binding using iMD-VR docking. iMD-VR has the advantage (compared to many docking approaches) that both the ligand and protein are flexible and so can adapt their structures to each other. Two iMD-VR protocols for docking X77 to the apo form of SARS-CoV-2 Mpro were tested: one with the aim of finding a low RMSD, the other instead focuses on forming two important hydrogen bonds (shown in Fig. 4.1). A challenge became immediately apparent with the apo crystal structure (Fig. 4.3). In the apo structure, the active site loop containing residues 41 to 54 (highlighted in orange in Fig. 4.1) is in a different position from the ligand-complexed structure, such that Tyr54 occupies part of the X77 binding pocket. MD performed on the apo structure showed this loop exhibits a high degree of flexibility, especially compared to X77-complexed Mpro (Fig. S4) [216]; due to this higher flexibility, we captured a state where the Tyr54 is blocking the pocket, hence X77 could not be fully replaced (Fig. 4.3c). We tested whether apo-docked structures generated by iMD-VR, with the ligand correctly oriented and forming important contacts with the protein, relaxed into a structure closer to the crystal structue of the complex with additional MD. During minimization and requilibration on the iMD-VR generated complexes, Tyr54 spontaneously moved back after X77 docking and, furthermore, the 41 to 54

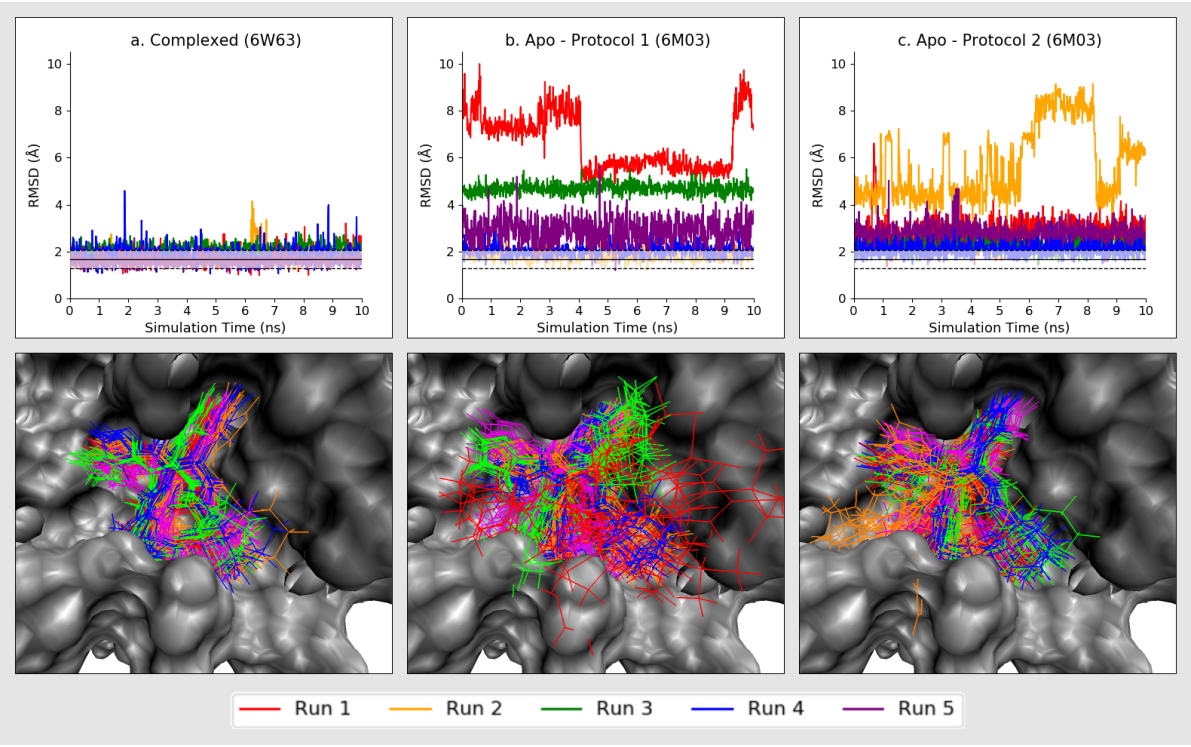

Figure 4.2: **iMD-VR docked X77 RMSD during 10 ns of validation MD**. (Top) Results from MD simulations for structures from iMD-VR docking of the X77 ligand into (a) its cognate crystal structure (ligand-complexed X77 docking) (b) the apo structure (using X77 docking protocol 1), and (c) the apo structure (using X77 docking protocol 2). For each 10 ns MD simulation starting from five independent iMD-VR docking experiments (5 runs, one for each iMD-VR docked structure), the heavy atom RMSD of X77 is shown. For reference, the black line represents the average X77 RMSD from 10 ns of MD for the original, unperturbed bound structure (6W63). The translucent bars represent the standard deviation around this mean. (Bottom) For each of the five runs for each of the three docking experiments, snapshots from the 10 ns of MD simulation (taken every nanosecond), superimposed on the X77 complex crystal structure. Each image corresponds to the graph directly above it.

loop exhibited a reduced degree of flexibility, comparable the complexed form of Mpro (Fig. S4). [216] Encouragingly, this suggests that the apo structure can be used for docking small ligands, so long as the structure is given opportunity to relax.

RMSD analysis Not surprisingly, docking to the apo structure (using either docking protocol) results in slightly higher RMSDs and less stable structures than docking to the cognate ligand complex structure, with less overall consistency between runs (Fig. 4.2). However, for each protocol, at least one structure was found with an average X77 RMSD lower than 2.5 Å. For reference, 10 ns of MD simulation of the unperturbed liganded (prior to iMD-VR) yielded an average RMSD of 1.7 Å, and the lowest average X77 RMSD for iMD-VR docking to the complexed structure was 1.6 Å. In comparison, the lowest average X77 RMSD for the apo X77 docking protocol 1 was 1.8 Å, and the lowest for apo X77 docking protocol 2 was 2.1 Å. Although the first protocol produced a pose with lower average RMSD during subsequent MD, overall, it performed

worse: the total average RMSD across five 10 ns MD runs for apo X77 docking protocol 1 was 3.6 Å (σ 1.9 Å), whilst the total average RMSD for apo X77 docking protocol 2 was 3.2 Å (σ 1.5 Å). Refer to Fig. 4.2 to see the overall variation in X77 positions between the two protocols. This indicates that a protocol in which the user aims to form important binding contacts gives better results than one in which selection is based on RMSD alone.

Hydrogen bond analysis Fig. 4.4 shows analysis of hydrogen bonds in the 10 ns validation MD simulations of structures from the two apo X77 iMD-VR docking protocols. For apo X77 docking protocol 1, runs 1 and 3 show poorest hydrogen bonding and highest X77 RMSD of the five runs (Fig. 4.4b). In iMD-VR docking, hydrogen bond 2 did not form in run 2 of the apo X77 docking protocol 2, and rarely in subsequent MD simulation (Fig. 4.4c), which resulted in the highest X77 RMSD (Fig. 4.2c). RMSD is clearly an important metric, but consideration of RMSD may not give structures with important binding interactions (as noted above). Therefore, as with other manual docking methods, consideration of key hydrogen bonds is important in creating ligand complexes with iMD-VR.

Additional analysis When a reference (e.g. crystal) structure is known, RMSD provides an objective value to rank iMD-VR generated poses but, as noted above, users should pay careful attention to interactions in generating structures by iMD-VR docking. [219] We tested other analyses of the iMD-VR generated poses. Fig. S2 [216] shows the fraction of contacts recreated for each of the five runs for each of the three docking experiments. Similarly, Figs. S3-8 [216] show the Root Mean Square Fluctuation (RMSF) of the five active site protein loops during MD simulations with no backbone restraints. These analyses are more extensively discussed in the ESI [216], however, while this lends further confidence to the iMD-VR generated structures, the

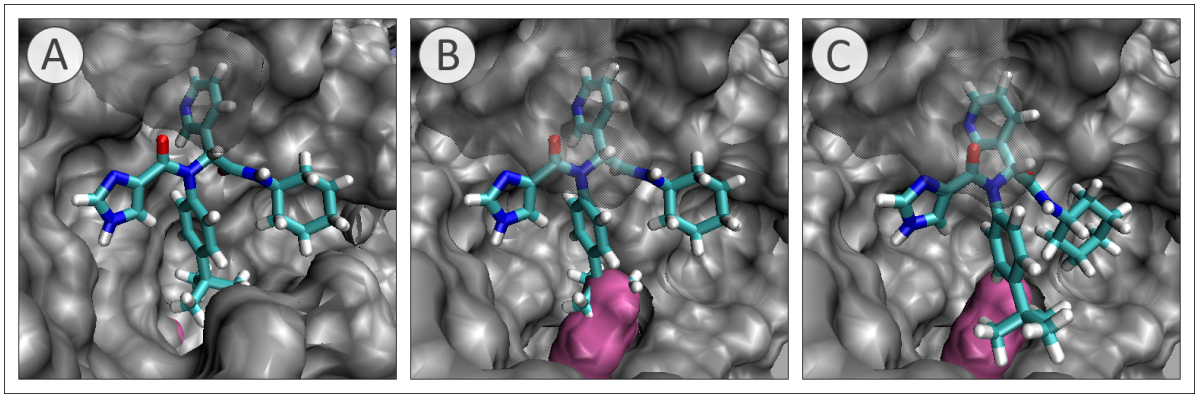

Figure 4.3: **X77 binding pose overlaid on SARS-CoV-2 Mpro structures**. (A) Crystal structure of X77 bound to the SARS-CoV-2 Mpro (PDB: 6W63). Tyr54 (highlighted in pink) is buried in the protein structure. (B) The X77 structure from 6W63 superimposed on the apo structure starting coordinates, used in the two apo X77 docking protocols. Tyr54 (highlighted in pink) has shifted so that it is no longer buried and is occupying the X77 binding pocket, causing a steric clash with the tert-butylbenzene group of X77. (C) A representative iMD-VR generated X77 bound atom positions (taken from apo X77 docking protocol 2), showing how X77 could no longer be docked correctly due to the presence of Tyr54 (highlighted in pink).

methods suggested here should not be treated as an exhaustive list. As has been previously recommended, users should pay attention to both protein-ligand interactions and dynamics when evaluating iMD-VR docked structures; with this in mind, more data analysis will always be preferable to less.

4.3.1.3 Discussion

At least one run from each docking experiment was deemed successful based on all the evaluation metrics (including those discussed in the ESI). [216] All the poses generated by iMD-VR docking, for each of the three protocols, are given in the ESI. [216] Overall, iMD-VR docking successfully recreated X77 and SARS-CoV-2 Mpro complexes. Docking to an apo structure gave complexes with higher RMSDs, but that were still usefully close to the crystallographically observed X77 complex. Based on these results, we make general recommendations for using iMD-VR docking for protein-ligand complexes. RMSD is useful for quickly evaluating the similarity between a known structure and a pose generated by iMD-VR docking, but has significant limitations. [219] RMSD of a ligand clearly only measures how well one ligand structure superimposes on another; it does not indicate whether binding interactions are present. Docking to apo structures is a challenge, but as we show here, iMD-VR docking of small molecule ligands to the apo structure of SARS-CoV-2 Mpro is successful, which is encouraging. This success reflects the flexibility of the protein and ligand in the iMD-VR approach. Users should focus on forming favourable interactions such as hydrogen bonds when docking in iMD-VR.

4.3.2 iMD-VR docking of an oligopeptide to Mpro

4.3.2.1 Docking the oligopeptide into complexed SARS-CoV Mpro

A particular advantage of iMD-VR is in the docking of large, flexible molecules because the user can manipulate both their structures and that of the protein. We tested this approach initially for an oligopeptide binding to the original SARS Mpro H41A mutant, for which a crystal structure is available (PDB: 2Q6G). [200] In this crystal structure, the catalytic histidine is replaced by alanine, rendering the enzyme inactive and allowing crystallization of a substrate complex. A 10 ns MD simulation of this crystal structure was performed to compare with structures generated by iMD-VR. The RMSD of the oligopeptide in this simulation was 3.7–5.6 Å.

Two docking protocols were tested for the oligopeptide substrate with the SARS-CoV Mpro H41A mutant: in the first, restraints were applied to the protease backbone (protocol 2); in the second, the protease was fully flexible (protocol 3). In both protocols, the aim was to reform 14 hydrogen bonds between the protease and substrate that are observed in the crystal structure. Docking was performed 5 times following each protocol, making a total of 10 iMD-VR oligopeptide docking experiments. From each, a structure in which hydrogen bonds 8 and 10 (the oxyanion hole, excluding hydrogen bond 9 as it is not strongly observed in the reference simulation) are

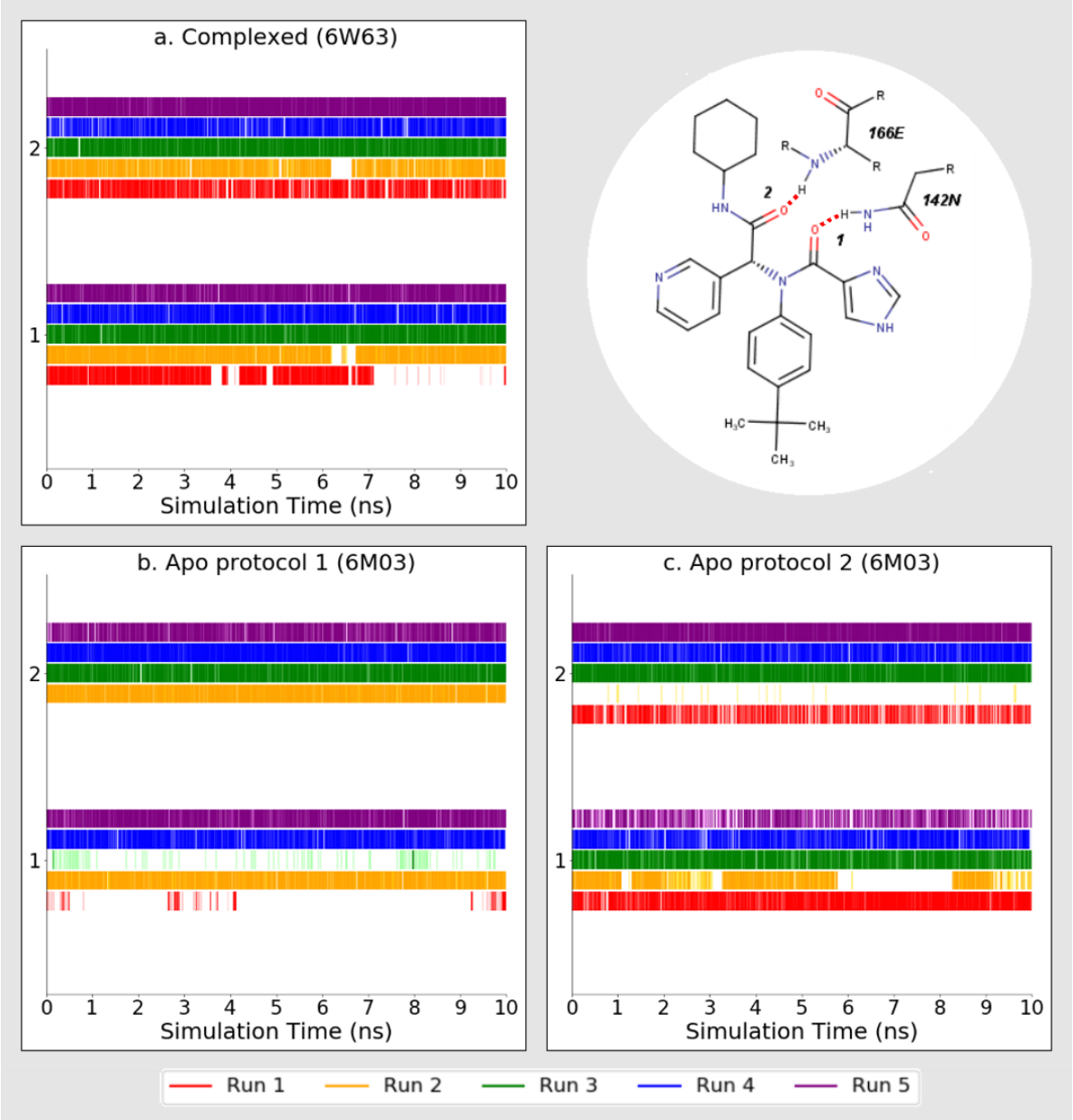

Figure 4.4: **iMD-VR docked X77 hydrogen bonding during 10 ns of validation MD**. Results from (a) ligand complexed X77 iMD-VR docking, (b) apo X77 docking protocol 1, and (c) apo X77 docking protocol 2, showing presence of two hydrogen bonds over 10 ns of MD simulations of the resulting structures. Hydrogen bonds were detected using the Wernett-Nilsson algorithm [220], where the cutoff distance depends on the angle between the donor and acceptor heavy atoms. Lines with a solid colour indicate that a hydrogen bond is present in that snapshot. Fainter lines indicate that a hydrogen bond is not present according to the above criteria, but the interatomic distance between the donor and acceptor atom is still less than 4 Å, with an applied gradient to become lighter as the atoms move further away. Therefore, faint lines which are harder to distinguish denote only slight displacement.

formed was extracted, and 10 ns of MD simulation was run for each of these docked structures. These interactions (which are shown in Fig. 4.1) were chosen because they play an integral part in the mechanism of proteolytic cleavage, stabilising the tetrahedral intermediate by interaction with the carbonyl oxygen of the substrate's scissile bond. [221]

As a test, substrate docking was also performed following the previous protocol (protocol 1), as for small ligand docking (section 4.3.1), where the focus was placing the oligopeptide atoms directly on top of the trace atoms. However, the docked structures generated from following this protocol did not resemble the crystal structure. While this protocol was successful for docking small molecules (including for the small ligand docking to the complexed SARS-CoV-2 Mpro), it was unsuitable for docking long, flexible molecules. Results from this docking protocol are detailed in the ESI. [216] We therefore recommend that novice iMD-VR users should follow protocol 2 (i.e. apply backbone restraints) when docking large, flexible molecules to not accidentally perturb the protease structure, and expert iMD-VR users should follow protocol 3 where the protease is fully flexible.

RMSD analysis RMSD analysis of the substrate in MD simulations of all the docked structures showed that the oligopeptide remains within 3.5–6.5 Å of the crystal structure (Fig. S8b-c). [216] This value is similar to the substrate RMSD values from the reference simulation (3.7–5.6 Å, Fig. S8a) [216], which indicates that the iMD-VR docked structures are similar to the crystal structure and are also stable in MD simulations. The residues with RMSDs above 5.6 Å are the terminal residues which are solvent exposed, less tightly bound and more mobile (see additional analysis).

Hydrogen bond analysis Structural determination performed by Xue et al. of the SARS-CoV Mpro H41A mutant complex with the 11-mer oligopeptide substrate revealed 13 hydrogen bonds important for substrate binding (Fig. 4.6a). [200] The stability of these 13 hydrogen bonds, plus an additional hydrogen bond between Ser144 and P1-GLN that is part of the oxyanion hole, were analysed in each simulation of the SARS-CoV docked structures. The hydrogen bonds in all these simulations are very similar to those observed in the reference simulation (Fig. 4.6b), in which the most stable interactions are hydrogen bonds 1, 2, 3, 6, 8, 10, 12, and 14 (Fig. S10 and S11). [216] It is especially encouraging that in all the simulations of iMD-VR docked structures, the oxyanion hole interactions are present.

Additional analysis RMSF analysis of the substrate iMD-VR docked structures showed that the P1-Gln residue (which is involved in proteolytic cleavage, and closest to the catalytic dyad) is tightly bound and fluctuates by less than 0.5 Å (Fig. S16b-c). [216] In contrast, the substrate terminal residues (P6-Thr and P5'-Lys) are much more mobile, with RMSF values ranging between 0.8–1.3 Å and 0.8–2.5 Å respectively (oligopeptide sequence shown in Section 4.2.3). This is not surprising because they are not involved with the 14-hydrogen bond network and not as deeply buried as those in the active site of the protease. Similar behaviour is observed in the reference simulation (RMSF of the P1-Gln residue below 0.5 Å and RMSFs for P6-Thr and

P5'-Lys of 1 Å and 2.5 Å respectively, Fig. S16a). [216] Altogether, this shows iMD-VR docking with protocols 2 or 3 produces stable structures, which are structurally and dynamically similar to MD simulations based directly on the crystal structure.This demonstrates the power of iMD-VR docking for flexible ligands, including peptide substrates.

4.3.2.2 Docking oligopeptide into two structures of SARS-CoV-2 Mpro

We then tested iMD-VR protocols 2 and 3 for docking the substrate interactively 5 times each into the active site of two SARS-CoV-2 Mpro structures (apo and inhibitor-complexed, PDB codes 6M03 and 6W63, respectively), a total of 20 iMD-VR docking simulations. While the SARS-CoV-2 Mpro has a very similar sequence to the SARS-CoV Mpro (96% sequence identity) [188], the structures are slightly different. Fig. 4.5 shows the SARS-CoV Mpro and both SARS-CoV-2 Mpro starting structures for iMD-VR simulations overlaid on the secondary structure. It shows that there are some small structural differences. As in the SARS-CoV Mpro iMD-VR docking, a structure in which the oxyanion hole interactions had been reformed was extracted from each VR simulation. 10 ns of implicit solvent MD was performed on each of the docked SARS-CoV-2 Mpro structures, giving a total of 20 MD simulations.

RMSD analysis RMSD analysis shows that the structures built by iMD-VR docking are close to the crystal structure. The substrate heavy atoms remain within 3–6 Å of the crystal structure coordinates (Fig. S8d-g) [216] in all the MD simulations of iMD-VR docked complexes. Visual inspection of the trajectories showed that the substrate remains bound to the protease in all simulations and that the cases where the RMSD is higher than 5 Å are due to the mobility of the terminal residues of the oligopeptide (see additional analysis). This is similar to the RMSD analysis of the reference simulation (Fig. S8) [216] and also to simulations of the SARS-CoV docked structures (Fig. S8). [216]

Hydrogen bond analysis As noted above, the SARS-CoV-2 Mpro has a very high sequence similarity to the SARS-CoV Mpro (96% and contains the same binding residues involved in the 14 hydrogen bonds). The same hydrogen bonds are likely to be involved in substrate binding and therefore are considered here. Docking to the apo SARS-CoV-2 Mpro generally formed the oxyanion hole interactions (hydrogen bond 8 and 10) using either protocol (Fig. 6c-d). Similarly, hydrogen bonds 2, 3, 6, 12, and 13 were maintained throughout simulations of all the docked poses, showing that a common, stable pose is obtained by iMD-VR docking (Fig. S12 and S13). [216] Hydrogen bond 9 is also present, although the interaction is weaker.

The simulations of the inhibitor SARS-CoV-2 Mpro docked structures showed hydrogen bonds are not always present (similar to results from docking to the apo structure, Fig. S14 and S15) [216], although they still show most of these hydrogen bonds. Among the most stable in all simulations built from inhibtor complexes are hydrogen bonds 2, 3, 12, and 14. Furthermore, the oxyanion hole interactions are present throughout the simulations (Fig. 4.6e-f, except inhibitor - protocol 2 run 1).

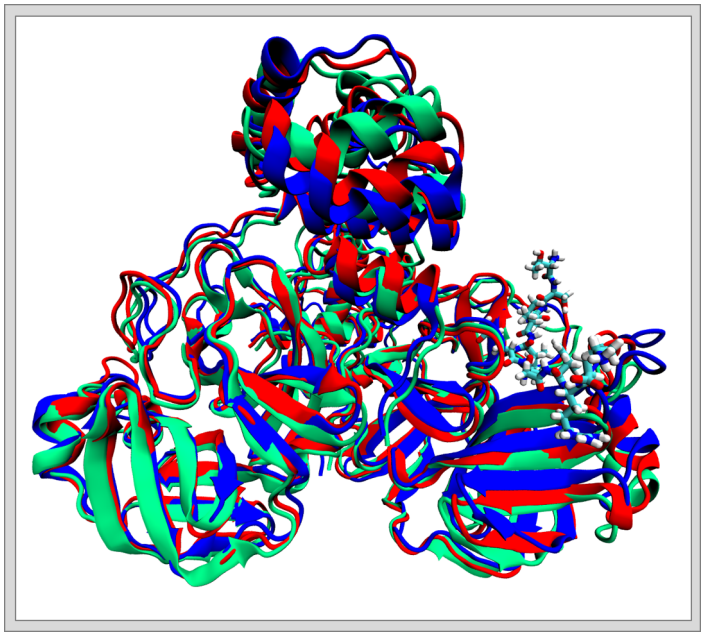

Figure 4.5: **Three Mpro structures used as input for iMD-VR docking overlaid**. The structures are SARS-CoV Mpro (red), the apo SARS-CoV-2 Mpro (blue) and the inhibitor-complexed SARS-CoV-2 Mpro (green). The oligopeptide is also shown on the right, bound to the SARS-CoV structure. The two SARS-CoV-2 structures are aligned against the secondary structure of the SARS-CoV structure, yielding an RMSD of 3.17 Å and 3.29 Å for the apo and inhibitor-complexed structures respectively. For consistency, the structures were also aligned on the secondary structure of the apo Mpro and the inhibitor-complexed Mpro. The RMSD of SARS-CoV Mpro and inhibitor-complexed Mpro aligned on the apo structure are 3.17 Å and 3.19 Å respectively, and the RMSD of the SARS-CoV Mpro and the apo Mpro aligned on the ligand-complexed structure are 3.29 Å and 3.19 Å repsectively.

Finally, hydrogen bonds 4 and 13 are the only two in this set that were not reformed in any iMD-VR docking attempts with either the SARS-CoV or SARS-CoV-2 Mpro. This could be because these two hydrogen bonds do not involve the enzyme backbone. Note that hydrogen bond 13 was also not observed in the reference simulations of the substrate complexes.

Additional analysis RMSF analysis of all 20 MD simulations of the SARS-CoV-2 docked structures showed that the α-carbon of the P1-Gln residue fluctuates by no more than 0.5 Å, whereas the terminal residues P6-Thr and P5'-Lys are more mobile (RMSF between 0.5–3 Å, Fig. S16d-g). [216] This is expected, as the ends of the substrate are bound more weakly than the central residues, as also observed for SARS-CoV Mpro (above) and the reference simulation. Altogether, this shows that substrate complexes built by iMD-VR docking are stable and will be suitable for further simulation of Mpro dynamics, binding and mechanism.

4.3.2.3 Discussion

Docking with iMD-VR was successful in both (i) reproducing the crystal structure of an oligopeptide substrate bound to SARS-CoV Mpro, and also (ii) in creating stable structures of SARS-CoV-2

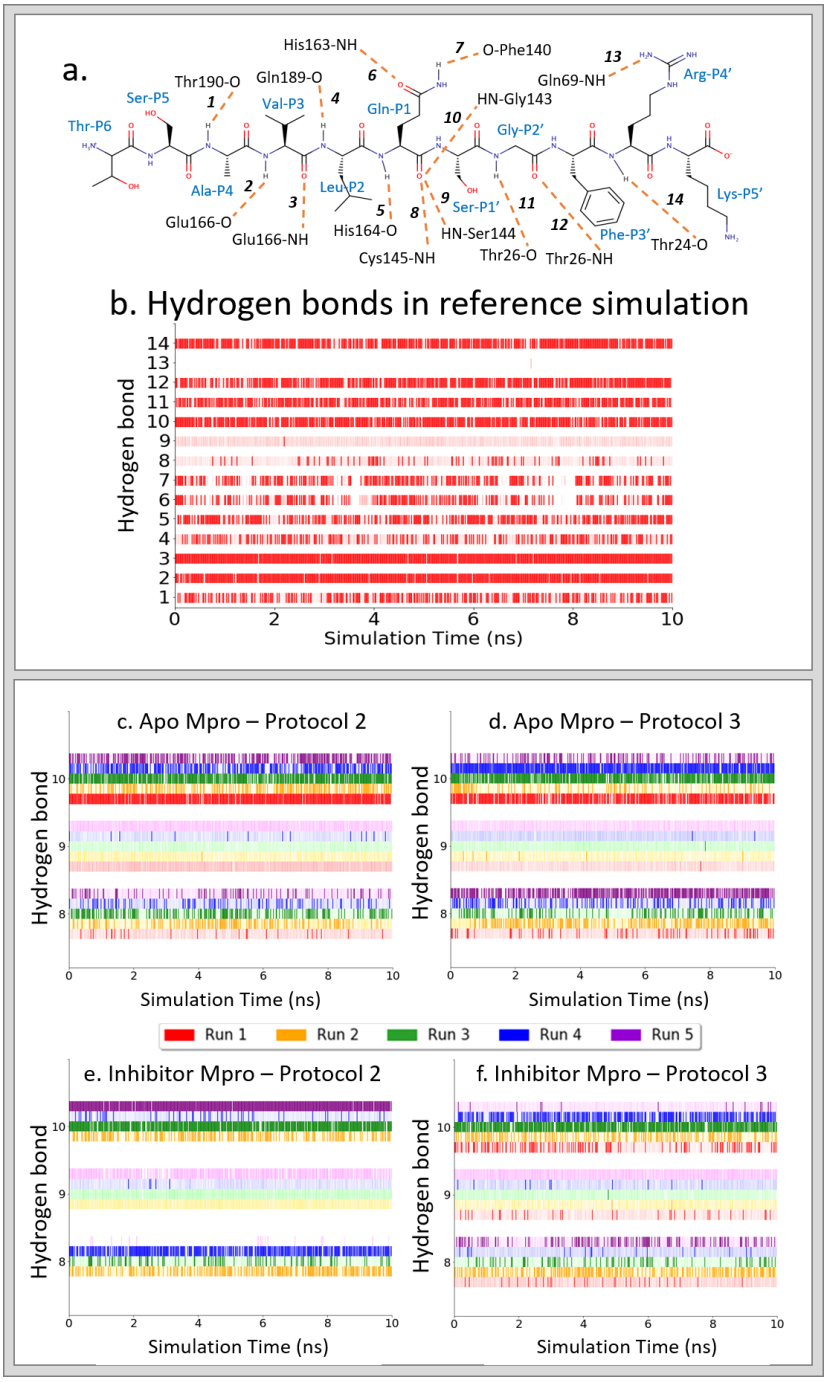

Figure 4.6: **iMD-VR docked oligopeptide hydrogen bonding during 10 ns of validation MD**. (a) The sequence of the 11-mer oligopeptide substrate and the 14 hydrogen bonds which were considered in analysis of VR generated structures. (b) The presence of the 14 hydrogen bonds throughout the MD simulation of the docked SARS-CoV Mpro crystal structure. The solid colour represents the hydrogen bond being present, and the lighter/translucent colour represents the donor and acceptor atoms being within 4 Å of each other. Hydrogen bond 13 is not included as it was never fully formed. The hydrogen bonds involved in the oxyanion hole (shown on the y-axis as 8, 9 and 10) are presented for throughout the simulations of the VR generated docked structures of the substrate to (c) the apo SARS-CoV-2 Mpro following VR docking protocol 2 and (d) following docking protocol 3, and of the substrate to (e) the inhibitor SARS-CoV-2 Mpro following docking protocol 2 and (f) docking protocol 3.

Mpro with this substrate. This docking was assisted by experience gained from docking the inhibitor, alongside chemical and spatial intuition. We tested different docking protocols, e.g. testing the effects of protein backbone restraints. The docked SARS-CoV Mpro structures reformed more of the hydrogen bonds in the 14 hydrogen bond network than in the SARS-CoV-2 structures. This is likely due to the fact docking to the original SARS protease used the cognate peptide complex structure, which is in a configuration to accommodate oligopeptide binding and so will form these hydrogen bonds more easily than apo enzyme structures or structures with small molecule inhibitors, which may have to undergo conformational changes. Nonetheless, the substrate RMSD in simulations of the apo and inhibitor SARS-CoV-2 Mpro docked structure stayed in the same range as the reference simulation. The iMD-VR docked structures also consistently reproduce the majority of the hydrogen bonds with the substrate, particularly the important oxyanion hole interactions and hydrogen bonds 2, 3, 12 and 14. This is very encouraging: iMD-VR docking to all the different crystal structures gave stable structures that were also in agreement with experiment. There is no significant discernible difference in the docked structures generated from protocols 2 or 3. We therefore recommend that expert iMD-VR users should follow protocol 3 (i.e. to treat the protease as fully flexible), and novice iMD-VR users should follow protocol 2 (applying backbone restraints, as to not accidentally disrupt the protein secondary structure during docking).

4.4 Conclusions

In this work, we have demonstrated that iMD-VR is an effective tool for generating structures of complexes of the SARS-CoV-2 Mpro with an inhibitor (X77) and an oligopeptide substrate. In previous work [61] we have shown that even novice users can quickly generate structures in good agreement with crystal structures, with minimal guidance. With a little practice, researchers can dock ligands to proteins in a few minutes. Here, we show that iMD-VR docking is effective for building and modelling inhibitor and substrate complexes of SARS-CoV-2 Mpro. Structures constructed by iMD-VR docking reproduce the key structural and binding motifs found in reference crystallographic structures. As expected, iMD-VR docking performs better on cognate protein models, i.e. redocking to an observed complex, than for docking to apo forms of the protein. However, the results with apo and other protein structures are in good agreement with experiment and stable in MD. This shows that iMD-VR docking can be used predictively to generate structures of complexes of Mpro even when specific experimental structural information is lacking. This is because the iMD-VR protocols described here allow for full flexibility of the enzyme, and of the ligand, and their conformational behaviour and interactions are modelled by a detailed atomistic forcefield, allowing the system to respond in a realistic manner.

In iMD-VR docking, users should pay attention to forming specific binding interactions. RMSD alone can be a poor indicator of the model quality. Other evaluation metrics should be

used in addition. Further MD simulations of docked complexes provide a test of stability, as here. Proteins are known to undergo conformational changes upon binding and, although some docking methods can account for this [222], high-throughput screening methods often treat the protein or ligand as rigid out of practical necessity; simplified interaction potentials are also typically used in automated docking. Our iMD-VR framework will complement high-throughput docking e.g. to test structures predicted by computational screening, taking advantage of the protein and ligand flexibility in iMD-VR, and human intuition, to refine these structures. iMD-VR can also be used as a predictive tool to model binding of potential inhibitors or substrates. It should be a useful tool for testing binding hypotheses. Any ligand can be modelled, given appropriate molecular mechanics parameters. The accuracy of the simulation is limited by the accuracy of the underlying MD forcefields. In this work, we used an implicit solvent model, which speeds the simulations and simplifies the binding problem a little, however, these models have limitations for modelling protein structure and binding. Explicit solvation can straightforwardly be included in iMD-VR; this simply increases computational cost (which would reduce responsiveness for large systems). In cases where specific solvent molecules are involved in binding, use of an explicit solvent representation may be preferable.

iMD-VR allows the user to 'step inside' the SARS-CoV-2 Mpro and manipulate its structure and interactions – and dynamics - in atomic-level detail. This allows the user to perceive ligand binding in three dimensions and to interact with molecules in an intuitive way, similar to how people interact with macroscopic objects. It is a better interface for molecular modelling tasks than traditional screen/mouse-based methods. [20] We believe that such technologies will find widespread application in structure-based drug design [61], in other molecular modelling, design and simulation applications, and in education. [21] iMD-VR should be directly useful in ongoing efforts to develop Mpro inhibitors as potential antivirals against COVID-19, especially as others look to crowd-source the problem. [223]

Narupa, the software framework that we have developed, is open source and uses commodity VR hardware, which is widely accessible. [20, 21, 61, 85] It can therefore readily be used. We make our Mpro simulations here freely available; these can be used for ligand discovery and structure-activity studies for SARS-CoV-2. They run straightforwardly on a suitably configured laptop computer. In future work, we will aim to have these simulations available via the cloud, such that anyone with a compatible VR headset can easily access them. We note that the cloud also offers the possibility of virtual collaboration and distributed worked via iMD-VR. We encourage others to use these potentially transformative tools and believe that they will be widely useful.

4.5 Supplementary Materials

Supplementary material for this chapter is available at `https://pubs.acs.org/doi/suppl/10.1021/acs.jcim.0c01030/suppl_file/ci0c01030_si_001.pdf`

CHAPTER 5

DESIGNING AND EVALUATING SONIFICATION STRATEGIES FOR iMD-VR

This chapter was developed with several other contributors and is adapted from a manuscript we all collaborated on. I developed and implemented the custom non-bonded interaction energy force field used in the sonification protocol (Sections 5.1 and 5.2), and also designed the docking tasks (see Chapter 3 for more detail). Myself and Alex Jones jointly designed, carried out and analysed the results of the feature sound feedback session and sonification evaluation session (Sections 5.3.3 and 5.4). Alex Jones, Tom Mitchell and Joseph Hyde designed and carried out the sonification design workshop (Section 5.3.2), performed analysis on the results of the design and feedback workshops to determine the final design principles (which is not detailed here), and implemented the sonification engine in the iMD-VR docking simulations. Simon Bennie and David R. Glowacki provided their knowledge and expertise towards this work.

5.1 Introduction

The plucking of a guitar string can be modelled with a simple harmonic oscillator, where it vibrates around an equilibrium and swings between two positions above and below that point; assuming perfect conservation of energy, as the string moves away from the most stable position, the resulting strain will pull it back in the opposite direction, and vice versa. Similarly, this behaviour is not unlike how interactions between atoms are modelled in molecular mechanics force fields, where bonds and interatomic interactions will oscillate around an optimum distance. [127] The potential energy function of a chemical system, which is accounted for in many MD force fields, is calculated as the sum of the energy of (i) all bonds, (ii) all bond angles, (iii) all bond dihedrals, and (iv) all non-bonded energy terms. The final component, the non-bonded energy

term, is the sum of two components, the Lennard-Jones and the electric potential of all atom interactions in a system. The Lennard-Jones potential is modelled using Eq. 5.1.

$$V_{LJ} = \sum_{i=1}^{N} \sum_{j=i+1}^{N} 4\varepsilon[(\frac{\sigma}{r_{ij}})^{12} - (\frac{\sigma}{r_{ij}})^{6}] \tag{5.1}$$

Where ε is the minima of the potential well, σ is the interatomic distance at which the potential is zero, and r_{ij} is the distance between two atoms, i and j, and N denotes the total number of atoms in a system.

Similarly, the electric potential is modelled using Eq. 5.2.

$$F = \sum_{i=1}^{N} \sum_{j=i+1}^{N} k_e \frac{q_i q_j}{r^2} \frac{1}{78.5} \tag{5.2}$$

Where k_e is Coloumb's constant (8.9876x10^9 kg·m^3·s^{-4}·A^{-2}), q_i is the partial charge of atom i, q_j is the partial charge of atom j, r_{ij} is the distance between the two atoms, i and j, and N denotes the total number of atoms in a system. Additionally, in order to account for the dampening effect that water molecules have on an electrostatic interaction, the whole term is multiplied by a solvent dielectric constant of 78.5 $^{-1}$ (this value was taken directly from protein-ligand simulation modelled with the Amber14 force field and OBC2 water model). [213, 215]

Eq. 5.3 shows the total non-bonded interaction energy, which sums the Lennard-Jones and electric contributions modelled by Eqs. 5.1 and 5.2 respectively. As an example of how non-bonded interactions can be modelled, the parameter terms from the Amber 14 force field [213] can be taken from the backbone oxygen of alanine (atom i) and the backbone amide hydrogen of alanine (atom j) and substituted into Eq. 5.3, the form of which can be found in Fig. 5.1.

$$E(r) = 4\varepsilon[(\frac{\sigma}{r_{ij}})^{12} - (\frac{\sigma}{r_{ij}})^{6}] + k_e \frac{q_i q_j}{78.5 r^2} \tag{5.3}$$

Similar to way a string oscillates, the non-bonded interaction will swing in the potential well of the function (in the case of Fig. 5.1, the hydrogen bond distance is modelled to vibrate around 0.22nm with a minimum energy of -1.47 kJ·mol^{-1}). If we know the input parameters of atom pairs ahead of time, we can understand which interatomic distances correspond to an optimal non-bonded interaction energy, and which indicate that an interaction is close to being formed (or not at all). As such, some indication (e.g. sound) could be used to signify that a non-bonded interaction is vibrating at the optimal distance. With further development, this could be used to convey meaningful information to a user attempting to establish a ligand binding pose, as in Chapters 3 and 4. This chapter describes a protocol for designing sounds which represent changes in molecular data features, including the non-bonded energy of atom pairs, and their implementation into an iMD-VR simulation. Expert sound designers, who have no familiarity

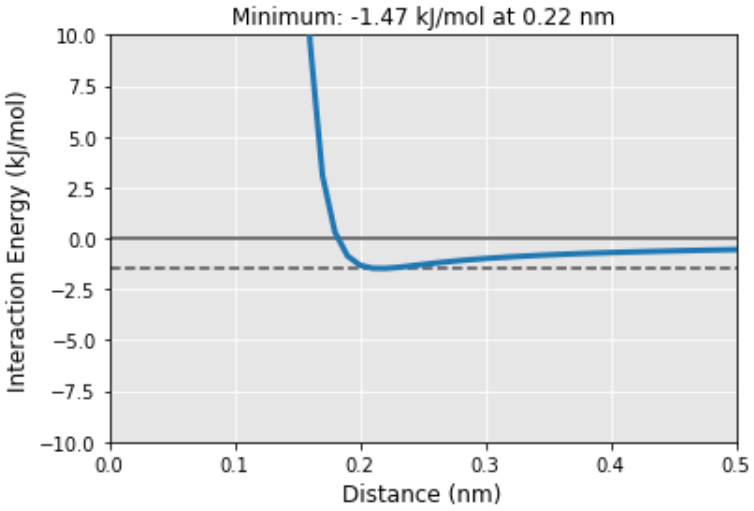

Figure 5.1: **Example non-bonded interaction potential**. The non-bonded potential of a hydrogen bond between the backbone oxygen and amide hydrogen of alanine, using parameters taken from the amber 14 force field. [213] The optimal distance that the interaction would oscillate around, and the corresponding energy at said distance, is given at the top of the graph.

with physical chemistry, were recruited to design the sounds, which were initially evaluated by domain experts listening and denoting how they think the change in the chemical feature is being represented. Design principles were taken from the sounds participants found the most intuitive and used to create new sonifications of the data features, which were then implemented into three protein-ligand iMD-VR simulations. The completed iMD-VR framework was then further evaluated in a study in which participants were asked to establish a protein-ligand binding pose using either (i) visuals and sound or (ii) visuals alone to guide them.

5.2 Selection of Chemical Features

Previous molecular sonification studies, which were integral in guiding this work, have highlighted example features for the sonification of chemical data. [213, 224] These include:

- *Surface complementarity*, the optimization of interatomic distances between two protein complexes.
- *Hotspots at the interface*, particular interactions which contribute towards the binding free energy.
- *Surface collisions*, the number of physical collisions between atoms on the surface of two proteins.

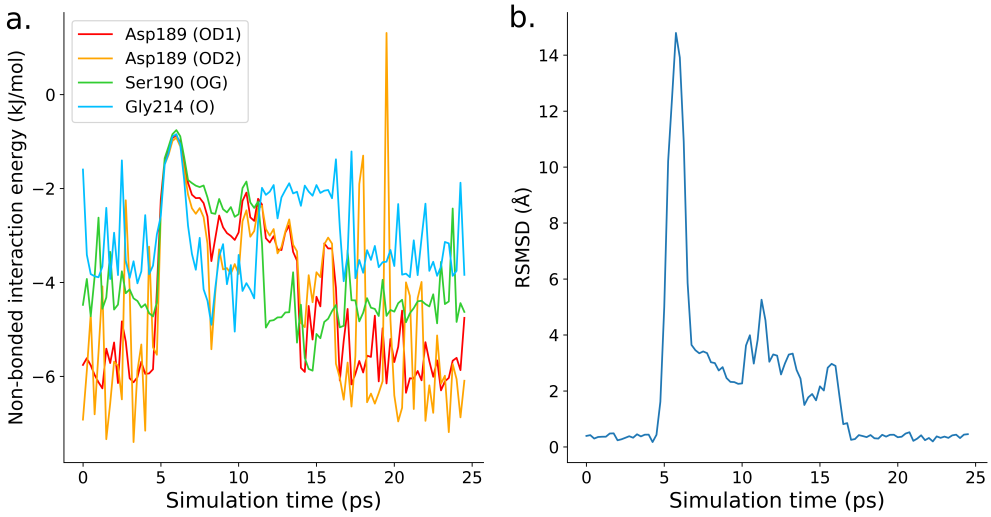

Figure 5.2: **Comparison of two methods of analysing an iMD-VR trajectory of benzamidine being undocked and redocked into trypsin**. For context, at around 5 ps is the point that benzamidine is pulled out of the binding pocket, and 16 ps is the point at which the original bound structure is re-established; between these two points represents the ligand being deliberately bound incorrectly by the iMD-VR user. (a) Plot of how the non-bonded interaction energy changes over the trajectory. This is calculated across four sets of atom interactions between the benzamidine and residues in the benzamidine binding pocket (the interaction sets are shown in Fig. 5.3, which the colours used correspond to). (b) Compared to the benzamidine heavy atoms in the starting bound structure, plot of the RMSD of benzamidine throughout the trajectory.

- *Electrostatic energy of the complex*, the electrostatic interaction energies between atoms (i.e. the electric potential component of the non-bonded interaction energy term of the potential energy).

- *Van der Waals energy of the complex*, the van der Waals interaction energies between atoms (i.e. the Lennard-Jones component of the non-bonded interaction energy term of the potential energy).

- *Atomic positional fluctuations*, known as B-factors which are drawn directly from experiment and reflect how much atoms fluctuate around an average position.

Although these features are more specific to protein-protein interactions, the principle of highlighting molecular data features as candidates for sonification can be applied to binding a ligand into a protein binding pocket. Three molecular data features, non-bonded interaction energy, interatomic distance and potential energy, are described in Sections 5.2.1-5.2.3.

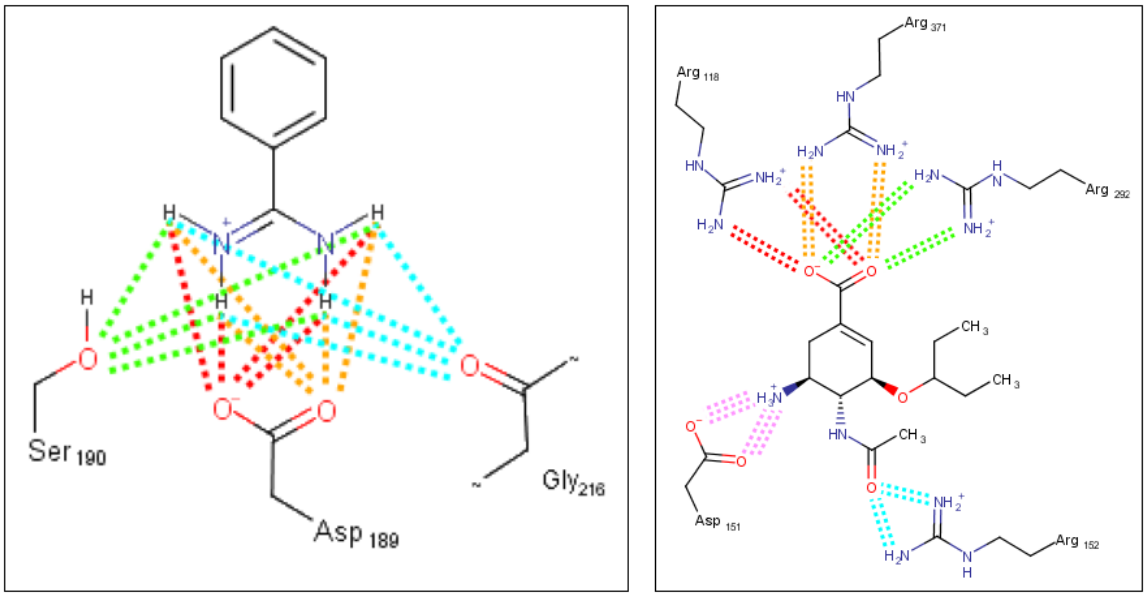

Figure 5.3: **Hydrogen bond interaction sets for two protein-ligand systems**. (left) Four interaction sets between an amidine group and the trypsin binding pocket, each denoted by a separate color. (right) Five interaction sets between oseltamivir and the neuraminidase active site, each denoted by a separate color. Where several parallel lines are drawn, each single line represents an interaction to an individual hydrogen.

5.2.1 Non-bonded interaction energy function

Non-bonded interactions are thought to be an essential component of the free energy of binding - concurrently, these interactions are thought to be significant in many kinds of biologically-relevant protein systems. [225–227]

By isolating out the key hydrogen bonds a ligand forms to a protein during an iMD-VR session, and modelling them using the non-bonded interaction term (Eq. 5.3), sound can relay whether an interaction is not formed at all (as the non-bonded interaction will be approximately zero and slow-changing), is formed optimally (as the non-bonded interaction energy will be close to the minima shown in Fig. 5.1), or is otherwise partially formed. A trajectory of benzamidine being unbound and rebound to trypsin was generated using iMD-VR where, on re-entry, the ligand was deliberately put into several non-optimal docked configurations. Across this trajectory, Fig. 5.2a shows the total non-bonded interaction energy of the four amidine nitrogens of benzamidine interacting with (i) OD1 of Asp189, (ii) OD2 of Asp189, (iii) OG of Ser190, and (iv) O of Gly214 - each of these interaction sets are shown in Fig. 5.3. Only at the end of this trajectory, when the user finally docks benzamidine correctly, does the energy of all four sets of interaction return to the baseline state, otherwise, at least one interaction is at a higher energy than it should be.

5.2.2 Interatomic distance function

A limitation of the non-bonded interaction energy function it is asymptotic to y=0, meaning it can only relay changes to an iMD-VR user once the ligand is in close proximity to the protein binding site. RMSD has been identified as a metric for understanding whether a binding pose has been reformed in iMD-VR where (i) an optimal reference pose is known and (ii) the protein is in a similar conformation to a known complex structure. [61] In particular, it is shown to be highly sensitive to whether or not the ligand is located in the protein binding pocket; unlike the non-bonded interaction function, the most rapid shifts in RMSD is when the user is steering the ligand to or away from the binding pocket. Conversely, although RMSD can detect large-scale movements of the ligand, it does not convey specific structural information to the user, in that alone it can only say how far off a pose is from a reference, not whether it is stable (Fig. 5.2b). However, as the relationship between RMSD and moving the ligand away from the binding pocket is not asymptotic, and therefore retains sensitivity to an iMD-VR user's inputs regardless of where the ligand is located, it can act as a 'warmer-colder' gauge as iMD-VR users move the ligand through the simulation space and towards the binding pocket. As this work is not concerned with curating specific atomic distances, instead it focuses on measuring the overall distance between the ligand and protein binding pocket, for clarity, RMSD will henceforth be referred to as the interatomic distance.

5.2.3 Potential energy function

Both the interatomic distance and RMSD functions are specific to the state of the ligand. Inversely, the potential energy - which is inherently calculated by the MD engine as it runs - can tell the users about the overall state of a system, including relative atomic movements, undesirable conformational states, molecular bond strains, and collisions. In particular, this can act as an indication that the iMD-VR user has caused perturbation to the structure of the protein. However, as it is calculated using parameters from potentially thousands of atoms, it will include a lot of noise, therefore, it is potentially only sensitive to extreme perturbations of the system by the user.

5.3 Design Workshops

5.3.1 Participants

Four expert sound designers were recruited to conceptualize how sound can be mapped onto the three features outlined in Section 5.2 as they increase or decrease in value. The participants were all male, between the ages of 30 and 50, and were incentivised to participate with a payment of £50. A summary of the four sound designers relevant experience and the sound design tools they used can be found in Table 5.1.

Sound Designer ID	Sound Design Experience	Sound Design Tools
SD1	Acousmatic composer and audio-visual performer	Ableton Live and Max for Live
SD2	Film and television	AVID Pro Tools and puredata
SD3	Muscician, designer and creative technologist	Teenage Engineering OP-1
SD4	Gaming and VR	FMOD, GRM Tools Plugins

Table 5.1: **Sound designer information**. Participant IDs, sound design backgrounds and a summary of tools used for the four expert sound designers recruited to partake in the sonification design workshop.

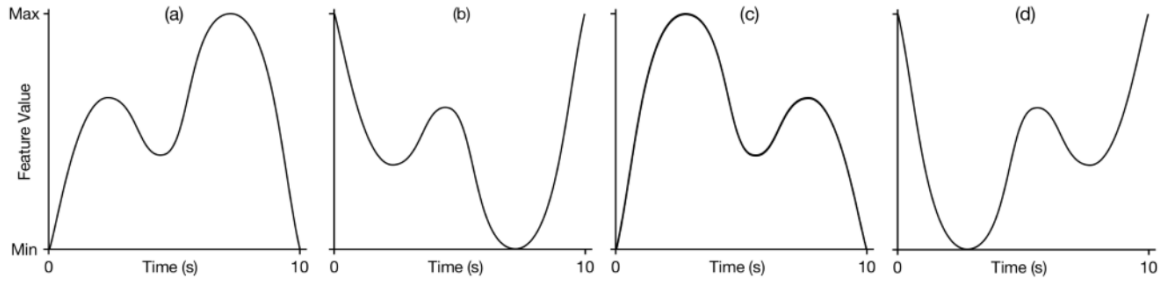

Figure 5.4: **Virtual feature value trajectories where the value shifts between an arbitrary range over an arbitrary timescale**. Plots were generated by taking a single trajectory and performing (a) no axis flipping, (b) an x-axis flip, (c) a y-axis flip, and (d) an xy-axis flip. This was done to encapsulate a range of changes in the virtual feature, whilst retaining a comparable degree of challenge.

5.3.2 Procedure

Fig. 5.4 shows a series of virtual feature trajectories (where the value shifts between an arbitrary value over an arbitrary range), showing how we might expect each of the three data features outlined in Section 5.2 to change during an iMD-VR simulation. Chiefly, the curves are designed to encapsulate: (i) movement of a feature from a global minimum to a local minimum, (ii) movement of a feature from a local minimum to a global minimum, (iii) rapid movement of a feature from a low value to a high value, (iv) rapid movement of a feature from a high value to a low value, (v) movement of a feature between minima with low, medium and high barriers.

The workshop was split into two individual sessions, totalling four hours. For each session, the participant was invited to design, create and discuss a series of 10 second auditory representations of the graphs shown in Fig. 5.4. Plots were distributed amongst the four participants to ensure a lack of carryon effect between designing different sounds and that all feature changes represented by the plots were designed in equal measure. Once both sessions were finished, the participant was asked to select the most effective auditory representation for each data feature; these sounds (12 in total) are used in a subsequent evaluation experiment, described in Section 5.3.3. More detail on the two sessions is given in Section 5.3.2.1.

5.3.2.1 Session One

Participants were given a design brief which asked them to design the features with no underlying understanding of molecular physics given. Instead, these features were described to them in more colloquial terms that a non-expert in physical chemistry could easily understand: Potential energy, non-bonded interaction energy, and interatomic distance were labelled as *energy*, *attraction (as opposed to repulsion)*, and *distance* respectively. Overall, an hour was allocated to this session.

5.3.2.2 Session Two

The second session of the workshop began with a 20-minute exercise which allowed the sound designers to conceptualize the relationships between the data features described in Section 5.2 and the subsequent effect changing them can have on a molecular system. A researcher with an academic background in chemical physics ran a closed-eyes experiment where each sound design expert was given two bipolar magnets and invited to feel the attractive and repulsive forces between them as they changed their relative orientation. The invisible forces between the magnets were then described as governing each of the three features: As a whole, the 'system' between the two magnets wants to have a low overall energy, so the magnets will try to align themselves along opposite poles: this invisible attractive force is why one alignment is favoured and the other is repulsed as a correct alignment corresponds to a lower overall energy. The distance between them governs the strength of the interaction - as the magnets are pulled closer together, the user would either feel a stronger pull or push between the them, whereas this got noticeably weaker as they were pulled apart. Holding two oppositely-charged poles closer together corresponds to a stronger physical attractive force and lower overall energy (and vice versa). Overall, two hours was allocated to this session, not including the 20 minute briefing exercise.

5.3.3 Feature sound feedback session

A second feedback session was designed to assess the 12 selected sounds from Section 5.3.2 and identify which of them best represent each of the features to an audience with a background in physical chemistry. Sound designers were chosen for the first session as they are able to quickly and effectively conceptualize molecular features as sounds, however, previous work has demonstrated that this does not always lead to a more intuitive sound design to the end-users. [228]

12 participants (6 male, 5 Female, 1 prefer not to say) from a molecular physics background (2 MSc students, 4 PhD students, 5 post-doctoral researchers, 1 faculty staff) volunteered to participate in the listening study. Participants were aged 22 to 54, with no reported hearing impediments. No incentive was offered to participants.

5.3.3.1 Procedure

Each participant was played the 12 sounds one by one, given a blank axis and instructed to draw how they perceived the data feature to change after the clip is played. Although each feature was assessed in turn, the order of each of the four corresponding sounds was randomized for each participant. Participants were made aware of the data feature which was being represented in each section. Each sound was played three times to the participant before they were given a chance to hand-graph it.

For each of the three features, after listening to the four sounds, a semi-scripted interview was conducted with the following questions as points to prompt further discussion from:

- Which auditory representations did you find the clearest, and why?
- Which auditory representations did you find least clear, and why?
- Do you have any other comments regarding the sounds?

5.3.3.2 Analysis of hand-drawn graphs

Rather than allowing participants to select the correct feature shape from a series of pre-drawn graphs, pen and paper was selected as the assessment tool as it affords a more organic representation of how the sounds were perceived (while also eliminating false positives from a correct guess). However, the major drawback of hand drawings is that, ultimately, the results are inherently subjective.

In order to understand more quantitatively how well each sound was understood by participants, each drawing was scanned into the computer and overlaid onto the original virtual feature trajectory that each sound was designed from (with no rescaling; the blank graph that participants drew on had the same proportions). As an example, Fig. 5.5 shows the 12 hand-drawn responses from each of participants for the potential energy sound created by sound designer 4 (SD4).

The original curves were given to the sound designers in order to encapsulate specific changes throughout the virtual trajectory, described in Section 5.3.2. With reference to this, the hand-drawn plots were assessed by asking the following questions about how the sounds were interpreted by the users:

Polarity Did the participant correctly understand that the feature started at a high value and decreased, or a low value and increased? For example, graph A1 of Fig. 5.5 shows understanding the potential energy started at a high value, dipped, before returning to a high-energy state.

Peaks/Troughs Did the participant correctly identify two peaks or troughs as the feature changed? For example, graph 2B of Fig. 5.5 shows understanding that two minima was being represented by the sound.

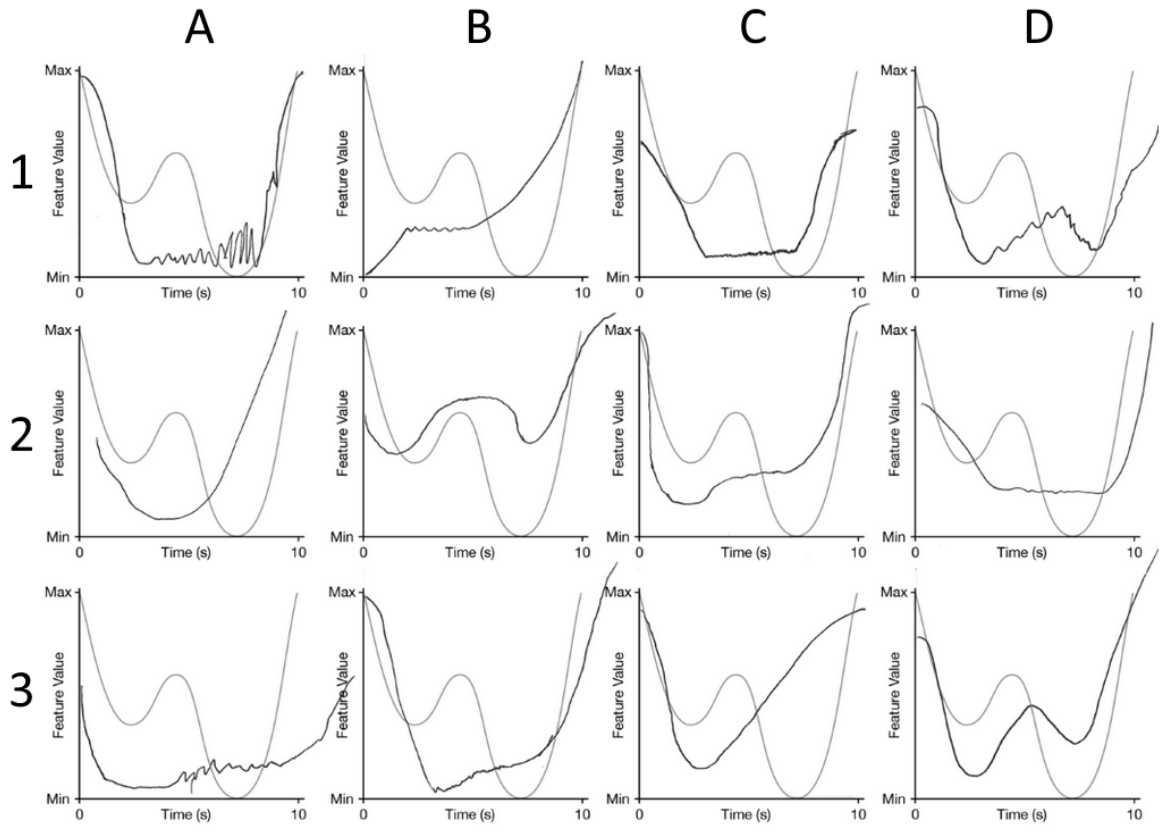

Figure 5.5: **Example hand-drawn participant responses**. Hand-drawn responses (black) produced by all 12 participants in response to the Potential Energy sound created by sound designer 4 (SD4). The original curve supplied to the sound designer is shown in grey for comparison.

Magnitude If more than one peak was detected, did the participant correctly identify the relative height differences them? For example, graph 3D of Fig. 5.5 shows an incorrect understanding that the first minima is lower in energy than the second.

Notably, smaller peaks along a larger trend (for example, graphs A1, D1, and A3) were interpreted as the participant trying to represent noise and not counted as individual peaks themselves; only larger scale shifts were included in this analysis. Based on the above three criteria, the responses from each participant for each sound was grouped together based on having a similar interpretation. As an example, for the responses in Fig. 5.5, the graphs were grouped into four categories:

1. (n=5) Participants got polarity correct, however, all drew only one peak. Three thought peak was prolonged.

2. (n=3) Participants got polarity correct. Drew correct number of peaks. Detected small change in height of peaks (not very detectable), but in wrong direction.

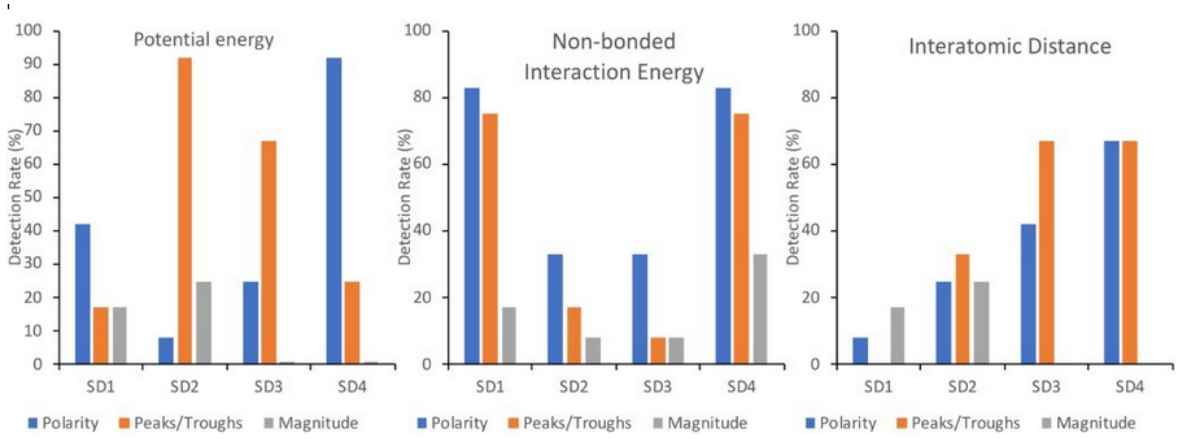

Figure 5.6: **Summary of results from sound design feedback session**. For each of the 12 designed sounds representing a chemical feature, detection rates for polarity, peaks/troughs, and magnitude.

3. (n=3) Participants got polarity correct. Only drew one peak, but did detect that the sound doesn't return back to higher until end.

4. (n=1) Participant got polarity incorrect, but similar to above groups, detected that sound was flat before sharply returning to positive.

One researcher performed this analysis, from which it was possible to see which sounds enabled perception of the three changes throughout the virtual trajectory. For example, of the 12 sounds shown in Fig. 5.5, it can be stated that participants understood the intended polarity of the sound, however, they had less success with detecting that there were two peaks and, furthermore, none were able to correctly identify the magnitude of the energy barrier separating the minima. The analysis was repeated for each individual sound; a summary of how well each feature was detected for the each of the 12 designed sounds can be found in Fig. 5.6.

5.4 Evaluation session

Based on the analysis detailed in Section 5.3.3.2, alongside qualitative analysis of participant interviews, general principles for designing sound representations of the three data features were determined. In short, the most easily intuited sounds for each feature were chosen by whether the feature sound feedback session participants (i) detected the correct virtual feature trajectory shape and (ii) self-reported liking the sound design in interview. By going back to how the expert sound designers described their design process, the underlying ideas behind the sounds were then extracted. Subsequently, these were used to design new sonified representations of the three data features. The new sonification framework was applied to a series of protein docking iMD-VR experiments [61] and a user study was conducted. 12 molecular physicists from the 2019 CCP-BioSim workshop volunteered to participate in the study (6 female, 6 male; aged 25 to

60). Participants were divided equally into an Sonification (S) group, who could hear the feature sounds during the experiment, and a No Sonification (NS) group who could not.

5.4.1 Procedure

Participants were asked to complete three iMD-VR docking tasks in total, each based on a protein-ligand complex structure downloaded from the Protein Data Bank: (i) starting from a correctly docked position, undocking and redocking benzamidine from trypsin (PDB: 1S0R), (ii) starting from an undocked position, docking indole-amidine into trypsin (PDB: 2G5N), and (iii) starting from an undocked position, docking oseltamivir into neuraminidase (PDB: 2QWK). Each task is based on those described in Chapter 3, corresponding to the expert and novice tasks for trypsin, and the expert task for neuraminidase. Each of the ligand structures, alongside their key hydrogen bonding interactions, is shown in Fig. 3.2. For each task, rather than calculating all non-bonded interactions between the ligand and protein, atom pairs which contribute to hydrogen bonds were isolated (as this reduces noise in the function). In order to limit the number of audio channels required, these hydrogen bonds were grouped according to which residue they were formed to and calculated as an average (these hydrogen bonding interaction groups can be found in Fig 5.3, note that benzamidine and indole-amidine used the same grouping). Tasks were designed to have increasing complexity, in that the first task (benzamidine and trypsin) showed the correctly docked structure to the participant via a 'trace representation' (more detail on this can be found in Chapter 3). The second task (indole-amidine and trypsin) does not show the correctly docked structure directly, but asked the same non-bonded interactions be formed as the previous task, only with a larger molecule, so users are more reliant on both their domain knowledge and auditory/visual feedback. The third task (neuraminidase and oseltamivir) is the most challenging as it gives no information about how the ligand should be docked, thus requiring the participants to explore different binding conformations based on their own intuition. Each task had a time limit of five minutes, however, once participants indicated that they thought a reasonable binding pose had been achieved, the task could be ended. As all three tasks were based on simulations described in [61], details on simulation parametrization and set up can be found there (or see Section 3.2.3). Simulations used the same iMD-VR representations as the previous work, except trace atoms were removed where relevant (tasks 2 and 3).

Before commencing with the three docking tasks, participants were provided with a verbal description of how to use the iMD-VR interface. After this explanation, users were placed into a simulation of buckyballs and given a chance to practice with the controls. Once participants indicated they understood the ways they could interact with the iMD-VR simulation, they were moved onto the three docking tasks. Additionally, members of the S group were also given a description of which features would be sonified, and verbal instructions on how to interpret the mappings, but no explicit instructions to use sound when completing the docking tasks.

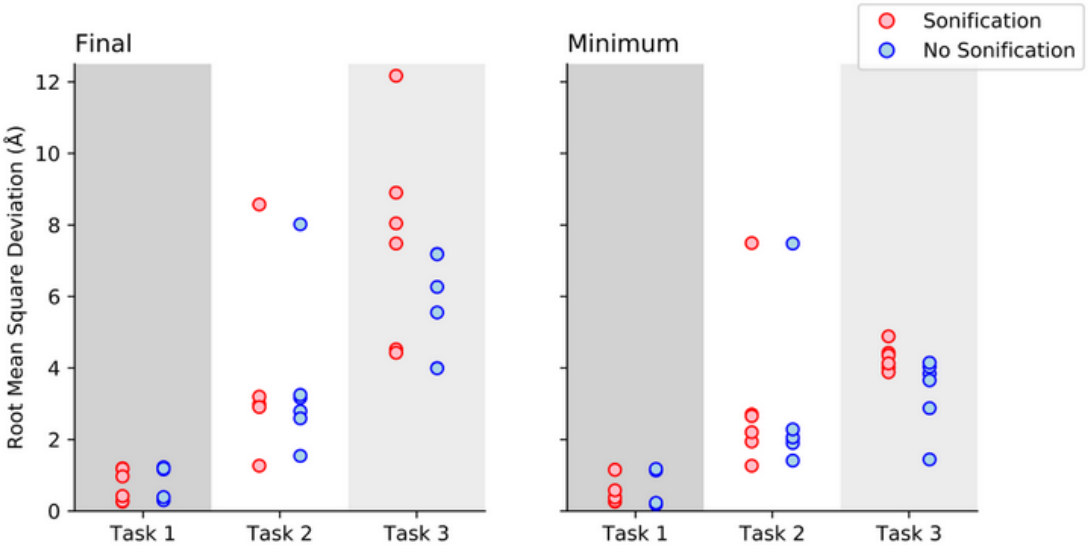

Figure 5.7: **Participant results for sound evaluation session**. Final and minimum RMSD values for the Sonification (S) and No Sonification (NS) groups for docking benzamidine into trypsin (task 1), docking indole-amidine into trypsin (task 2), and docking oseltamivir into neuraminidase (task 3). More detailed descriptions of each of the three tasks can be found in 5.4.1. The S group is denoted with red dots, and the NS group is denoted with blue dots.

5.4.2 Results

The following data was gathered from each participant-generated iMD-VR simulation. Compared to the starting structure, the minimum achieved RMSD throughout the task was recorded to gauge how close the participant got to the correct answer overall. Additionally, the RMSD from the final recorded frame was calculated to gauge how close participants were at the end point of the simulation. Ideally, a participant would generate the correct, stable bound configuration and know to end the task at that point, leading to a low degree of variance between the corresponding two data points. A plot summarizing the RMSD data is shown in Fig. 5.7.

5.5 Discussion and Conclusions

This chapter presents a participatory design and evaluation method where both sound design and domain experts are engaged to derive design principles for the mapping of sounds onto data features in physical chemistry. The aim was to create sonified representations which were both transparent and meaningful for the intended audience. In particular, this approach helps ensure the sound mapping onto a data feature considers both the intuitiveness and aesthetic elements of the composition. Compared to conventional and *ad hoc* methods, this work presents a more methodologically robust means of sound design as the process and rationale for choosing features is clearly stated; although these design choices will always have subjectivity baked in, a greater

degree of reproducibility is afforded.

The design principles for sonification of molecular data features is assessed in a small-scale study (n=12) in which two groups of participants, Sonification and No Sonification, were asked to complete a short series of molecular docking tasks in iMD-VR. Both groups were able to successfully locate the binding pocket in each task and recreated the original binding pose for the first two, which demonstrates the success of an iMD-VR interface for molecular docking where guidance is given to what interatomic contacts need to be formed, but less so where this information isn't clearly stated. As it stands, whether sonification proffers any advantage for molecular docking in iMD-VR remains to be demonstrated. Achievement for tasks 1 and 2, where users had some guidance to the correct solution, was consistent between the two groups. However, overall, the NS group found the lower minimum RMSDs for Task 3. It should be noted however, that the groups were not strictly controlled for having similar levels of expertise, and that the aim of having two groups was to gain an understanding of task performance with no sound (as to not falsely conclude that sonification of data features is explicitly leading participants to the correct answer); we cannot yet make any statement on whether there are any advantages or disadvantages to the sonification of iMD-VR simulations.

A future study could more rigorously test the sonification framework. One limitation of this work is the high task load and limited time frame given for participants to learn both how to use the iMD-VR interface and to interpret the sound mappings. In post-task interviews, participants in the S group can be quoted as saying:

S4: *"I think I did but because of lack of using this thing I wasn't able to process or implement it as well as I did visually because I'm used to these interactions, so if you show me I can tell you about them but with the sound I still need more experience."*

S5: *"I wasn't too sure what the sounds meant – I was aware that there were sounds going on, but I didn't know if they were good sounds or bad sounds.... once I was getting closer, there was more of a ... it was going to a crescendo, but I didn't know what that meant."*

Although it was a deliberate design choice to not extensively coach users on how the sound designs should be interpreted, as we wanted to observe if the sonification was easy or difficult to understand, it may in fact be advantageous to provide more explicit guidance in future work. We anticipate sonification in iMD-VR as a long-term tool that can be familiarized with at a user's own pace (and could be personally customized by those who are more adept). While this initial user test does not show any overtly negative outcomes from using sonification - which is still an encouraging first step - the study design itself should be revisited to more explicitly answer the question of how sonfication can be effectively implemented in iMD-VR.

Another area for improvement is developing the sonification framework to be more easily generalized. Here, the customized force field requires you to define a set of non-bonded interactions ahead of calculation, thus requiring an understanding of what a 'correct' binding solution is. Similarly, the distance metric is derived from the RMSD, which is also reliant on having a pre-

defined binding pose for comparison. New targets of significant pharmacological relevance can emerge at any time [229], and iMD-VR can be potentially used as a strategic tool for intuitively finding key interactions between a ligand and protein binding pocket. In the context of evaluating docking in iMD-VR, pre-defined poses were an essential component of defining efficacy [61], however, sonification could be further developed to convey information to a user during an iMD-VR simulation where the 'ideal' solution is yet to be understood. In initial tests of how to effectively use sonification in iMD-VR, known binding poses should still be used, however, developers should be cognizant of how they can be extended outside of these specific use-cases, towards using iMD-VR as a predictive tool for drug design.

CHAPTER 6

CALCULATING FREE ENERGIES FOR PROTEIN-LIGAND BINDING ALONG PATHWAYS SAMPLED IN iMD-VR

The data for this chapter was obtained in collaboration with another contributor, Kirill Zinovjev, who I am currently working on a manuscript with (which this chapter is been adapted from). Kirill performed the reaction coordinate definition, Umbrella Sampling, and Adaptive String Method analysis on the seven iMD-VR pathways, as well as calculating the estimates for computational sampling times given in Section 6.4, and writing Section 6.2.3. More detail on Kirill's contributions can be found in Appendix A. I created the seven unbinding pathways for benzamidine exiting the trypsin binding pocket in iMD-VR and performed more detailed structural analysis of the free energy data. David R. Glowacki provided his valuable expertise towards this work.

6.1 Introduction

Protein systems typically contain thousands of atoms. Owing to the number of degrees of freedom (3N – 6, where N is the number of atoms), the energetic landscapes of protein systems are typically high-dimensional. Given this large conformational search space, the system can enter a near-infinite number of states. Because of this, protein energetic landscapes are characterized as 'rugged' in nature: Instead of directly moving between two areas of conformational space (e.g. ligand bound to ligand in solvent), the system may need to instead first pass through a series of metastable states (each with their own energetic barriers surrounding them). Depending on the complexity of the system, this results in protein binding energetic landscapes which can take milliseconds or seconds on average to traverse. [230] As a result, simulating these processes during MD is inaccessible to even very sophisticated computer architectures unless a

biasing method is employed. Given the high number of degrees of freedom a chemical system can possess, it is standard to 'simplify' the system by selecting out a simple feature (e.g. an interatomic distance or a bond angle), known as a Collective Variable, and use it to represent changes occurring; so long as the CV is well-coupled to the process under study (e.g. using the distance between two atoms to signify bond formation), there is little need to consider other data in the system. Where using a simple feature is inadequate, a CV can also represent an ensemble of features or, alternatively, a collection of CVs can be used together. In practice, these descriptions can tell a biasing method which of the many degrees of freedom in a system should be explored, thus allowing sampling to be directed towards certain states or processes. Given the near-infinite number of ways a system can be reduced however, to be meaningful, CVs need to both capture and differentiate between the metastable states which occur during a given chemical process, furthermore, it is preferable that they follow a MFEP. [231] While low dimensional CVs for describing protein-ligand (un)binding can be intuitive to derive [153], it can be difficult to identify in advance meaningful CVs, particularly where complex protein motions need to be considered alongside a ligand entering or exiting the binding pocket. Chapter 3 describes how PathReducer [130] can be used to analyze VR generated ligand unbinding and rebinding pathways to create 2D and 3D descriptions of these processes, however, there is no exploration of whether these reduced pathways either (i) capture metastable states or (ii) follow a MFEP. Here, the utility of iMD-VR for producing a series of distinct unbinding pathways for a protein-ligand system (trypsin-benzamidine) is explored and these pathways are used as a means of intelligently guiding Umbrella Sampling to obtain an estimate of the free energy of unbinding.

Trypsin is a serine protease enzyme which catalyses the hydrolysis of peptide bonds via the His57-Asp102-Ser195 catalytic triad. Trypsin also has a secondary, negatively charged binding pocket, S1, which contains Asp189 and thus drives specificity to lysine and arginine (which are positively charged) by binding them during catalysis. [148] In order to inhibit trypsin, benzamidine blocks this secondary pocket by mimicking lysine or arginine, an interaction which is thought to be a primary driver of the binding process. [232] Benzamidine is a small molecule with only one rotatable bond that only needs to form a single electrostatic bridge with trypsin, therefore, inhibition has relatively fast kinetics - case in point, trypsin-benzamidine is frequently used to evaluate theoretical methods for characterizing ligand-protein (un)binding pathways, kinetics, and energetics. [60, 154, 233, 234] Alongside having been previously tested in iMD-VR [61], these features lend suitability to evaluating a protocol for generating free energies from iMD-VR generated unbinding pathways.

Based on trypsin-benzamidine having an easily-characterized binding mode, it may be tempting to intuit a two-state mode of bound and solvated, however, binding is thought to be facilitated by numerous metastable states along a series of different protein surface pathways. Short range, the unbinding of benzamidine to Asp189 is stabilized via water intercalation, allowing benzamidine to form longer-range interactions with S1 pocket residues as it dissociates. [149] Through

interacting with the residues surrounding Asp189, instead of directly pulling itself away from the S1 binding pocket, benzamidine can rotate itself as it rolls out of the pocket - potentially to the extent that the charged amidine group is pointing towards the solvent and the hydrophobic benzyl group is buried. [235, 236] Beyond the immediate dissociation with the S1 pocket, benzamidine is thought to exit trypsin through an ensemble of different pathways. Previous work has characterized several metastable states on the protein surface which benzamidine exchanges between as it unbinds, including one where the benzyl group intercalates between Tyr39 and Tyr151. [153] Additional independent studies also found this metastable state. [233, 237] Unbinding pathways have characterized benzamidine as being non-solvent exposed [153, 234, 238], indicating that it runs over the surface of trypsin as it unbinds. Furthermore, in the case of benzamidine entering the protein, longer range van der Waals interactions are thought to play a role in pulling benzamidine towards the S1 pocket. [237] Additionally, it should be noted that the conformational state of trypsin itself influences benzamidine unbinding. [136, 238]

In previous chapters, iMD-VR has offered a reliable tool for experts and novices alike to generate reversible protein-ligand binding and unbinding pathways. Here, this work is extended to show user-generated iMD-VR pathways can be used to estimate the free energy of unbinding. Specifically, iMD-VR is used to create a series of unbinding trajectories that are collapsed into six CVs. These six-dimensional pathway descriptions were then used as 'guess nodes' in Umbrella Sampling to obtain a free energy profile, with the further optimization of the nodes towards a MFEP using the Adaptive String Method. [239] Here, it is demonstrated that it is possible to calculate reliable free energies along user-generated iMD-VR pathways. Fig 6.1 shows a schematic for the workflow developed here.

6.2 Methodology

6.2.1 System parameterization and set up

Protein system preparation for iMD-VR is similar to previously described work. [183] Hydrogen atoms were added to the protein and ligand using the reduce module. Trypsin was parameterized with the Amber 14 forcefield [213], benzamidine was parameterized with the general amber forcefield (GAFF) in antechamber [214], and the solvent was modelled implicitly using OBC2. [215] Prior to simulating in iMD-VR, the structure was minimized and equilibrated. First, the structure was iteratively energy minimized four times, each stage using slowly decreasing degrees of positional restraint. 5 kcal·mol^{-1}·Å^{-2}, 2.5 kcal·mol^{-1}·Å^{-2}, and 1.25 kcal·mol^{-1}·Å^{-2} was applied to all backbone and ligand atoms for the first three rounds of minimization respectively, and no restraints were applied for the final round. Next, the system was heated by running 10 stages total of 20 ps of MD, starting at 0 K and linearly increasing the temperature by 30 K at each stage until a temperature of 298 K was reached (each step had a backbone and ligand atom restraint of 5 kcal·mol^{-1}·Å^{-2}). Finally, 8 rounds of 500 ps of MD with slowly decreasing backbone and ligand

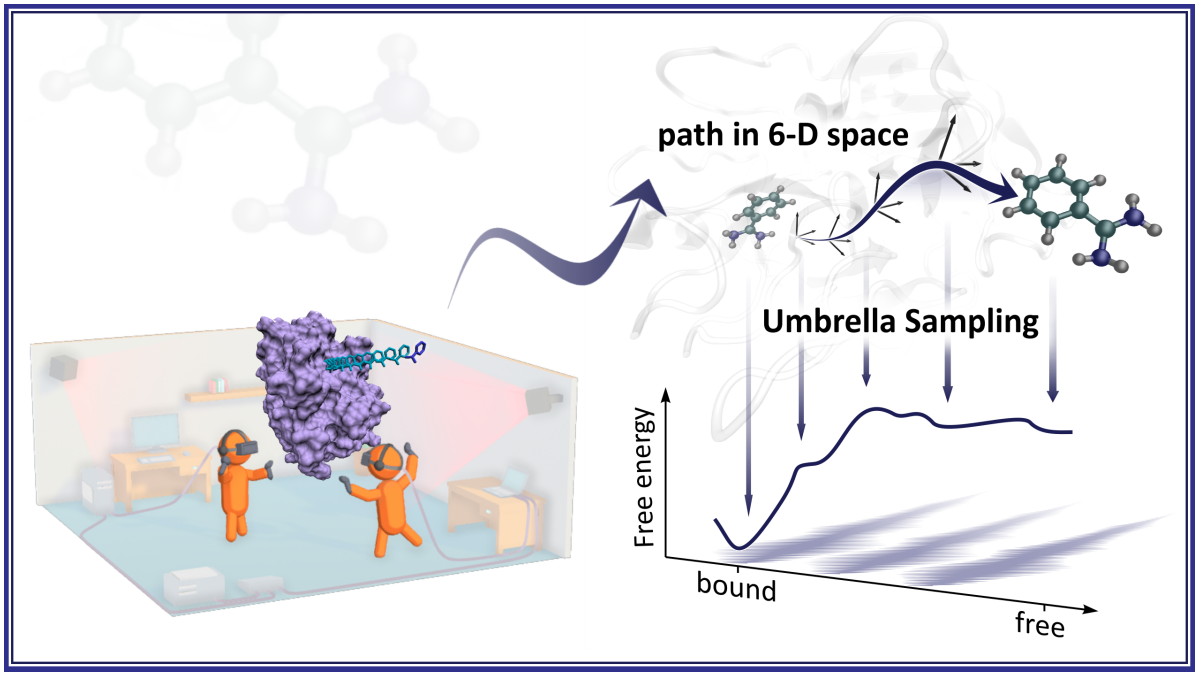

Figure 6.1: **iMD-VR to free energy pipeline**. Schematic showing the pipeline between creating a ligand unbinding pathway in iMD-VR, reducing the dimensional space to six CVs, and generating a free energy profile using Umbrella Sampling.

atom restraints were run to equilibrate the structure. Restraints were initially 5 kcal·mol^{-1}·Å^{-2} and halved after each step; once backbone restraints were below 1 kcal·mol^{-1}·Å^{-2}, the restraint atoms were relaxed to only alpha backbone and ligand atoms. The eighth and final stage had no restraints on the protein and ligand at all. All stages of minimization had a 20 kcal·mol^{-1}·Å^{-2} positional restraints on the calcium ion embedded within the trypsin structure.

Due to the introduction of artificially high forces during iMD-VR, a 500 kJ·mol^{-1} backbone positional restraint was applied to the trypsin structure during interactive simulations, and a 500 kJ·mol^{-1} positional restraint was applied to the calcium ion in the simulation. All other parameters were taken directly from the minimization MD. For all iMD-VR simulations, a temperature of 300 K was used with a timestep of 0.5 fs. Snapshots of the iMD-VR simulations were taken every 500 timesteps, equal to every 0.25 ps.

6.2.2 Generation of seven distinct unbinding pathways in iMD-VR

6.2.2.1 Starting coordinates

A minimized and equilibrated frame where benzamidine starts in the bound position was used as the iMD-VR starting coordinates. A user who is proficient in iMD-VR docking then proceeded to carefully manipulate the ligand so that it was extracted from the active site; this process was repeated seven times, each time steering the benzamidine molecule so that it takes a different

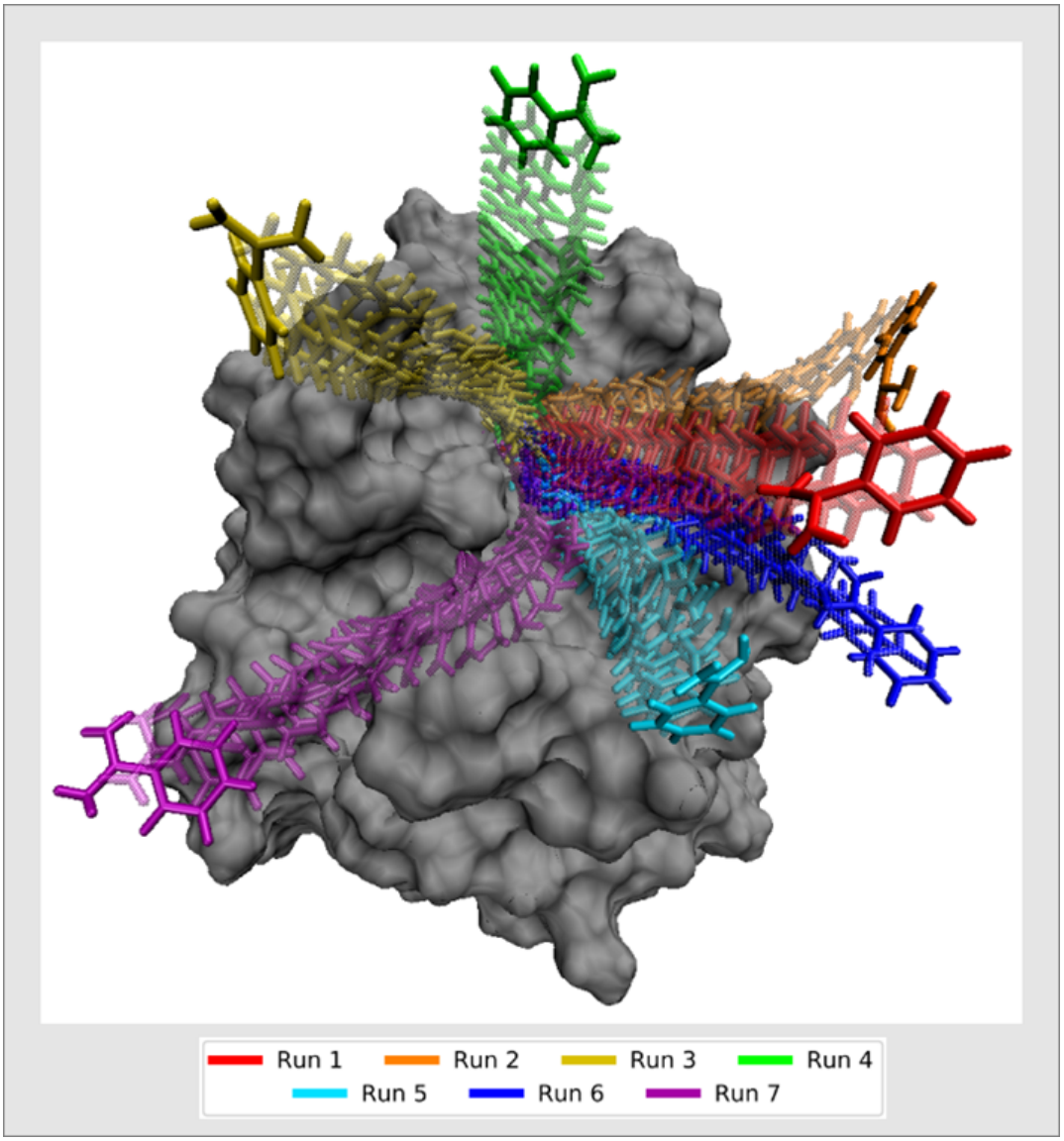

Figure 6.2: **Seven iMD-VR generated unbinding pathways**. Overlay of each of the seven iMD-VR generated unbinding pathways onto the structure of trypsin, showing the extent to which the surface was interactively explored. Each pathway has been assigned a unique colour.

path. Therefore, a total of seven different unbinding pathways were generated.

Additionally, a set of incorrectly-bound starting coordinates were generated using iMD-VR. Benzamidine was pulled out into the solvent area of the simulation and then replaced in the binding pocket upside down (so that the charged amidine group is pointing away from Asp189). From there, the user generated a pathway in which the incorrectly bound benzamidine was pulled out from the binding pocket.

6.2.2.2 Pathway descriptions

All iMD-VR generated pathways that used the correctly orientated benzamidine as starting coordinates are shown in Fig. 6.2.

Path 1 (Shown in red, Fig. 6.2) was the simplest. Here, no particular interactions were made with the trypsin surface, instead the ligand was pulled directly away from Asp189 and into the free space of the simulation.

Paths 2, 3, and 4 pulled benzamidine away from the catalytic triad and along the steep 'back wall' of the trypsin binding pocket (denoted as it is pointed away from the catalytic triad). Paths 2, 3, and 4 are distinguished from one another by the direction that the ligand is pulled along this 'back wall'. Orientating the protein as in Fig. 6.2, Path 2 steers the ligand to the right and towards Trp211. Inversely, Path 3 steers the ligand to the left, over Gln192. Path 4 continues to pull benzamidine straight across the 'back wall' of the protein binding pocket, straight over the disulphide bridge between Cys191 and Cys215.

Path 5 instead pulls benzamidine straight over the catalytic triad and continues to pull it in that direction until the ligand is in the free space of the simulation. Path 6 and 7 both mimic path 5 in pulling benzamidine over the catalytic triad, however, once the ligand is past the triad, these paths diverge in opposing directions. Path 6 pulls the ligand towards a surface groove formed between the loops containing Tyr59 and Tyr94, whereas path 7 pulls the ligand through the groove formed between the loops containing Tyr39 and Tyr151, therefore, these paths explored areas of chemical space close to previously established metastable states (S1 and S2 respectively in Buch et. al). [153] For path 6, the user ran the benzamidine over the grooves on the protein surface, whereas for path 7 the user deliberately pulled benzamidine through them.

6.2.3 Free energy calculations

Details of the protocol, including how the six CVs of the reaction coordinate are defined, can be found in Appendix A. Briefly, each pathway was reduced into six dimensional space and the free energy profiles along these CV pathways were calculated using the Umbrella Sampling method [63], which consists of running a set of simulations biased to different values of the chosen RC with harmonic biasing potentials and subsequent integration of the obtained sampling to recover the full free energy profile. The same setup and simulation protocol were used for all seven iMD-VR pathways. All the simulations were performed with the modified version of sander from AmberTools19. Generalized Born implicit solvation method was used to describe the water solution. 56 Umbrella Sampling windows were used. The initial structures for Umbrella Sampling windows were obtained by taking the closest snapshot from the iMD-VR pathway and running 1 ps MD, gradually increasing the force constant from 0 to the target value. 1 ns of sampling was acquired during production simulations. The resulting potentials of mean force were integrated using the WHAM procedure. [240] Additionally, the Adaptive String method [239] was performed on a path with the most favourable energy profile, as to try and optimize the

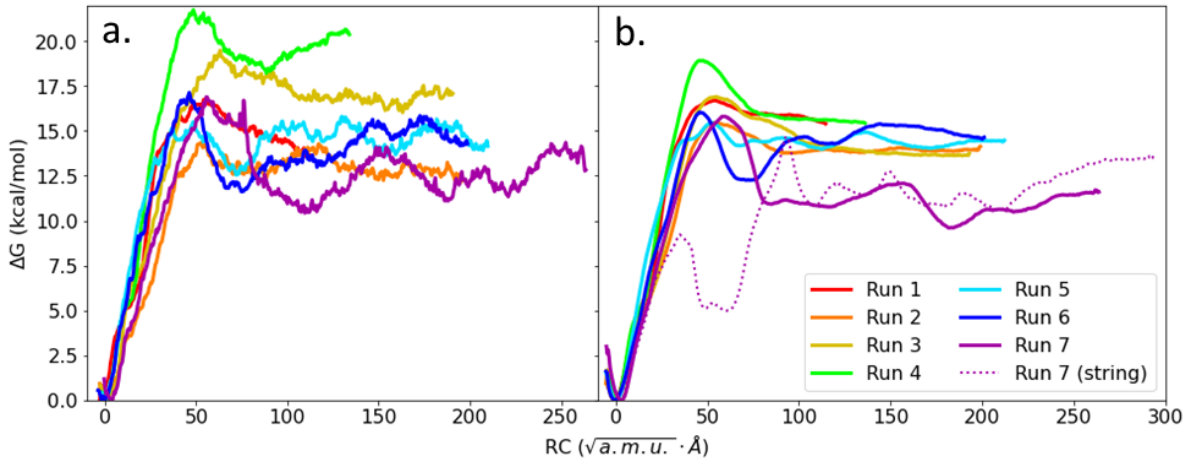

Figure 6.3: **Free energies calculated from iMD-VR generated pathways**. (a) Initial free energies derived using each of the seven free energy paths where sampling was limited (10 ps per run). (b) Free energies derived each of the seven free energy paths were sampling was more extensive (1 ns per run). The free energy of path 7 with optimization with the Adaptive String Method is also shown as a dotted line.

initial iMD-VR guess pathway towards a MFEP.

6.3 Results

6.3.1 Free energy calculations of seven distinct unbinding pathways

Fig. 6.3 shows the seven free energies calculated from each path using the Umbrella Sampling method. With limited sampling (10 ps; Fig. 6.3a), the pathways have some variance, especially at the point of the reaction coordinate which represents the ligand being in the free simulation space. However, with increased sampling (1 ns; Fig. 6.3b), although the unbinding routes show some slight variance, they mostly converge to a free energy difference between bound and unbound of around 15 kcal·mol^{-1}. The exception to this is path 7: although the barrier is similar to other paths, the energy past this maxima is notably lower, possibly because the user is close to a metastable area of the protein surface. [153] Additionally, path 7 is distinct from others as the user deliberately ran the ligand through grooves in the protein surface before returning it to the free simulation space, thus heightening the extent of protein-ligand interactions along the path. Although this path is more favourable, it should be noted that the free energy does not return to the same point as other paths, indicating a potential issue with complete sampling or convergence.

An initial free energy 'guess' required 10 ps of sampling per MD run (Fig. 6.3a), whereas the more converged pathways were sampled for 1 ns (Fig. 6.3b). We anticipate this method being used to screen a larger array of initial guesses from iMD-VR, therefore, focus should initially

be on gleaning initial insights before performing more extensive analysis on the paths which appear more favourable. The calculations presented here yielded 150 ps of MD per day using a single CPU, however, this implementation used unoptimized code. Modern GPUs however, can provide much faster MD sampling for larger systems (such as proteins) [241], so there is room for yet further optimization. While the initial iMD-VR trajectories do not adequately sample the available conformational space to calculate a free energy, combined with the Umbrella Sampling method, an initial approximation can be obtained (Fig. 6.3a). In this case, energy profiles obtained were found to be generally consistent, however, path 7 had a more distinctive energy profile. Subsequently, this path was further refined using the Adaptive String Method [239] to try and move the initial guess pathway provided by iMD-VR towards a MFEP, represented by the dotted line in Fig. 6.3b. More detail on this can be found in Section 6.3.2, and further details of the implementation of the Adaptive String Method can be found in Appendix A.

6.3.2 Characterization of MFEP obtained using the adaptive string method

Of each of the pathways, path 7 (shown in purple in Figs. 6.2 and 6.3) was found to have the most distinct free energy profile when evaluated with Umbrella Sampling, in that the energies are lower after passing over the initial energy barrier. In the case of path 7, this was noted to be of particular interest as the iMD-VR user was more deliberate when pulling benzamidine across the trypsin surface, pushing the ligand between the grooves on the protein surface which contain Tyr39 and Try151. Although this had the initial goal of testing whether free energy methods are sensitive to less carefully-generated iMD-VR generated paths, instead, the most favourable energy path was formed. As such, path 7 was selected for further analysis with the Adaptive String Method, the results of which are shown as the dotted line in Fig. 6.3.

While running the Adaptive String Method, representative states along the optimized pathway were taken, which were subsequently inspected to ascertain what interactions are formed as the ligand unbinds. Initially, as benzamidine is pulled out of the binding pocket there is a steady increase in the free energy, likely as the stabilising electrostatic contact is lost. However, closer inspection of the trajectory shows that the ligand rotates itself so that the amidine group more closely interacts with Ser190 while it exits (Fig. 6.4a). Next, the ligand passes itself from Ser190 to between the catalytic residue Ser195 and the carboxyl oxygen of Ser210; from here, it appears to interact with the catalytic triad, denoted by the local energy minimum at around 50 $\sqrt{a.m.u.} \cdot$ Å of the reaction coordinate (Fig. 6.4b). To dissociate with the catalytic residues, benzamidine leapfrogs over them, using the charged amidine group to 'hold' these residues as it passes over (Fig. 6.4c). Benzamidine then moves between the loops containing Tyr39 and Tyr151, before returning to the free area of the simulation (Fig. 6.4d) - notably, this transition has been observed in previous work as a viable path to exit. [153] Finally, as the ligand moves away from interacting with the protein surface to the free simulation space, there is a gradual increase in free energy, encouragingly, to the point that the other paths converged to. Additionally, where

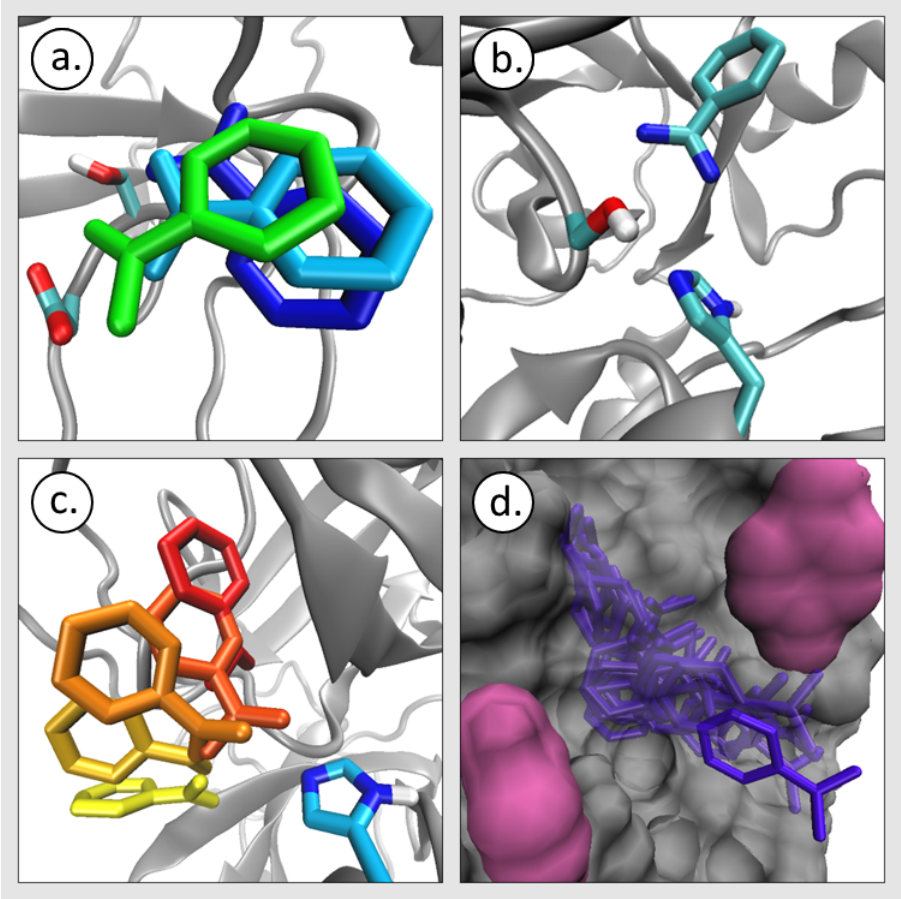

Figure 6.4: **A series of states sampled from the MFEP generated using string optimization for path 7**. (a) Showing benzamidine rotating itself away from Asp189 (b) Showing benzamidine with the amidine group directed towards the catalytic residues, His57 and Ser195. (c) Showing how benzamidine directs the amidine group towards His57 as it passes by it. (d) Showing benzamidine passing through the surface grooves that contain Tyr39 and Tyr151, coloured in pink.

other paths were quick to reach an energy indicating the ligand is no longer associated with the protein, this path does not reach this point until the end of the reaction coordinate, showing better surface exploration. Overall, the free energy profile remains similar when the Adaptive String Method is used, however, there is a divergence at around 40 $\sqrt{a.m.u.}\cdot$Å of the reaction coordinate and a distinctive local minimum is formed. When pulling benzamidine out of the iMD-VR pocket, the user was not especially conscientious about forming specific interactions with residues, instead, the focus was placed on the overall path taken out of the pocket. The guess nodes used in the initial Umbrella Sampling run likely did not adequately capture this minimum, however, with the addition of the Adaptive String Method, the interactions between benzamidine and the catalytic triad were presumably better captured.

6.3.3 Free energy of unbinding pathway starting from incorrectly bound benzamidine

In order to test whether this protocol is sensitive to less energetically-favourable pathways, the free energy of an unbinding trajectory which starts from incorrectly docked benzamidine was calculated (Fig. 6.5).

All free energies generated using this method are relative; the lowest energy state is at zero, whilst all other changes in energy are in respect to this point. Strikingly, unlike trajectories spawned from benzamidine in the correct orientation, this trajectory does not start at lowest energy point, instead, the minimum free energy is found at around 25 $\sqrt{a.m.u.}\cdot$Å of the reaction coordinate. Inspection of the states sampled which correspond to that point show that benzamidine has left the S1 pocket and the positively-charged amidine group is directed towards the catalytic triad. An observation noted in previous work docking benzamidine into trypsin using iMD-VR was that incorrectly bound benzamidine has a tendency to float out and get 'caught' on the catalytic triad. [61] As was implied by the previous iMD-VR experiment, the free energy profile shows the misdocked conformation is short-lived as it is energetically unfavourable (compared to being in the free space of the simulation), however, there is potential for instead forming a more stable complex with the catalytic triad as it spontaneously exits.

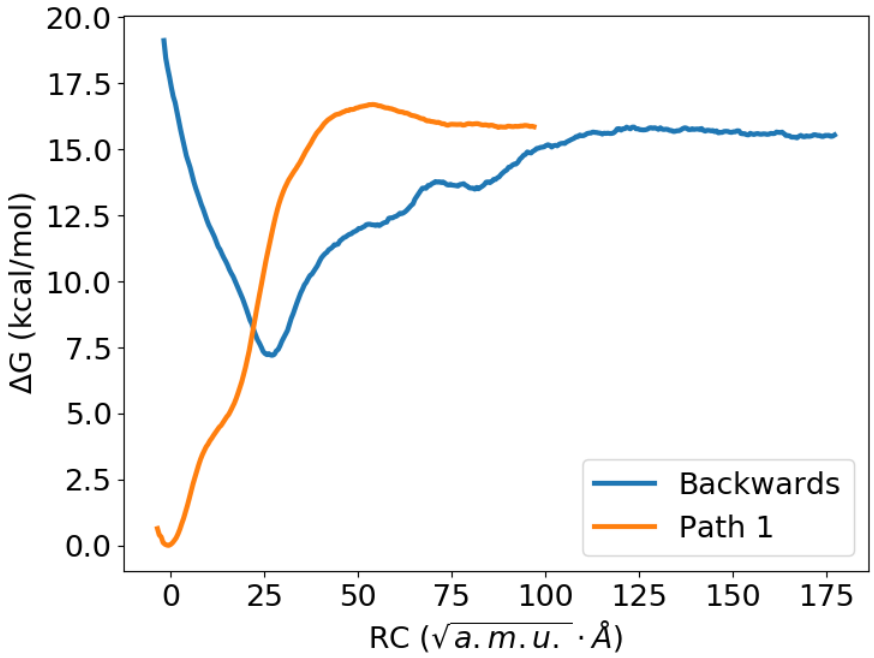

Figure 6.5: **Free energy of incorrectly bound benzamidine**. The free energy of the incorrectly docked unbinding pathway, denoted here as backwards, is shown in blue. For comparison, the free energy of path 1 is overlaid in orange.

6.4 Discussion and Conclusions

Previous chapters have focused on characterizing a stable, bound protein-ligand complex with key interactions accurately reformed, however, these discussions did not pay any heed to the overall energetic pathway the ligand traverses to enter the protein binding pocket. Understanding the route a ligand takes along a protein surface – and the speed at which it transitions between metastable points on this pathway – is considered a key component of understanding protein-ligand binding: A ligand could have a low overall binding free energy, however, if the rate at which binding occurs is slow, and/or the rate of dissociation is fast, then the molecule is arguably of limited use compared to one with a weaker binding energy but a more favourable binding profile. Therefore, to gain a truly comprehensive understanding of binding pathways, energetics, and kinetics, more extensive sampling of conformations outside of the binding pose is required (however, this is more resource- and time-expensive to perform). The difficulty of converging information about binding pathways is further exacerbated when the energy landscape is complex, such as when many degrees of freedom need to be accounted for (e.g. protein loop motions, ligand torsions). Even in the case of apparently simple protein-ligand complexes, such as trypsin and benzamidine, many distinct pathways can be elucidated. Therefore, timescales of sampling should be reflective of the slowest unbinding pathways, not just those which can be obtained with minimal computational time.

The ability to sample complex energetic landscapes is arguably limited in unbiased MD; according to the Boltzmann distribution, the probability of overcoming a given energy barrier is proportional to the height. Where many barriers need to be overcome, as is the case with ligand unbinding, this results in long average timescales as the system navigates a rugged, high-dimensional search space. However, iMD-VR allows these states to be sampled irrespective of the complexity of the energetic landscape, offering a means to enhance the speed protein conformational space is explored. For example, Fig. 6.2 shows the extent of protein surface exploration by a ligand within a single iMD-VR session (undertaken in less than one hour of real-time). On a comparable timescale, independently sampling these distinct unbinding pathways within MD is not readily feasible. Subsequently, the points sampled along the iMD-VR trajectories can be used as an initial guess, which in turn can be used to draw routes within a set of CVs to feed into path-based sampling methods (such as Umbrella Sampling). With this protocol, we can gain an estimate of (i) the overall free energy barrier between bound and unbound states, and (ii) whether the user has sampled any lower energy points, which could potentially indicate the existence of a metastable state. Comparatively, the seven iMD-VR generated pathways had similar free energy profiles, however, path 7 exhibited a somewhat more favourable energy along the reaction coordinate; this trajectory was further explored using the Adaptive String Method to move the initial 'guess nodes' used in Umbrella Sampling towards a potential MFEP, from which, a new free energy profile was calculated. Additionally, a less favourable path, where benzamidine started incorrectly docked, was tested and found to have a distinct energy profile compared to the

original seven paths.

Due to current limitations of iMD-VR, the unbinding pathways were sampled in implicit solvent, a simulation detail which was retained during any additional non-interactive MD. Although this enhanced the rate of sampling, compared to experiment, the estimated free energies were incorrect by around a magnitude of around 10 kcal·mol^{-1} compared to experiment. [242] Some degree of error is expected from employing a classical forcefield, however, water is also known to play a role in trypsin-benzamidine binding. [149] Therefore, the use of implicit solvent is a consideration for why the free energy of binding has been estimated as higher, particularly in comparison to previous theoretical methods in the literature which have used explicit solvation. [60, 154, 233, 234] While more computationally expensive, the Umbrella Sampling could be repeated starting from a solvated structure, giving us a better idea of how the use of implicit water has contributed to the discrepancy in free energy compared to experiment. This workflow could also be applied to different inhibitors of trypsin, as has been done with other related work. [242] Furthermore, previous work has established that the conformational state of trypsin can influence unbinding - here, we only tested one trypsin structure. Therefore, a future improvement would be to repeat this workflow with a range of conformations. [136, 238]

Nonetheless, this new method enables the exploration of differences in thermodynamics between various ligand unbinding pathways. Many of the paths sampled by the iMD-VR user converged towards a similar overall free energy profile, however, one path appeared more favourable as to warrant more detailed analysis. The workflow describes how a series of iMD-VR generated pathways can be used to quickly generate a pathway along a set of CVs, which can then be used as an initial guess to guide Umbrella Sampling. Furthermore, this initial path can then potentially be further optimized towards a MFEP with the Adaptive String Method. A development of this work would be to see if unbinding free energies can be obtained for systems with more complex dynamics, such as those detailed in Chapter 3, where finding useful CVs, and points along the reaction coordinate to start sampling from, is less easily intuitive. While benzamidine is a good starting use-case for this workflow, a human-intuitive, 2D reaction coordinate can already be used to find metastable states along various binding pathways. [153] Previously, we have shown that a reversible reaction coordinate which distinguishes between bound and unbound states can be obtained for more complex systems using an iMD-VR generated pathway [61], however, these are yet to be validated as capturing crucial metastable states. While it is unlikely that a single researcher generating a single unbinding pathway is going to perfectly encapsulate a MFEP along a series of metastable states, it is apparent that iMD-VR can be used to quickly sample a range of distinct pathways, some of which will be more optimal than others. Here, one researcher was able to quickly generate seven distinct unbinding pathways (within a single iMD-VR session), however, with new advances in running simulations remotely hosted on the cloud, scientists from around the world could be recruited to generate a larger array of paths. Using the established protocol to analyze these results, multiple researchers working collaboratively can potentially find new low

energy pathways of unbinding. These data can then be used to intelligently guide accelerated sampling methods toward potential metastable states, thus enhancing the rate protein systems can be explored.

CHAPTER 7

DISCUSSION AND FUTURE OUTLOOK

7.1 Discussion and Future Outlook

Biological machines orchestrate our cellular processes on the nanomolecular level, yet we have only recently been able to fully appreciate their structure and function. Early examples of protein models were static physical sculptures [1], however, advances in computing technology led to virtual molecular representations becoming the status quo. Although computational renderings sacrifice a sense of physicality, they do proffer one key advantage: Dynamics. The advent of MD allowed proteins to be represented as machines which undergo conformational transformations to function. Therefore, these models afford us an even more detailed understanding. However, one drawback is that 3D molecular processes are frequently projected onto 2D screens; advances in Augmented and Virtual Reality provide an intriguing counter to this problem. Early approaches to render molecules in VR often required access to specialized hardware, computing resources and physical space however, so, although these methods showed promise, they were not broadly accessible. [77, 78] Recently, AR technology has allowed us to bring virtual molecular representations into the room with us using commercial cameras or smartphones, meaning that tangible renderings can be created using hardware the user likely already owns. [33, 34] Furthermore, HMDs, such as the Microsoft Hololens, Oculus Rift, Valve Index or HTC Vive, can be bought commercially and allow representations to be built which track with a user's head movements and are well co-located within a bespoke virtual space. Additionally, there have also been numerous attempts to incorporate haptic interaction devices with these fully 3D representations [80, 86], bringing them further away from the virtual and towards reality. Advances in optimizing MD to run on increasingly advanced GPUs allows simulations to be updated in real time, meaning users can use an HMD to immerse themselves within a dynamic representation of a chemical system.

With proper integration of input devices, a user can reach out and interact with individual atoms which the system is responsive to - this makes them not just a spectator, but a part of the molecular world itself. [84]

Recent work by the Glowacki group has highlighted iMD-VR as an emergent field and this thesis develops it to study protein-ligand complexes. Chiefly, proteins are globular molecules with function that can either be induced or inhibited by small molecules complexing with a binding pocket, i.e. by slotting into grooves along a molecular surface. Therefore, the principle being explored here is that protein-ligand binding can be thought of as a shape fitting puzzle of sorts, in which one molecule needs to be correctly orientated so that (i) the two shapes have a complementary fit and (ii) functional groups are aligned with residues that favourable interactions are formed with. Computers do have some capability to predict how these molecular shapes fit together [180], however, depending on what allowances have been made, the quality of these predictions can be variable. In particular, as accounting for bond rotations introduces more degrees of freedom, treating either the ligand or protein as flexible is thought to increase the size of the corresponding search space, reducing the accuracy of predictions made using conventional high-throughput drug screening methods. [243] Protein folding is thought to have a similar complexity issue, however, gamification combined with crowd sourcing has been used to solve problems in this field to great success. [9, 74, 75] FoldIt proposes the idea that humans have an innate sense of chemical and spatial intuition which allows them to 'see' solutions that a computer would be reliant on methodically processing an algorithm to reach (if at all), thereby bypassing a rather extensive search space through employing 'high risk' strategies over high energy barriers. Here, a framework for using iMD-VR to dock fully-flexible ligands into proteins during molecular dynamics is presented. Though the use of iMD-VR, users are able to directly manipulate the position and orientation of molecules in the simulation space and hence drive protein-ligand binding processes to occur. Depending on the system under evaluation, this may take extensive computational time to observe using an unbiased simulation, thus the formation (or deformation) of a protein-ligand complex can be accelerated.

Initially, iMD-VR was evaluated as an interface for performing molecular manipulations, where three simple tasks were used to encompass the kinds of more complex spatial reasoning an iMD-VR user may perform. However, compared to more conventional input methods (i.e. mouse, touchscreen), here it is questioned whether or not VR can afford more sophisticated molecular operations. [20] Three molecular manipulation tasks, threading a methane through a nanotube, reversing the screw sense of helicene, and tying a knot in 17-alanine, were evaluated, where a cohort of molecular scientists were recruited to perform each task in an iMD simulation using (i) a mouse and keyboard, (ii) a tablet computer, or (iii) an HTC Vive VR headset. Each task involves some aspect of spatial reasoning, be it to accurately locate the entrance of a nanotube in 3D space, recognize the direction a helical molecule is turning itself, or to perceive when certain atoms are in front or behind one another in the plane of view. Interestingly, it was with the third task, tying

a knot in 17-alanine, that we saw the most dramatic benefit for VR compared to the two other interfaces. 72% of participants were able to complete this task, compared to only a few instances with the mouse and keyboard or tablet computer. In particular, VR was found to be successful for virtual knot tying as it is an inherently 3D process, requiring concerted depth perception throughout: an iMD-VR user must first pull one end of the protein string behind the other, pull it to the front, and then successfully pull it around and through the resulting loop. Being able to easily perceive depth - and also having the VR camera and controller positions co-located to the user's head and hands respectively - accelerated the accomplishment of this task, demonstrating that the HTC Vive VR interface enabled a greater degree of control over the iMD simulation. Overall, this observation has interesting implications for other molecular applications, such as docking ligands into proteins, which is further explored below.

To bind a ligand to a protein in iMD-VR, users need to be able to locate the binding pocket and location of any key residues, rotate the ligand so that it is correctly aligned, and then place it in the pocket so that functional groups form good interatomic contacts, the structure is not strained, and steric clashing is minimized. Furthermore, a user who is not careful when manipulating the system may cause disruption to the structure of the protein; if this is significant enough, there is danger the protein will be pushed into a state where docking a small ligand is less favourable (e.g. if key residue(s) are misplaced). On the other hand, if interactions are poorly formed or a functional group is clashing with the protein structure, under more rigorous and extensive MD simulations, the ligand may not stay in place. Therefore, the user needs to be able to quickly and precisely manipulate the position and orientation of the ligand in the simulation space as the atoms remain in constant motion - especially once the ligand has entered the binding pocket and specific interactions need to be carefully curated. Because the virtual reality platform was most performant in initial tests (Chapter 2), it was prioritized as the platform for performing ligand docking using iMD.

To evaluate the performance of iMD-VR in completing ligand docking tasks, a series of unbinding and rebinding experiments were designed to test how iMD-VR performs (i) as the ligand becomes larger and more rotationally flexible, (ii) where the user has to also manipulate the protein structure to perform docking, and (iii) between expert and novice users. Therefore, three systems of increasing complexity were selected. The first task, docking benzamidine into trypsin, was chosen as benzamidine is a small, planar, and symmetrical molecule which only has one rotational bond. Additionally, the user does not need to induce any conformational change in trypsin, it is simply a matter of pulling benzamidine out and then replacing it, ensuring that a single electrostatic contact has been reformed. Therefore, benzamidine and trypsin represents an easy use case: if users are not able to recreate the starting binding pose, this would suggest that the iMD-VR interface needs rethinking at a rather fundamental level. The second task, docking oseltamivir into neuraminidase, increases task complexity in two ways. Firstly, oseltamivir is a larger molecule with eight rotatable bonds and multiple hydrogen bonds to the neuraminidase

pocket. Secondly, although the protein secondary structure does not need to be manipulated, the residues Asp150 and Arg151 act as a molecular 'hinge' which sit over the ligand and help secure it in place with two hydrogen bonds. If the user knocks the position of either of these two residues when pulling oseltamivir out, they will need to be adjusted back into position, thus this represents a task where the user needs to be cognizant of the position of both ligand and protein atoms. The final task, docking amprenavir into HIV-1 protease, was the most complex as it required a conformational shift in the protein secondary structure. Before amprenavir could be removed from the binding pocket, a user needs to move two protein loops so that the protein is in an open configuration and then place them back once the ligand had been redocked.

Two expert users, who have extensive experience manipulating biomolecular systems in iMD-VR, completed the three tasks between them: In each case, the user was able to get the ligand within 2.5 Å of the original starting pose, furthermore, it remained in place during a separate, explicit solvent 200 ns MD simulation, showing iMD-VR can be used to quickly and effectively sample bound and unbound states (within tens of picoseconds of simulation time). Novice users - who only had a limited timespan familiarize themselves with the interface - were also able to correctly re-establish the position of five ligands in the binding pockets of trypsin, neuraminidase and HIV-1 protease (however, to reduce the task load during the tests, participants were not asked to manipulate the backbone of HIV-1 protease, instead, this was moved to the open conformation in a previous iMD-VR session). Although task accomplishment for trypsin and benzamidine docking was consistent with expert users, as the tasks became more complex, there was more variation seen in the RMSD of the docked poses. Nonetheless, these results show that docking in iMD-VR is intuitive and affords sufficient control to recreate crystallographic poses - even when the user is not familar with the system being studied. In practice, we would anticipate that iMD-VR users (i) are looking at systems of specific interest to them and (ii) will have more than the hour-long session to become proficient in using the iMD-VR system. Therefore, it is likely a novice user would benefit from more time and training prior to being assessed, similar to the expert users who were familiar with both the protein systems and the iMD-VR interface discussed here.

An arguable limitation of the results discussed in Chapter 3 is that only already-complexed conformations of proteins were evaluated (thus we were reasonably confident iMD-VR binding would be stable). Furthermore, systems were only tested where a reference docking solution was already known. For iMD-VR to be used as a predictive tool, these conditions are not fully reflective of the potential to generate new docking solutions. To further develop the protocol established in Chapter 3, several new use cases were evaluated with a protein target of high pharmacological relevance: SARS-CoV-2 Main Protease (Mpro) has been identified as a key protein in the life cycle of the coronavirus responsible for a global pandemic [190, 200–202], thus, there exists an extraordinarily strong impetus for effective therapies. Here, we first tested a potential inhibitor with an established crystallographic binding pose, X77, using the protocol described in Chapter 3

where (i) a set of atom coordinates for the complexed structure was known ahead of time, and (ii) the protein was in the already-complexed conformation. The X77 starting bound pose was undocked and then redocked to a comparable degree of accuracy to previous work (Chapter 3), showing that SARS-CoV-2 MPro is a potential candidate for iMD-VR docking. X77 was then interactively docked into an apo form of SARS-CoV-2 Mpro using two seperate protocols, one where the user focused on closely recreating the same ligand atom positions in the binding pocket as in the complexed structure, and one where the user focused on the reformation of two key hydrogen bonds. Overall, compared to docking to the already-complexed structure, the results for the apo form showed the position of X77 in the binding pocket to be less consistent over 10 ns of validation MD. As such, this implies that selecting a protein structure which is in a favourable conformation is an important consideration for future iMD-VR docking experiments, and it may be the case that a series of structures need to be tested. With repeated iMD-VR docking experiments however, both protocols were able to re-establish the starting bound structure to a comparable degree of accuracy with docking to the already-complexed structure, particularly after allowing the protein structure to relax. A series of heuristic tests were developed to further validate the iMD-VR generated structures, however, the general recommendation was made that the analysis presented was not exhaustive and researchers using iMD-VR should feel free to add their own additional evaluation metrics.

As a further development of iMD-VR, a protocol for building protein-substrates complexes was also developed in tandem with work evaluating X77. It is extremely challenging to characterize an enzyme-substrate pre-reaction complex as they are typically short-lived, however, iMD-VR proffers a means to try and build these complexes in a non-reactive environment. A reactive 11-mer oligopeptide structure was docked into SARS-CoV-2 MPro (where, to the best of our knowledge, no such structure exists) using coordinates from a deactivated SARS-CoV-1 MPro mutant complex as a guide for how the oligopeptide should be placed. Similar to work with X77, multiple docking protocols were tested with multiple protein conformations (ligand-complexed and apo), where focus was placed on forming hydrogen bonds to structures with either (i) light backbone restraints or (ii) no backbone restraints. Compared to a drug-like compound, oligopeptides are large and have a high degree of rotational flexibility, therefore, docking them presents a new and greater degree of challenge. Overall, we were able to use iMD-VR to generate structures with an oligopeptide RMSD between 3 and 6.5 Å compared to the original mutated complex during 10 ns of validation molecular dynamics; however, it should be noted that higher RMSD structures were due to 'floppy' peptide termini that were not stabilized by hydrogen bonds. Inversely, inspecting reactive centre of the complex showed good formation of electrostatic interactions within the catalytic oxyanion hole. Most significantly, we were able to use iMD-VR to create new docked complexes between both apo and ligand-complexed structures of SARS-CoV-2 MPro.

Thus far, this thesis has explored the development of a framework for performing complex

manipulations of protein-ligand systems in iMD-VR, however, these solutions have focused on VR as a visual medium alone. In a typical iMD-VR simulation, there are a series of invisible calculations happening which drive the stability of a given complex, for example, van der Waals interactions, torsional angles, and electrostatic contacts can all play a role. Here, a process for the sonification of specific molecular data features was developed (non-bonded interaction energy of specific hydrogen bonds, interatomic distance between the ligand and the binding pocket, and total potential energy of the system). However, as these data features are abstract concepts, conceptualizing them as sounds involves an inherent degree of subjectivity; how one intuits a data feature to sound can potentially vary from person to person. In order to help mitigate subjectivity, sound designers, who have minimal biases as they are non-experts in chemical physics, were recruited to design sounds which can represent changes in these data features. Once an array of sounds had been created, domain experts were recruited to assess whether the sounds could meaningfully convey specific changes in a virtual trajectory, such as detecting the correct number of minima or understanding that two maxima points are of different heights to one another. Design principles from the most performant sounds were then used to create a new sonification of each data feature, which were then successfully incorporated into an iMD-VR simulation of a protein-ligand system. As a further evaluation, biomolecular experts were recruited to try and bind ligands to proteins using either (i) visuals and sound or (ii) visuals alone to guide them. Due to the study design, we could not conclude the sonification of data features had any benefit, however, their inclusion into the iMD-VR framework was not found to be detrimental and shows potential with further development. Therefore, future work should explore how sound can be included in an iMD-VR simulation to portray meaningful information to the user. In particular, a major limitation of this initial study was that the time allowed for users to familiarize themselves with the iMD-VR framework was low, where in practice a user will have more time to learn the interface. Additionally, as with other work discussed here, the framework was built off knowing a correct binding pose ahead of time, therefore, another key development would be to generalize how these methods can be applied so that they are useful in situations where there is no known ideal binding pose. Nonetheless, this initial exploration has shown how sonification can be applied to convey information that would otherwise be invisible during iMD-VR ligand docking.

iMD-VR has the potential to enhance the rate chemical systems are explored, in this case, a user can apply directed force to a protein-ligand system and a series of different unbinding pathways can be quickly generated. Subsequently, trajectories from iMD-VR can be used as an initial guess for path-based biasing methods, allowing free energy profiles for ligand disassociation to be estimated. Seven distinct unbinding pathways of benzamidine from trypsin were generated using iMD-VR, translated into six-dimensional space using a set of CVs, and Umbrella Sampling was used to estimate the free energy along these routes. Subsequently, one of the seven iMD-VR pathways exhibited a slightly more favourable free energy profile, as to warrant more detailed analysis; interestingly, it was this pathway which sampled areas along the protein surface which

were close to a known metastable state. [153, 233, 237] With the Adaptive String Method [239], we were able to further refine this iMD-VR initial guess pathway towards a MFEP. Additionally, a less favourable path, where benzamidine started incorrectly docked, was tested and found to have a distinctly poorer energy profile compared to the original seven paths. Between all paths, the estimated energy of unbinding had a degree of error (around 10 kcal·mol^{-1}, however, a likely culprit was the use of an implicit solvent model. Nonetheless, this method has enabled exploration of differences in thermodynamics between various ligand unbinding pathways with limited computational cost (1 ns of sampling per run). In particular, this analysis may be able to indicate whether the user has sampled a route containing lower energy, potentially metastable, states, prompting further investigation. With new advances in remote simulation hosting on the cloud [84], scientists from around the world can potentially generate pathways which can then be quickly evaluated to see if a potentially optimal pathway has been found. With the identification of low energy areas along a protein surface, it is hoped that biased sampling methods can be intelligently guided to these areas of conformational space.

Throughout this work, several limitations have been recurrent. Due to bottlenecks in the speed of the iMD-VR framework, all interactive simulations presented here used an implicit solvent model. Water is thought to play a role in protein-ligand binding and unbinding processes [149], therefore, it should be acknowledged that any sampled configurations could have some degree of inaccuracy as solvent effects are not fully accounted for. Chapter 3 shows how iMD-VR structures can be solvated, equilibrated and minimized after-the-fact, however, this possibility has only been explored with structures that we are reasonably confident are stable (and thus will not be significantly perturbed during this process). Future work could address how solvent could directly be included in iMD-VR simulations, and even go so far as to try to understand the degree of error introduced from current implicit models. Although the protocols described here still afford more protein and ligand flexibility than many current docking software packages, backbone restraints were still employed in most simulations, largely to ensure the iMD-VR user does not inadvertently push the protein into a less dockable state. Although Chapters 3 and 4 show that fully-flexible proteins can still be docked in iMD-VR, it is a general recommendation that backbone restraints should be used initially to test whether a given protocol will work, or where the iMD-VR user is unfamiliar with the system (such as with any novice user tests, where we wanted to mitigate accidental protein structure disruption as a factor for why a docking attempt was unsuccessful). However, it should be acknowledged that allowing full protein flexibility is preferable. In any case, docked and undocked configurations can be generated at faster timescales than would happen with no simulation biasing, so it may very well be the case that protein motions have not been adequately captured due to this. Therefore, iMD-VR users should not place confidence in a single complexed structure and should instead perform additional molecular dynamics to allow the protein structure to relax, particularly when docking to conformations where binding could be less favourable (such as the apo form).

A second limitation of these tests is that they are all based on systems where a stable docking solution was known ahead of time. Although the groundwork for using iMD-VR as a predictive tool has been established here, it has not yet been demonstrated whether it is effective at generating protein-ligand complexes where an optimal docking pose is not known ahead of time. A way to test this could be to perform a 'blind' comparison with conventional methods, where a series of drug-like compounds are tested against a protein target using a computational high-throughput screening method. Once a series of hit compounds have been established, iMD-VR users could be recruited to try to dock those same compounds and the results between the two methods can be compared. Alternatively, iMD-VR can be developed as a tool which works in tandem with conventional drug docking approaches. Once a potential hit compound has been identified, a user could be put into iMD-VR with the identified complex; from here, they could make adjustments to the position of the ligand or even suggest new chemical changes to improve binding efficacy. In either use-case for iMD-VR, a robust evaluation method for generated complexes is required. The advantage of metrics such as RMSD and hydrogen bonding is that they can be derived directly from a simulation trajectory, therefore, where a lot of conformations need to be evaluated, this lends itself to fast processing of iMD-VR docked poses. However, at best, we can say these metrics correlate to a stable binding free energy, but do not directly tell us which of an array of many different poses are the most energetically favourable. Alternatively, the free energies of iMD-VR generated poses can be directly calculated, however, these methods require more extensive sampling or calculations to be performed. We have typically recorded a trajectory from iMD-VR simulations, so each docking experiment yields a handful of unique docking poses – it may not be practical to run calculations on every recorded step, especially as some will be more optimal than others. However, metrics such as the existence of hydrogen bonds could be used to perform quick initial analysis on an iMD-VR trajectory to identify at which points the user is close to a stable configuration, which in turn could be more extensively analysed. Alternatively, to gain a more quantitative understanding of the whole energy change as a ligand enters or exits a protein binding pocket, an iMD-VR generated pathway could be used to create a description of the (un)binding process along a set of CVs. In turn, this path in reduced dimensional space could then be used with a biased sampling method, such as Umbrella Sampling, from which a free energy profile for the entire process can be estimated. Although it is unlikely a single researcher generating a single pathway is going to perfectly recreate the MFEP across a series of relevant metastable states, nor expansively explore the entire system, with repeated experiments areas close to potential metastable states can be identified. More pertinently, these states can be described using CVs and, from this, biased sampling methods can be intelligently lead towards these more energetically favourable areas of conformational space.

The iMD-VR framework itself could also be improved. Notably, there is currently no capability for non-bonded interactions to be visually displayed to the user. Electrostatic contacts and hydrogen bonds are thought to be key in the formation of a stable binding pose and for catalytic

processes to occur, therefore, it may be useful to visually indicate interatomic distances, presence of hydrogen bonds, bond torsions etc. Alternatively, with further development of the sonification framework, this information could also be conveyed to an iMD-VR user with the use of sound. Methods employed to convert work performed during sMD into a potential of mean force could also be used with iMD-VR, giving a heuristic means of estimating the energy of pathways which have been generated. This should first be applied to test systems, such as pulling a methane through a nanotube, as these are the kinds of tasks used to validate these methods [69, 70], but the same principles could be applied to protein-ligand docking at a future date.

The user studies discussed in this thesis were performed in person, which caused other limitations in the amount of time afforded for each user and the extent of their expertise. Tests employed participants who were unfamiliar with iMD-VR and, very often, the protein-ligand systems being studied. Due to (i) general inexperience with iMD-VR and (ii) there only being a limited time window to perform the tests, participants often had an additional learning pressure: although it is still highly encouraging that novice users could reestablish known crystallographic poses under these circumstances, they are not fully representative of how iMD-VR for ligand docking could optimally be used. If a user has more than 40 to 60 minutes to learn how to use iMD-VR, and is already knowledgeable about the protein-ligand system, the results presented here could likely be improved upon. Advances in networking technology has allowed iMD-VR simulations to be hosted remotely on the cloud [84]; the ability to connect to a pre-set simulation from anywhere around the world using a front-end client could improve the accessibility of iMD-VR. Specialist knowledge of how to parameterize a system (and then convert those parameters into an iMD-VR simulation) would not be required, nor is there a need to understand how to set up and run an iMD server. Instead, users would only need a compatible VR headset and an executable file which allows them to connect to a cloud-hosted server and run the front end VR client. Therefore, participants could be recruited without the need for them to present at a specific place and time, instead, they can complete docking tasks on their own schedule. With proper development, the iMD-VR front end could provide feedback to the user about the quality of docked poses, such as through integration of a scoring function, or even gamification of the problem. Currently, the docking protocols presented here require extensive analysis of sampled states after-the-fact, however, enabling end-users to self-evaluate docked poses on-the-fly and submit only their best solutions could simplify this process. Although a longer-term idea, the end-goal would be an iMD-VR interface which allows people to connect to a hosted simulation of a protein-ligand system, attempt different docking solutions, and then submit them for further ranking and possible analysis, thus crowd-sourcing the problem of interactive drug design. Additionally, by being able to recruit people with diverse backgrounds and interests, it is hoped that these problems will be approached in a variety of ways, thus increasing the breadth of solutions offered.

Here, we have utilized recent advantages in both computational processing and VR technology to develop an iMD-VR framework for interactively docking ligands into proteins. The conforma-

tional search space of chemical systems ranges from low to high dimensionality. For example, to observe bond breaking, a simulation can be directed along a one-dimensional path, i.e. going from a small interatomic distance to a larger one. However, as degrees of freedom in a system increases, so does the complexity of the energetic landscape. A poor CV (or other descriptor) of a given process can lead a simulation down an inefficient route, or get the system lost or stuck within energetic peaks. Proteins are large, complex molecules which exhibit many degrees of freedom. Typically, this results in an energetic landscape which is rugged and has many variable routes: A unique challenge is describing high-quality pathways in these conformational spaces. However, human spatial and chemical intuition grant a 'bird's eye view' of an energetic landscape – principally, it is this perspective that iMD-VR takes advantage of. Irrespective of system complexity, these interfaces allow human observers to guide molecules towards a specific state of interest. As demonstrated in this thesis, a ligand can be placed into a protein binding pocket; with careful formation of key contacts, a stable binding complex can be formed. Alternatively, a series of distinct unbinding pathways can be generated within a single interactive session. As energetic barriers are navigated by will, not probability, interactive molecular environments proffer a way to explore chemical space. Given the size and complexity of biological systems, this approach is especially pertinent. Considering this, protocols for performing iMD-VR docking have been developed and applied, including performing additional analysis on a generated pose or pathway. Future work should focus on both developing the interface to make finding good binding solutions intuitive to the user, thus enhancing the utility as a tool for building predictive models. Nonetheless, this work presents a foundation for the use of iMD-VR for studying protein-ligand systems.

APPENDIX A

APPENDIX A

Appendix A describes some of the underlying methodology for the Umbrella Sampling and Adaptive String Method employed to generate ligand unbinding free energies described in Chapter 6. This methodology was developed by Kirill Zinovjev; it should be acknowledged that this appendix is his work and is largely based off previous publications. [239, 244, 245] Although I cannot claim this as my own work, it is included in this thesis to provide more detail to those who are interested in how the methodology was employed.

A.1 Reaction Coordinate Definition

The unbinding pathways obtained from iMD-VR were characterized by six CVs describing relative orientation of the two species as proposed in previous work. [246]

- r = $distance\mathrm{P}_1\mathrm{L}_1$
- θ = $angle\mathrm{P}_1\mathrm{L}_1\mathrm{L}_2$
- ϕ = $dihedral\mathrm{P}_1\mathrm{L}_1\mathrm{L}_2\mathrm{L}_3$
- Θ = $angle\mathrm{P}_2\mathrm{P}_1\mathrm{L}_1$
- Φ = $dihedral\mathrm{P}_2\mathrm{P}_1\mathrm{L}_1\mathrm{L}_2$
- Ψ = $dihedral\mathrm{P}_3\mathrm{P}_2\mathrm{P}_1\mathrm{P}_1$

Where P1-P3 and L1-L3 are reference centres in the protein and the ligand respectively, defined as geometric centres of the atom groups defined in Table A.1.

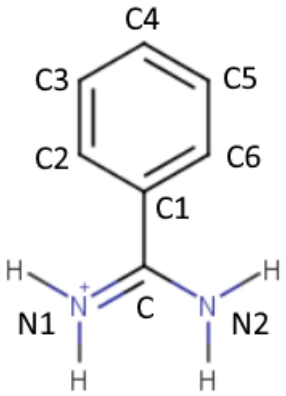

Figure A.1: **Benzamidine atom labels**. With regard to defining reference geometric centres, how each atom is labelled in benzamidine.

By choosing this representation we assume that the internal degrees of freedom (such as vibrations and conformational changes) are not coupled to the unbinding and therefore can be excluded from the reaction coordinate. While this assumption is valid for the trypsin-benzamidine case, it would fail if there were a significant conformational rearrangement during the unbinding (e.g. lid opening-like motion). In such case, an additional CVs describing the conformational change must be included.

To obtain the free energy profiles along iMD-VR pathways one needs to (i) define a reaction coordinate that changes smoothly along the path and (ii) ensure that the simulation system stays in the vicinity of the path. The latter is especially important when the user intentionally generates a sub-optimal path to explore alternative unbinding mechanism. Without any additional restraint there is a high chance of the system falling to a more favorable path, which might have already been explored. Both tasks can be accomplished with path CVs (pathCVs) defined along the paths in the chosen CV space [244]:

$$s\boldsymbol{r} = \frac{\sum_{i=1}^{n} t_i e^{-\lambda d\boldsymbol{\theta}\boldsymbol{r},\boldsymbol{z}(t_i)}}{\sum_{i=1}^{n} e^{-\lambda d\boldsymbol{\theta}\boldsymbol{r},\boldsymbol{z}(t_i)}} \tag{A1}$$

Protein centres (all heavy atoms of the following residues):	Ligand centers:
P1: Cys136, Leu137, Ile138, Cys157, Leu158, Lys159, Pro198, Val199, Val200	**L1**: C, C1, N1, N2
P2: Phe181, Cys182, Ala183, Val213, Ser214, Trp215, Gly226, Val227, Tyr228	**L2**: C2, C3
P3: Val31, Ser32, Leu33, Gln64, Phe41, Cys42, Gly43, Gln64, Val65, Arg65A	**L3**: C5, C6

Table A.1: **Reference geometric centres**. Definitions the six reference geometric centres P1-P3 and L1-L3. Ligand atom names are defined in Fig. A.1

(A2) $$z\boldsymbol{r} = -\lambda^{-1} ln \sum_{i=1}^{n} e^{-\lambda \boldsymbol{\theta r}, \boldsymbol{z}(t_i)}$$

(A3) $$t_i = \frac{i-1}{n-1} L$$

Where $\boldsymbol{z}t$ is the reference path parameterized by the arc length, L is the total length of the path and $d\boldsymbol{\theta r}$, $\boldsymbol{z}$ is some distance measure between the given state of the system $\boldsymbol{r}$ and a point $\boldsymbol{z}$ on the reference path, and $d\boldsymbol{\theta r}$ is the 6-vector of CVs defined above. λ is set to inverse of the distance between the points $\boldsymbol{z}t_i$. To account for interdependency and different nature of the CVs, the following measure was used [245]:

(A4) $$d\boldsymbol{\theta r}, z(t_i) = \sqrt{\boldsymbol{\theta r} - \boldsymbol{z}t_i^T \boldsymbol{M} t_i^{-1} \boldsymbol{\theta r} - \boldsymbol{z}t_i}$$

Where $\boldsymbol{M}$ is the variable distance metric tensor defined as:

(A5) $$\boldsymbol{M}t_{i_{jk}} = \nabla\theta_j \boldsymbol{r} \cdot \nabla\theta_k \boldsymbol{r}_{\boldsymbol{\theta r} = \boldsymbol{z}t_i}$$

Where gradients are taken w.r.t. mass-weighted Cartesian coordinates and $\ldots_{\boldsymbol{\theta r}=\boldsymbol{z}t_i}$ denotes canonical ensemble average over configurations constrained to the point $\boldsymbol{z}t_i$ in the CV space.

A.2 Umbrella Sampling

The same setup and simulation protocol were used for all 7 VR pathways. All the simulations were performed with the modified version of sander from AmberTools19. Generalized Born implicit solvation method was used to describe the water solution. Temperature was set to 300 K and was controlled with Langevin thermostat. The bonds involving hydrogen were constrained using SHAKE, which allowed an integration timestep to 2 fs. 56 Umbrella Sampling windows were used. Harmonic biases were equally spaced along the range of pathCV values with force constants determined automatically to guarantee uniform sampling assuming flat underlying free energy profile (see Ref. [239] for details). The initial structures for Umbrella Sampling windows were obtained by taking the closest snapshot from the iMD-VR pathway and running 1 ps MD gradually increasing the force constant from 0 to the target value. 1 ns of sampling was acquired during production simulations. Hamiltonian replica exchange between windows was attempted every 500 fs. To restrain the sampling to the vicinity of the path, a harmonic bias was added along the z-coordinate at z=0 with force constant equal to 1 kcal·mol^{-1}·a.m.u.$^{-1}$·Å^{-2}. The resulting potentials of mean force were integrated using the WHAM procedure. [240]

A.3 Adaptive String Method

The adaptive version of on-the-fly string method [239] was used to obtain the minimum free energy path in the vicinity of path 7. The following adaptive string method parameters were changed from their default values to ensure faster convergence and stability of the simulations:

- γ = 500 ps^{-1}
- $K^{\perp}$ = 1 kcal· mol^{-1}·a.m.u.$^{-1}$·$Å^{-2}$
- γ_{α} = 200 kcal·mol^{-1}·a.m.u.$^{-1}$·$Å^{-2}$·ps
- κ = 1 a.m.u.$^{-2}$·$Å^{-4}$

The same CVs as the pathCV Umbrella Sampling calculations were used in the string method. Path 7 was used as the initial guess. Endpoints of the path were fixed in the CVs space. The MD protocol was identical to the one used for Umbrella Sampling. The string optimization converged after 1.7 ns of simulation. The free energy along the converged path was obtained using the same procedure as for the paths obtained directly from iMD-VR.

Acronyms

2D two dimensional. 2, 3, 6, 13, 14, 16, 18, 23, 30, 33–35, 88, 98, 101

3D three dimensional. 1–4, 6, 9, 12, 14, 16, 18, 20, 23, 30–32, 34–36, 42, 49, 50, 55, 56, 88, 101–103

AR Augmented Reality. 2, 3, 101

CPU Computational Processing Unit. 5, 94

CV Collective Variable. 32, 88–90, 92, 97, 98, 106, 108, 111–114

GPU Graphical Processing Unit. 5, 13, 15, 16, 23, 94, 101

HMD Head Mounted Display. 3, 4, 7, 15, 101

HPC High-Performance Computing. 13, 21, 30

iMD Interactive Molecular Dynamics. 5–7, 11, 22, 102, 103, 109

iMD-VR Interactive Molecular Dynamics in Virtual Reality. i, ix, xi, xvii, xix, 6–9, 11, 15, 26, 27, 29–36, 38–44, 46–50, 53, 55–77, 81–85, 87–98, 102–114

iMS Interactive Molecular Simulation. xvii, 13, 14, 17, 19

MD Molecular Dynamics. i, ix, xvii, 5, 6, 9, 13, 15–17, 21–23, 29–31, 39, 40, 42, 44, 48, 49, 54–56, 59–71, 76, 87, 89, 90, 92–94, 97, 98, 101, 103–105, 113, 114

MFEP Minimum Free Energy Path. xiii, xix, 7, 50, 88, 89, 93–95, 97, 98, 107, 108

PC Principal Components. 40–42, 44

PCA Principal Component Analysis. 29, 39, 40, 44

RMSD Root Mean Square Deviation. xvii, 2, 39–49, 55, 58–63, 65–67, 69, 74, 76, 83, 84, 104, 105, 108

RMSF Root Mean Square Fluctuation. 62, 65, 67

sMD Steered Molecular Dynamics. 5, 6, 109

VR Virtual Reality. i, xvii, 2–9, 14–16, 18, 20, 21, 23–26, 55, 66, 70, 77, 88, 101–103, 106, 109, 113

BIBLIOGRAPHY

[1] J. C. Kendrew, G. Bodo, H. M. Dintzis, R. Parrish, H. Wyckoff, and D. C. Phillips, "A three-dimensional model of the myoglobin molecule obtained by x-ray analysis," *Nature*, vol. 181, no. 4610, pp. 662–666, 1958.

[2] J. S. Richardson, "Early ribbon drawings of proteins," *nature structural biology*, vol. 7, no. 8, pp. 624–625, 2000.

[3] M. Gerstein, J. Tsai, and M. Levitt, "The volume of atoms on the protein surface: calculated from simulation, using voronoi polyhedra," *Journal of molecular biology*, vol. 249, no. 5, pp. 955–966, 1995.

[4] "molymod - the original dual-scale system of molecular models." `http://www.molymod.com/`.
Accessed: 2020-07-08.

[5] "Crystalproteins - 3d laser data etched in glass." `https://crystalproteins.com/`.
Accessed: 2020-07-08.

[6] S. Rossi, M. Benaglia, D. Brenna, R. Porta, and M. Orlandi, "Three dimensional (3d) printing: A straightforward, user-friendly protocol to convert virtual chemical models to real-life objects," 2015.

[7] F. M. Richards, "The matching of physical models to three-dimensional electron-density maps: a simple optical device," *Journal of molecular biology*, vol. 37, no. 1, pp. 225–230, 1968.

[8] T. A. Jones, "A graphics model building and refinement system for macromolecules," *Journal of Applied Crystallography*, vol. 11, no. 4, pp. 268–272, 1978.

[9] S. Cooper, F. Khatib, A. Treuille, J. Barbero, J. Lee, M. Beenen, A. Leaver-Fay, D. Baker, Z. Popović, *et al.*, "Predicting protein structures with a multiplayer online game," *Nature*, vol. 466, no. 7307, pp. 756–760, 2010.

[10] K. M. Beem, D. C. Richardson, and K. V. Rajagopalan, "Metal sites of copper-zinc superoxide dismutase," *Biochemistry*, vol. 16, no. 9, pp. 1930–1936, 1977.

[11] J. A. Tainer, E. D. Getzoff, K. M. Beem, J. S. Richardson, and D. C. Richardson, "Determination and analysis of the 2 Å structure of copper, zinc superoxide dismutase," *Journal of Molecular Biology*, vol. 160, no. 2, pp. 181 – 217, 1982.

[12] J. Lejeune, A. G Michel, and D. P Vercauteren, "Interactive flexible molecular fitting program to be integrated into computer-aided molecular modelling systems," *Journal of Molecular Graphics*, vol. 4, no. 4, pp. 194 – 199, 1986.

[13] P. Cozzini, P. Pavesi, and G. D Andreetti, "Computer graphic tool for colour structure display on personal computers," *Journal of Molecular Graphics*, vol. 3, no. 3, pp. 90 – 92, 1985.

[14] R. A. Sayle and E. Milner-White, "Rasmol: biomolecular graphics for all," *Trends in Biochemical Sciences*, vol. 20, no. 9, pp. 374 – 376, 1995.

[15] W. Humphrey, A. Dalke, K. Schulten, *et al.*, "Vmd: visual molecular dynamics," *Journal of molecular graphics*, vol. 14, no. 1, pp. 33–38, 1996.

[16] "Unity real-time development platform | 3d, 2d vr and ar visualizations." `https://unity.com/`.
Accessed: 2020-07-08.

[17] J. Laureanti, J. Brandi, E. Offor, D. Engel, R. Rallo, B. Ginovska, X. Martinez, M. Baaden, and N. A. Baker, "Visualizing biomolecular electrostatics in virtual reality with unitymol-apbs," *Protein Science*, vol. 29, no. 1, pp. 237–246, 2020.

[18] L. J. Kingsley, V. Brunet, G. Lelais, S. McCloskey, K. Milliken, E. Leija, S. R. Fuhs, K. Wang, E. Zhou, and G. Spraggon, "Development of a virtual reality platform for effective communication of structural data in drug discovery," *Journal of Molecular Graphics and Modelling*, vol. 89, pp. 234 – 241, 2019.

[19] "Vrtk - virtual reality toolkit." `https://vrtoolkit.readme.io/`.
Accessed: 2020-07-08.

[20] M. O'Connor, H. M. Deeks, E. Dawn, O. Metatla, A. Roudaut, M. Sutton, L. M. Thomas, B. R. Glowacki, R. Sage, P. Tew, *et al.*, "Sampling molecular conformations and dynamics in a multiuser virtual reality framework," *Science advances*, vol. 4, no. 6, p. eaat2731, 2018.

[21] S. J. Bennie, K. E. Ranaghan, H. Deeks, H. E. Goldsmith, M. B. O'Connor, A. J. Mulholland, and D. R. Glowacki, "Teaching enzyme catalysis using interactive molecular dynamics in virtual reality," *Journal of Chemical Education*, vol. 96, no. 11, pp. 2488–2496, 2019.

[22] M. Won, M. Mocerino, K.-S. Tang, D. F. Treagust, and R. Tasker, "Interactive immersive virtual reality to enhance students' visualisation of complex molecules," in *Research and Practice in Chemistry Education*, pp. 51–64, Springer, 2019.

[23] L. A. L. F. da Costa and L. P. Nedel, "An immersive visualization study on molecules manipulation," in *2017 19th Symposium on Virtual and Augmented Reality (SVR)*, pp. 169–177, IEEE, 2017.

[24] P. Milgram, H. Takemura, A. Utsumi, and F. Kishino, "Augmented reality: A class of displays on the reality-virtuality continuum," in *Telemanipulator and telepresence technologies*, vol. 2351, pp. 282–292, International Society for Optics and Photonics, 1995.

[25] A. V. Savchenkov, "Designing three-dimensional models that can be printed on demand and used with students to facilitate teaching molecular structure, symmetry, and related topics," 2020.

[26] B. R. Kent, *3D scientific visualization with blender*.
Morgan & Claypool Publishers San Rafael, CA, 2015.

[27] D. OShaughnessy, "Visualization of molecular structures using augmented reality," in *Educational Media and Technology Yearbook*, pp. 105–120, Springer, 2019.

[28] L. A. Abriata, "Building blocks for commodity augmented reality-based molecular visualization and modeling in web browsers," *PeerJ Computer Science*, vol. 6, p. e260, 2020.

[29] P. Safadel and D. White, "Facilitating molecular biology teaching by using augmented reality (ar) and protein data bank (pdb)," *TechTrends*, vol. 63, no. 2, pp. 188–193, 2019.

[30] K. Eriksen, B. E. Nielsen, and M. Pittelkow, "Visualizing 3d molecular structures using an augmented reality app," 2020.

[31] C. Berry and J. Board, "A protein in the palm of your hand through augmented reality," *Biochemistry and Molecular Biology Education*, vol. 42, no. 5, pp. 446–449, 2014.

[32] P. Maier and G. Klinker, "Augmented chemical reactions: An augmented reality tool to support chemistry teaching," in *2013 2nd Experiment@ International Conference (exp. at'13)*, pp. 164–165, IEEE, 2013.

[33] A. Borrel and D. Fourches, "Realityconvert: a tool for preparing 3d models of biochemical structures for augmented and virtual reality," *Bioinformatics*, vol. 33, no. 23, pp. 3816–3818, 2017.

[34] P. Wolle, M. P. Müller, and D. Rauh, "Augmented reality in scientific publications—taking the visualization of 3d structures to the next level," 2018.

[35] C. Müller, M. Krone, M. Huber, V. Biener, D. Herr, S. Koch, G. Reina, D. Weiskopf, and T. Ertl, "Interactive molecular graphics for augmented reality using hololens," *Journal of integrative bioinformatics*, vol. 15, no. 2, 2018.

[36] C. Müller, M. Braun, and T. Ertl, "Optimised molecular graphics on the hololens," in *2019 IEEE Conference on Virtual Reality and 3D User Interfaces (VR)*, pp. 97–102, IEEE, 2019.

[37] C. N. Peterson, S. Z. Tavana, O. P. Akinleye, W. H. Johnson, and M. B. Berkmen, "An idea to explore: Use of augmented reality for teaching three-dimensional biomolecular structures," *Biochemistry and Molecular Biology Education*, 2020.

[38] M. Zheng and M. P. Waller, "Chempreview: an augmented reality-based molecular interface," *Journal of Molecular Graphics and Modelling*, vol. 73, pp. 18 – 23, 2017.

[39] M. Limniou, D. Roberts, and N. Papadopoulos, "Full immersive virtual environment cavetm in chemistry education," *Computers & Education*, vol. 51, no. 2, pp. 584 – 593, 2008.

[40] N. Akkiraju, H. Edelsbrunner, P. Fu, and J. Qian, "Viewing geometric protein structures from inside a cave," *IEEE Computer Graphics and Applications*, vol. 16, no. 4, pp. 58–61, 1996.

[41] A. Salvadori, M. Fusè, G. Mancini, S. Rampino, and V. Barone, "Diving into chemical bonding: An immersive analysis of the electron charge rearrangement through virtual reality," *Journal of computational chemistry*, vol. 39, no. 31, pp. 2607–2617, 2018.

[42] T. Mitchell, J. Hyde, P. Tew, and D. R. Glowacki, "Danceroom spectroscopy: At the frontiers of physics, performance, interactive art and technology," *Leonardo*, vol. 49, no. 2, pp. 138–147, 2016.

[43] K. Sabir, C. Stolte, B. Tabor, and S. I. O'Donoghue, "The molecular control toolkit: Controlling 3d molecular graphics via gesture and voice," in *2013 IEEE Symposium on Biological Data Visualization (BioVis)*, pp. 49–56, IEEE, 2013.

[44] O. Legetth, J. Rodhe, J. Pålsson, M. Wallergård, S. Lang, and S. Soneji, "Cellexalvr: A virtual reality platform for the visualisation and analysis of single-cell gene expression data," *BioRxiv*, p. 329102, 2019.

[45] T. Davison, F. Samavati, and C. Jacob, "Lifebrush: painting, simulating, and visualizing dense biomolecular environments," *Computers & Graphics*, vol. 82, pp. 232–242, 2019.

[46] D. Probst and J.-L. Reymond, "Exploring drugbank in virtual reality chemical space," *Journal of chemical information and modeling*, vol. 58, no. 9, pp. 1731–1735, 2018.

[47] P. Leinen, M. F. Green, T. Esat, C. Wagner, F. S. Tautz, and R. Temirov, "Hand controlled manipulation of single molecules via a scanning probe microscope with a 3d virtual reality interface," *JoVE (Journal of Visualized Experiments)*, no. 116, p. e54506, 2016.

[48] E. M. Ratamero, D. Bellini, C. G. Dowson, and R. A. Römer, "Touching proteins with virtual bare hands," *Journal of computer-aided molecular design*, vol. 32, no. 6, pp. 703–709, 2018.

[49] K. C. Cassidy, J. Šefčík, Y. Raghav, A. Chang, and J. D. Durrant, "Proteinvr: Web-based molecular visualization in virtual reality," *PLOS Computational Biology*, vol. 16, pp. 1–17, 03 2020.

[50] A. R. Balo, M. Wang, and O. P. Ernst, "Accessible virtual reality of biomolecular structural models using the autodesk molecule viewer," *Nature methods*, vol. 14, no. 12, pp. 1122–1123, 2017.

[51] A. Pramudwiatmoko, S. Tsutoh, G. Gutmann, Y. Ueno, and A. Konagaya, "A high-performance haptic rendering system for virtual reality molecular modeling," *Artificial Life and Robotics*, vol. 24, no. 4, pp. 542–549, 2019.

[52] R. Roebuck Williams, X. Varcoe, B. R. Glowacki, E. M. Gale, A. Jamieson-Binnie, and D. R. Glowacki, "Subtle sensing: Detecting differences in the flexibility of virtually simulated molecular objects," in *Extended Abstracts of the 2020 CHI Conference on Human Factors in Computing Systems*, pp. 1–8, 2020.

[53] J. F. Zhang, A. R. Paciorkowski, P. A. Craig, and F. Cui, "Biovr: a platform for virtual reality assisted biological data integration and visualization," *BMC bioinformatics*, vol. 20, no. 1, pp. 1–10, 2019.

[54] J. Laureanti, J. Brandi, E. Offor, D. Engel, R. Rallo, B. Ginovska, X. Martinez, M. Baaden, and N. A. Baker, "Visualizing biomolecular electrostatics in virtual reality with unitymol-apbs," *Protein Science*, vol. 29, no. 1, pp. 237–246, 2020.

[55] H. Li, K.-S. Leung, T. Nakane, and M.-H. Wong, "iview: an interactive webgl visualizer for protein-ligand complex," *BMC bioinformatics*, vol. 15, no. 1, pp. 1–6, 2014.

[56] K. Xu, N. Liu, J. Xu, C. Guo, L. Zhao, H.-W. Wang, and Q. C. Zhang, "Vrmol: an integrative cloud-based virtual reality system to explore macromolecular structure," *bioRxiv*, p. 589366, 2019.

[57] R. J. García-Hernández and D. Kranzlmüller, "Nomad vr: Multiplatform virtual reality viewer for chemistry simulations," *Computer Physics Communications*, vol. 237, pp. 230 – 237, 2019.

[58] H. J. Berendsen, "Bio-molecular dynamics comes of age," *Science*, vol. 271, no. 5251, pp. 954–954, 1996.

[59] B. E. Husic and V. S. Pande, "Markov state models: From an art to a science," *Journal of the American Chemical Society*, vol. 140, no. 7, pp. 2386–2396, 2018.

[60] L. W. Votapka, B. R. Jagger, A. L. Heyneman, and R. E. Amaro, "Seekr: simulation enabled estimation of kinetic rates, a computational tool to estimate molecular kinetics and its application to trypsin–benzamidine binding," *The Journal of Physical Chemistry B*, vol. 121, no. 15, pp. 3597–3606, 2017.

[61] H. M. Deeks, R. K. Walters, S. R. Hare, M. B. O'Connor, A. J. Mulholland, and D. R. Glowacki, "Interactive molecular dynamics in virtual reality for accurate flexible protein-ligand docking," *PLOS ONE*, vol. 15, pp. 1–21, 03 2020.

[62] P. G. Bolhuis, D. Chandler, C. Dellago, and P. L. Geissler, "Transition path sampling: Throwing ropes over rough mountain passes, in the dark," *Annual review of physical chemistry*, vol. 53, no. 1, pp. 291–318, 2002.

[63] J. Kästner, "Umbrella sampling," *Wiley Interdisciplinary Reviews: Computational Molecular Science*, vol. 1, no. 6, pp. 932–942, 2011.

[64] A. Barducci, M. Bonomi, and M. Parrinello, "Metadynamics," *Wiley Interdisciplinary Reviews: Computational Molecular Science*, vol. 1, no. 5, pp. 826–843, 2011.

[65] R. J. Allen, C. Valeriani, and P. R. ten Wolde, "Forward flux sampling for rare event simulations," *Journal of physics: Condensed matter*, vol. 21, no. 46, p. 463102, 2009.

[66] E. Weinan, W. Ren, and E. Vanden-Eijnden, "Finite temperature string method for the study of rare events," *J. Phys. Chem. B*, vol. 109, no. 14, pp. 6688–6693, 2005.

[67] M. O'Connor, E. Paci, S. McIntosh-Smith, and D. R. Glowacki, "Adaptive free energy sampling in multidimensional collective variable space using boxed molecular dynamics," *Faraday Discussions*, vol. 195, pp. 395–419, 2017.

[68] B. Isralewitz, M. Gao, and K. Schulten, "Steered molecular dynamics and mechanical functions of proteins," *Current Opinion in Structural Biology*, vol. 11, no. 2, pp. 224 – 230, 2001.

[69] S. Park and K. Schulten, "Calculating potentials of mean force from steered molecular dynamics simulations," *The Journal of chemical physics*, vol. 120, no. 13, pp. 5946–5961, 2004.

[70] F. M. Boubeta, R. M. Contestín García, E. N. Lorenzo, L. Boechi, D. Estrin, M. Sued, and M. Arrar, "Lessons learned about steered molecular dynamics simulations and free energy calculations," *Chemical biology & drug design*, vol. 93, no. 6, pp. 1129–1138, 2019.

[71] J. F. Prins, J. Hermans, G. Mann, L. S. Nyland, and M. Simons, "A virtual environment for steered molecular dynamics," *Future Generation Computer Systems*, vol. 15, no. 4, pp. 485 – 495, 1999.

[72] D. Rapaport, "Interactive molecular dynamics," *Physica A: Statistical Mechanics and its Applications*, vol. 240, no. 1-2, pp. 246–254, 1997.

[73] M. C. Surles, J. S. Richardson, D. C. Richardson, and F. P. Brooks Jr, "Sculpting proteins interactively: continual energy minimization embedded in a graphical modeling system," *Protein Science*, vol. 3, no. 2, pp. 198–210, 1994.

[74] S. Cooper, F. Khatib, I. Makedon, H. Lu, J. Barbero, D. Baker, J. Fogarty, Z. Popović, and F. Players, "Analysis of social gameplay macros in the foldit cookbook," in *Proceedings of the 6th International Conference on Foundations of Digital Games*, pp. 9–14, 2011.

[75] C. B. Eiben, J. B. Siegel, J. B. Bale, S. Cooper, F. Khatib, B. W. Shen, B. L. Stoddard, Z. Popovic, and D. Baker, "Increased diels-alderase activity through backbone remodeling guided by foldit players," *Nature biotechnology*, vol. 30, no. 2, pp. 190–192, 2012.

[76] B. Koepnick, J. Flatten, T. Husain, A. Ford, D.-A. Silva, M. J. Bick, A. Bauer, G. Liu, Y. Ishida, A. Boykov, *et al.*, "De novo protein design by citizen scientists," *Nature*, vol. 570, no. 7761, pp. 390–394, 2019.

[77] C. Cruz-Neira, R. Langley, and P. A. Bash, "Vibe: A virtual biomolecular environment for interactive molecular modeling," *Computers & Chemistry*, vol. 20, no. 4, pp. 469–477, 1996.

[78] Z. Ai and T. Fröhlich, "Molecular dynamics simulation in virtual environments," in *Computer Graphics Forum*, vol. 17, pp. 267–273, Wiley Online Library, 1998.

[79] J. E. Stone, J. Gullingsrud, and K. Schulten, "A system for interactive molecular dynamics simulation," in *Proceedings of the 2001 symposium on Interactive 3D graphics*, pp. 191–194, 2001.

[80] P. Grayson, E. Tajkhorshid, and K. Schulten, "Mechanisms of selectivity in channels and enzymes studied with interactive molecular dynamics," *Biophysical Journal*, vol. 85, no. 1, pp. 36–48, 2003.

[81] M. Dreher, M. Piuzzi, A. Turki, M. Chavent, M. Baaden, N. Férey, S. Limet, B. Raffin, and S. Robert, "Interactive molecular dynamics: Scaling up to large systems," *Procedia Computer Science*, vol. 18, pp. 20–29, 2013.

[82] N. Luehr, A. G. Jin, and T. J. Martínez, "Ab initio interactive molecular dynamics on graphical processing units (gpus)," *Journal of chemical theory and computation*, vol. 11, no. 10, pp. 4536–4544, 2015.

[83] M. P. Haag, A. C. Vaucher, M. Bosson, S. Redon, and M. Reiher, "Interactive chemical reactivity exploration," *ChemPhysChem*, vol. 15, no. 15, pp. 3301–3319, 2014.

[84] M. B. O'Connor, S. J. Bennie, H. M. Deeks, A. Jamieson-Binnie, A. J. Jones, R. J. Shannon, R. Walters, T. J. Mitchell, A. J. Mulholland, and D. R. Glowacki, "Interactive molecular dynamics in virtual reality from quantum chemistry to drug binding: An open-source multi-person framework," *The Journal of chemical physics*, vol. 150, no. 22, p. 220901, 2019.

[85] S. Amabilino, L. A. Bratholm, S. J. Bennie, A. C. Vaucher, M. Reiher, and D. R. Glowacki, "Training neural nets to learn reactive potential energy surfaces using interactive quantum chemistry in virtual reality," *The Journal of Physical Chemistry A*, vol. 123, no. 20, pp. 4486–4499, 2019.

[86] R. Freire, B. R. Glowacki, R. Roebuck Williams, M. Wonnacott, A. Jamieson-Binnie, and D. R. Glowacki, "Omg-vr: Open-source mudra gloves for manipulating molecular simulations in vr," *arXiv*, pp. arXiv–1901, 2019.

[87] D. R. Glowacki, M. D. Wonnacott, R. Freire, B. R. Glowacki, E. M. Gale, J. E. Pike, T. de Haan, M. Chatziapostolou, and O. Metatla, "Isness: Using multi-person vr to design peak mystical type experiences comparable to psychedelics," in *Proceedings of the 2020 CHI Conference on Human Factors in Computing Systems*, pp. 1–14, 2020.

[88] I. Sutherland, "The ultimate display. information processing techniques," in *Proceedings of the IFIP Congress*, pp. 506–508, 1965.

[89] D. Crowfoot, C. W. Bunn, B. W. Rogers-Low, and A. Turner-Jones, "X-ray crystallographic investigation of the structure of penicillin," *The chemistry of penicillin*, pp. 310–367, 1949.

[90] L. Pauling, R. B. Corey, and H. R. Branson, "The structure of proteins: two hydrogen-bonded helical configurations of the polypeptide chain," *Proceedings of the National Academy of Sciences*, vol. 37, no. 4, pp. 205–211, 1951.

[91] F. H. C. Crick and J. D. Watson, "The complementary structure of deoxyribonucleic acid," *Proceedings of the Royal Society of London. Series A. Mathematical and Physical Sciences*, vol. 223, no. 1152, pp. 80–96, 1954.

[92] M. F. Perutz, M. G. Rossmann, A. F. Cullis, H. Muirhead, G. Will, and A. North, "Structure of hæmoglobin: a three-dimensional fourier synthesis at 5.5-å. resolution, obtained by x-ray analysis," *Nature*, vol. 185, no. 4711, pp. 416–422, 1960.

[93] M. Levitt, "Birth and future of multiscale modeling for macromolecular systems (nobel lecture)," *Angewandte Chemie International Edition*, vol. 53, no. 38, pp. 10006–10018, 2014.

[94] J. D. Bernal, "The bakerian lecture, 1962. the structure of liquids," *Proceedings of the Royal Society of London. Series A, Mathematical and Physical Sciences*, vol. 280, no. 1382, pp. 299–322, 1964.

[95] M. Levitt and A. Warshel, "Computer simulation of protein folding," *Nature*, vol. 253, no. 5494, pp. 694–698, 1975.

[96] J. A. McCammon, B. R. Gelin, and M. Karplus, "Dynamics of folded proteins," *Nature*, vol. 267, no. 5612, pp. 585–590, 1977.

[97] J. E. Stone, D. J. Hardy, I. S. Ufimtsev, and K. Schulten, "Gpu-accelerated molecular modeling coming of age," *Journal of Molecular Graphics and Modelling*, vol. 29, no. 2, pp. 116–125, 2010.

[98] K. A. Dill and J. L. MacCallum, "The protein-folding problem, 50 years on," *science*, vol. 338, no. 6110, pp. 1042–1046, 2012.

[99] M. W. van der Kamp and A. J. Mulholland, "Combined quantum mechanics/molecular mechanics (qm/mm) methods in computational enzymology," *Biochemistry*, vol. 52, no. 16, pp. 2708–2728, 2013.

[100] A. Ganesan, M. L. Coote, and K. Barakat, "Molecular dynamics-driven drug discovery: leaping forward with confidence," *Drug discovery today*, vol. 22, no. 2, pp. 249–269, 2017.

[101] K. Lindorff-Larsen, S. Piana, R. O. Dror, and D. E. Shaw, "How fast-folding proteins fold," *Science*, vol. 334, no. 6055, pp. 517–520, 2011.

[102] K. J. Kohlhoff, D. Shukla, M. Lawrenz, G. R. Bowman, D. E. Konerding, D. Belov, R. B. Altman, and V. S. Pande, "Cloud-based simulations on google exacycle reveal ligand modulation of gpcr activation pathways," *Nature chemistry*, vol. 6, no. 1, p. 15, 2014.

[103] A. L. Beberg, D. L. Ensign, G. Jayachandran, S. Khaliq, and V. S. Pande, "Folding@ home: Lessons from eight years of volunteer distributed computing," in *2009 IEEE International Symposium on Parallel & Distributed Processing*, pp. 1–8, IEEE, 2009.

[104] W. E. Hart and S. Istrail, "Robust proofs of np-hardness for protein folding: general lattices and energy potentials," *Journal of Computational Biology*, vol. 4, no. 1, pp. 1–22, 1997.

[105] F. P. Brooks Jr, M. Ouh-Young, J. J. Batter, and P. Jerome Kilpatrick, "Project gropehaptic displays for scientific visualization," *ACM SIGGraph computer graphics*, vol. 24, no. 4, pp. 177–185, 1990.

[106] W. D. Atkinson, K. E. Bond, G. L. Tribble III, and K. R. Wilson, "Computing with feeling," *Computers & Graphics*, vol. 2, no. 2, pp. 97–103, 1977.

[107] L. Pollack, "Vmd: Twenty years of history and innovation." `http://www.ks.uiuc.edu/History/VMD/` (26/06/2020).

[108] D. Swapp, V. Pawar, and C. Loscos, "Interaction with co-located haptic feedback in virtual reality," *Virtual Reality*, vol. 10, no. 1, pp. 24–30, 2006.

[109] F. Khatib, S. Cooper, M. D. Tyka, K. Xu, I. Makedon, Z. Popović, and D. Baker, "Algorithm discovery by protein folding game players," *Proceedings of the National Academy of Sciences*, vol. 108, no. 47, pp. 18949–18953, 2011.

[110] "Sampling molecular conformations and dynamics in a multiuser virtual reality framework: Supplementary materials." `https://advances.sciencemag.org/content/suppl/2018/06/25/4.6.eaat2731.DC1`.
Accessed: 2020-12-22.

[111] "Sampling molecular conformations and dynamics in a multiuser virtual reality framework: Movie s1." `https://vimeo.com/244670465`.
Accessed: 2020-12-22.

[112] J. Lanier, *Dawn of the new everything: A journey through virtual reality*.
Random House, 2017.

[113] N. E. Seymour, A. G. Gallagher, S. A. Roman, M. K. O'brien, V. K. Bansal, D. K. Andersen, and R. M. Satava, "Virtual reality training improves operating room performance: results of a randomized, double-blinded study," *Annals of surgery*, vol. 236, no. 4, p. 458, 2002.

[114] D. R. Glowacki, M. O'Connor, G. Calabró, J. Price, P. Tew, T. Mitchell, J. Hyde, D. P. Tew, D. J. Coughtrie, and S. McIntosh-Smith, "A gpu-accelerated immersive audio-visual framework for interaction with molecular dynamics using consumer depth sensors," *Faraday discussions*, vol. 169, pp. 63–87, 2014.

[115] C. Cruz-Neira, D. J. Sandin, and T. A. DeFanti, "Surround-screen projection-based virtual reality: the design and implementation of the cave," in *Proceedings of the 20th annual conference on Computer graphics and interactive techniques*, pp. 135–142, 1993.

[116] "Sampling molecular conformations and dynamics in a multiuser virtual reality framework: Movie s2." `https://vimeo.com/235894288`.
Accessed: 2020-12-22.

[117] E. I. Chudyk, M. A. Limb, C. Jones, J. Spencer, M. W. van der Kamp, and A. J. Mulholland, "Qm/mm simulations as an assay for carbapenemase activity in class a β-lactamases," *Chemical Communications*, vol. 50, no. 94, pp. 14736–14739, 2014.

[118] P. Eastman, M. S. Friedrichs, J. D. Chodera, R. J. Radmer, C. M. Bruns, J. P. Ku, K. A. Beauchamp, T. J. Lane, L.-P. Wang, D. Shukla, *et al.*, "Openmm 4: a reusable, extensible, hardware independent library for high performance molecular simulation," *Journal of chemical theory and computation*, vol. 9, no. 1, pp. 461–469, 2013.

[119] M. Bonomi, D. Branduardi, G. Bussi, C. Camilloni, D. Provasi, P. Raiteri, D. Donadio, F. Marinelli, F. Pietrucci, R. A. Broglia, *et al.*, "Plumed: A portable plugin for free-energy calculations with molecular dynamics," *Computer Physics Communications*, vol. 180, no. 10, pp. 1961–1972, 2009.

[120] V. Oleinikovas, G. Saladino, B. P. Cossins, and F. L. Gervasio, "Understanding cryptic pocket formation in protein targets by enhanced sampling simulations," *Journal of the American Chemical Society*, vol. 138, no. 43, pp. 14257–14263, 2016.

[121] A. Kalra, G. Hummer, and S. Garde, "Methane partitioning and transport in hydrated carbon nanotubes," *The Journal of Physical Chemistry B*, vol. 108, no. 2, pp. 544–549, 2004.

[122] M. De Poli, W. Zawodny, O. Quinonero, M. Lorch, S. J. Webb, and J. Clayden, "Conformational photoswitching of a synthetic peptide foldamer bound within a phospholipid bilayer," *Science*, vol. 352, no. 6285, pp. 575–580, 2016.

[123] F. Ziegler, N. C. Lim, S. S. Mandal, B. Pelz, W.-P. Ng, M. Schlierf, S. E. Jackson, and M. Rief, "Knotting and unknotting of a protein in single molecule experiments," *Proceedings of the National Academy of Sciences*, vol. 113, no. 27, pp. 7533–7538, 2016.

[124] A. H. Muhlbach, A. C. Vaucher, and M. Reiher, "Accelerating wave function convergence in interactive quantum chemical reactivity studies," *Journal of chemical theory and computation*, vol. 12, no. 3, pp. 1228–1235, 2016.

[125] A. Aspuru-Guzik, R. Lindh, and M. Reiher, "The matter simulation (r) evolution," *ACS central science*, vol. 4, no. 2, pp. 144–152, 2018.

[126] R. E. Arbon, A. J. Jones, L. A. Bratholm, T. Mitchell, and D. R. Glowacki, "Sonifying stochastic walks on biomolecular energy landscapes," *arXiv preprint arXiv:1803.05805*, 2018.

[127] N. L. Allinger, Y. H. Yuh, and J. H. Lii, "Molecular mechanics. the mm3 force field for hydrocarbons. 1," *Journal of the American Chemical Society*, vol. 111, no. 23, pp. 8551–8566, 1989.

[128] H. J. Berendsen, J. v. Postma, W. F. van Gunsteren, A. DiNola, and J. R. Haak, "Molecular dynamics with coupling to an external bath," *The Journal of chemical physics*, vol. 81, no. 8, pp. 3684–3690, 1984.

[129] V. Braun and V. Clarke, "Using thematic analysis in psychology," *Qualitative research in psychology*, vol. 3, no. 2, pp. 77–101, 2006.

[130] S. R. Hare, L. A. Bratholm, D. R. Glowacki, and B. K. Carpenter, "Low dimensional representations along intrinsic reaction coordinates and molecular dynamics trajectories using interatomic distance matrices," *Chemical science*, vol. 10, no. 43, pp. 9954–9968, 2019.

[131] B. Nardi, B. Tomlinson, D. J. Patterson, J. Chen, D. Pargman, B. Raghavan, and B. Penzenstadler, "Computing within limits," *Communications of the ACM*, vol. 61, no. 10, pp. 86–93, 2018.

[132] M. Levitt, "A simplified representation of protein conformations for rapid simulation of protein folding," *Journal of molecular biology*, vol. 104, no. 1, pp. 59–107, 1976.

[133] S. Patodia, A. Bagaria, and D. Chopra, "Molecular dynamics simulation of proteins: A brief overview," *Journal of Physical Chemistry & Biophysics*, vol. 4, no. 6, p. 1, 2014.

[134] M. Karplus and J. Kuriyan, "Molecular dynamics and protein function," *Proceedings of the National Academy of Sciences*, vol. 102, no. 19, pp. 6679–6685, 2005.

[135] J. Mortier, C. Rakers, M. Bermudez, M. S. Murgueitio, S. Riniker, and G. Wolber, "The impact of molecular dynamics on drug design: applications for the characterization of ligand–macromolecule complexes," *Drug Discovery Today*, vol. 20, no. 6, pp. 686–702, 2015.

[136] N. Plattner and F. Noé, "Protein conformational plasticity and complex ligand-binding kinetics explored by atomistic simulations and markov models," *Nature communications*, vol. 6, p. 7653, 2015.

[137] D. Gioia, M. Bertazzo, M. Recanatini, M. Masetti, and A. Cavalli, "Dynamic docking: a paradigm shift in computational drug discovery," *Molecules*, vol. 22, no. 11, p. 2029, 2017.

[138] H. Zhao and A. Caflisch, "Molecular dynamics in drug design," *European journal of medicinal chemistry*, vol. 91, pp. 4–14, 2015.

[139] R. E. Amaro, J. Baudry, J. Chodera, Ö. Demir, J. A. McCammon, Y. Miao, and J. C. Smith, "Ensemble docking in drug discovery," *Biophysical journal*, vol. 114, no. 10, pp. 2271–2278, 2018.

[140] P. Śledź and A. Caflisch, "Protein structure-based drug design: from docking to molecular dynamics," *Current opinion in structural biology*, vol. 48, pp. 93–102, 2018.

[141] S. A. Hollingsworth and R. O. Dror, "Molecular dynamics simulation for all," *Neuron*, vol. 99, no. 6, pp. 1129–1143, 2018.

[142] O.-Y. Ming, D. V. Beard, and F. P. Brooks, "Force display performs better than visual display in a simple 6-d docking task," in *Proceedings, 1989 International Conference on Robotics and Automation*, pp. 1462–1466, IEEE, 1989.

[143] "imd-vr for accurate flexible protein-ligand docking: Supplementary materials." `https://doi.org/10.1371/journal.pone.0228461.s001`.
Accessed: 2020-12-22.

[144] "imd-vr for accurate flexible protein-ligand docking: Supplementary video a1." `https://vimeo.com/354833443`.
Accessed: 2020-12-22.

[145] "imd-vr for accurate flexible protein-ligand docking: Supplementary video a2." `https://vimeo.com/380015176`.
Accessed: 2020-12-22.

[146] "imd-vr for accurate flexible protein-ligand docking: Supplementary video b." `https://vimeo.com/354833800`.
Accessed: 2020-12-22.

[147] "imd-vr for accurate flexible protein-ligand docking: Supplementary video c." `https://vimeo.com/354834013`.
Accessed: 2020-12-22.

[148] J. J. Perona, L. Hedstrom, W. J. Rutter, and R. J. Fletterick, "Structural origins of substrate discrimination in trypsin and chymotrypsin," *Biochemistry*, vol. 34, no. 5, pp. 1489–1499, 1995.

[149] J. Schiebel, R. Gaspari, T. Wulsdorf, K. Ngo, C. Sohn, T. E. Schrader, A. Cavalli, A. Ostermann, A. Heine, and G. Klebe, "Intriguing role of water in protein-ligand binding studied by neutron crystallography on trypsin complexes," *Nature communications*, vol. 9, no. 1, pp. 1–15, 2018.

[150] F. Polticelli, B. Honig, P. Ascenzi, and M. Bolognesi, "Structural determinants of trypsin affinity and specificity for cationic inhibitors," *Protein Science*, vol. 8, no. 12, pp. 2621–2629, 1999.

[151] Y. Yonetani, "Water access and ligand dissociation at the binding site of proteins," *The Journal of Chemical Physics*, vol. 149, no. 17, p. 175102, 2018.

[152] M. Krieger, L. Kay, and R. Stroud, "Structure and specific binding of trypsin: comparison of inhibited derivatives and a model for substrate binding," *Journal of molecular biology*, vol. 83, no. 2, pp. 209–230, 1974.

[153] I. Buch, T. Giorgino, and G. De Fabritiis, "Complete reconstruction of an enzyme-inhibitor binding process by molecular dynamics simulations," *Proceedings of the National Academy of Sciences*, vol. 108, no. 25, pp. 10184–10189, 2011.

[154] I. Teo, C. G. Mayne, K. Schulten, and T. Lelièvre, "Adaptive multilevel splitting method for molecular dynamics calculation of benzamidine-trypsin dissociation time," *Journal of chemical theory and computation*, vol. 12, no. 6, pp. 2983–2989, 2016.

[155] S. Doerr and G. De Fabritiis, "On-the-fly learning and sampling of ligand binding by high-throughput molecular simulations," *Journal of chemical theory and computation*, vol. 10, no. 5, pp. 2064–2069, 2014.

[156] T. Horimoto and Y. Kawaoka, "Influenza: lessons from past pandemics, warnings from current incidents," *Nature Reviews Microbiology*, vol. 3, no. 8, pp. 591–600, 2005.

[157] M. Von Itzstein, "The war against influenza: discovery and development of sialidase inhibitors," *Nature reviews Drug discovery*, vol. 6, no. 12, pp. 967–974, 2007.

[158] C. J. Woods, M. Malaisree, B. Long, S. McIntosh-Smith, and A. J. Mulholland, "Computational assay of h7n9 influenza neuraminidase reveals r292k mutation reduces drug binding affinity," *Scientific reports*, vol. 3, p. 3561, 2013.

[159] M. von Itzstein, W.-Y. Wu, G. B. Kok, M. S. Pegg, J. C. Dyason, B. Jin, T. Van Phan, M. L. Smythe, H. F. White, S. W. Oliver, *et al.*, "Rational design of potent sialidase-based inhibitors of influenza virus replication," *Nature*, vol. 363, no. 6428, pp. 418–423, 1993.

[160] C. U. Kim, W. Lew, M. A. Williams, H. Liu, L. Zhang, S. Swaminathan, N. Bischofberger, M. S. Chen, D. B. Mendel, C. Y. Tai, *et al.*, "Influenza neuraminidase inhibitors possessing a novel hydrophobic interaction in the enzyme active site: design, synthesis, and structural analysis of carbocyclic sialic acid analogues with potent anti-influenza activity," *Journal of the American Chemical Society*, vol. 119, no. 4, pp. 681–690, 1997.

[161] N. Shahrour, "The role of neuraminidase inhibitors in the treatment and prevention of influenza," *Journal of Biomedicine and Biotechnology*, vol. 1, 2001.

[162] R. E. Amaro, R. V. Swift, L. Votapka, W. W. Li, R. C. Walker, and R. M. Bush, "Mechanism of 150-cavity formation in influenza neuraminidase," *Nature communications*, vol. 2, no. 1, pp. 1–7, 2011.

[163] Y. Wu, G. Qin, F. Gao, Y. Liu, C. J. Vavricka, J. Qi, H. Jiang, K. Yu, and G. F. Gao, "Induced opening of influenza virus neuraminidase n2 150-loop suggests an important role in inhibitor binding," *Scientific reports*, vol. 3, p. 1551, 2013.

[164] A. Brik and C.-H. Wong, "Hiv-1 protease: mechanism and drug discovery," *Organic & biomolecular chemistry*, vol. 1, no. 1, pp. 5–14, 2003.

[165] E. Kim, C. Baker, M. Dwyer, M. Murcko, B. Rao, R. Tung, and M. Navia, "Crystal structure of hiv-1 protease in complex with vx-478, a potent and orally bioavailable inhibitor of the enzyme," *Journal of the American Chemical Society*, vol. 117, no. 3, pp. 1181–1182, 1995.

[166] T. D. McGee Jr, J. Edwards, and A. E. Roitberg, "ph-remd simulations indicate that the catalytic aspartates of hiv-1 protease exist primarily in a monoprotonated state," *The Journal of Physical Chemistry B*, vol. 118, no. 44, pp. 12577–12585, 2014.

[167] J. Chen, Z. Liang, W. Wang, C. Yi, S. Zhang, and Q. Zhang, "Revealing origin of decrease in potency of darunavir and amprenavir against hiv-2 relative to hiv-1 protease by molecular dynamics simulations," *Scientific reports*, vol. 4, p. 6872, 2014.

[168] T. Hou and R. Yu, "Molecular dynamics and free energy studies on the wild-type and double mutant hiv-1 protease complexed with amprenavir and two amprenavir-related inhibitors: mechanism for binding and drug resistance," *Journal of medicinal chemistry*, vol. 50, no. 6, pp. 1177–1188, 2007.

[169] P. Kar and V. Knecht, "Energetic basis for drug resistance of hiv-1 protease mutants against amprenavir," *Journal of computer-aided molecular design*, vol. 26, no. 2, pp. 215–232, 2012.

[170] K. Wittayanarakul, S. Hannongbua, and M. Feig, "Accurate prediction of protonation state as a prerequisite for reliable mm-pb (gb) sa binding free energy calculations of hiv-1 protease inhibitors," *Journal of computational chemistry*, vol. 29, no. 5, pp. 673–685, 2008.

[171] A. Hosseini, A. Alibés, M. Noguera-Julian, V. Gil, R. Paredes, R. Soliva, M. Orozco, and V. Guallar, "Computational prediction of hiv-1 resistance to protease inhibitors," *Journal of Chemical Information and Modeling*, vol. 56, no. 5, pp. 915–923, 2016.

[172] M. Mahanti, S. Bhakat, U. J. Nilsson, and P. Söderhjelm, "Flap dynamics in aspartic proteases: a computational perspective," *Chemical biology & drug design*, vol. 88, no. 2, pp. 159–177, 2016.

[173] "imd-vr for accurate flexible protein-ligand docking: Supplementary animation a." `https://vimeo.com/354828618`.
Accessed: 2020-12-22.

[174] "imd-vr for accurate flexible protein-ligand docking: Supplementary animation b." `https://vimeo.com/354829098`.
Accessed: 2020-12-22.

[175] "imd-vr for accurate flexible protein-ligand docking: Supplementary animation c." `https://vimeo.com/354829412`.
Accessed: 2020-12-22.

[176] G. Leonis, Z. Czyznikowska, G. Megariotis, H. Reis, and M. G. Papadopoulos, "Computational studies of darunavir into hiv-1 protease and dmpc bilayer: necessary conditions for effective binding and the role of the flaps," *Journal of chemical information and modeling*, vol. 52, no. 6, pp. 1542–1558, 2012.

[177] Z. Zhu, D. I. Schuster, and M. E. Tuckerman, "Molecular dynamics study of the connection between flap closing and binding of fullerene-based inhibitors of the hiv-1 protease," *Biochemistry*, vol. 42, no. 5, pp. 1326–1333, 2003.

[178] I. Dierynck, M. De Wit, E. Gustin, I. Keuleers, J. Vandersmissen, S. Hallenberger, and K. Hertogs, "Binding kinetics of darunavir to human immunodeficiency virus type 1 protease explain the potent antiviral activity and high genetic barrier," *Journal of virology*, vol. 81, no. 24, pp. 13845–13851, 2007.

[179] C. F. Shuman, P.-O. Markgren, M. Hämäläinen, and U. H. Danielson, "Elucidation of hiv-1 protease resistance by characterization of interaction kinetics between inhibitors and enzyme variants," *Antiviral research*, vol. 58, no. 3, pp. 235–242, 2003.

[180] N. S. Pagadala, K. Syed, and J. Tuszynski, "Software for molecular docking: a review," *Biophysical reviews*, vol. 9, no. 2, pp. 91–102, 2017.

[181] E. Baker and R. Hubbard, "Hydrogen bonding in globular proteins," *Progress in biophysics and molecular biology*, vol. 44, no. 2, pp. 97–179, 1984.

[182] M. I. Zimmerman and G. R. Bowman, "Fast conformational searches by balancing exploration/exploitation trade-offs," *Journal of chemical theory and computation*, vol. 11, no. 12, pp. 5747–5757, 2015.

[183] H. M. Deeks, R. K. Walters, J. Barnoud, D. R. Glowacki, and A. J. Mulholland, "Interactive molecular dynamics in virtual reality is an effective tool for flexible substrate and inhibitor docking to the sars-cov-2 main protease," *Journal of Chemical Information and Modeling*.
DOI: https://doi.org/10.1021/acs.jcim.0c01030 (advance online publication).

[184] A. R. Fehr and S. Perlman, "Coronaviruses: an overview of their replication and pathogenesis," in *Coronaviruses*, pp. 1–23, Springer, 2015.

[185] L.-F. Wang, Z. Shi, S. Zhang, H. Field, P. Daszak, and B. T. Eaton, "Review of bats and sars," *Emerging infectious diseases*, vol. 12, no. 12, p. 1834, 2006.

[186] Y. Chen, Q. Liu, and D. Guo, "Emerging coronaviruses: genome structure, replication, and pathogenesis," *Journal of medical virology*, vol. 92, no. 4, pp. 418–423, 2020.

[187] L. Zhang, D. Lin, X. Sun, U. Curth, C. Drosten, L. Sauerhering, S. Becker, K. Rox, and R. Hilgenfeld, "Crystal structure of sars-cov-2 main protease provides a basis for design of improved α-ketoamide inhibitors," *Science*, vol. 368, no. 6489, pp. 409–412, 2020.

[188] W. Liu, J. S. Morse, T. Lalonde, and S. Xu, "Learning from the past: possible urgent prevention and treatment options for severe acute respiratory infections caused by 2019-ncov," *Chembiochem*, 2020.

[189] L. Kiemer, O. Lund, S. Brunak, and N. Blom, "Coronavirus 3cl pro proteinase cleavage sites: Possible relevance to sars virus pathology," *BMC bioinformatics*, vol. 5, no. 1, p. 72, 2004.

[190] C.-P. Chuck, L.-T. Chong, C. Chen, H.-F. Chow, D. C.-C. Wan, and K.-B. Wong, "Profiling of substrate specificity of sars-cov 3clpro," *PloS one*, vol. 5, no. 10, p. e13197, 2010.

[191] K. Anand, J. Ziebuhr, P. Wadhwani, J. R. Mesters, and R. Hilgenfeld, "Coronavirus main proteinase (3clpro) structure: basis for design of anti-sars drugs," *Science*, vol. 300, no. 5626, pp. 1763–1767, 2003.

[192] A. Grottesi, N. Bešker, A. Emerson, C. Manelfi, A. R. Beccari, F. Frigerio, E. Lindahl, C. Cerchia, and C. Talarico, "Computational studies of sars-cov-2 3clpro: Insights from md simulations," *International Journal of Molecular Sciences*, vol. 21, no. 15, p. 5346, 2020.

[193] S. Chen, F. Jonas, C. Shen, and R. Higenfeld, "Liberation of sars-cov main protease from the viral polyprotein: N-terminal autocleavage does not depend on the mature dimerization mode," *Protein & cell*, vol. 1, no. 1, pp. 59–74, 2010.

[194] M. A. Marra, S. J. Jones, C. R. Astell, R. A. Holt, A. Brooks-Wilson, Y. S. Butterfield, J. Khattra, J. K. Asano, S. A. Barber, S. Y. Chan, *et al.*, "The genome sequence of the sars-associated coronavirus," *Science*, vol. 300, no. 5624, pp. 1399–1404, 2003.

[195] B. Krichel, S. Falke, R. Hilgenfeld, L. Redecke, and C. Uetrecht, "Processing of the sars-cov pp1a/ab nsp7–10 region," *Biochemical Journal*, vol. 477, no. 5, pp. 1009–1019, 2020.

[196] A. Hegyi and J. Ziebuhr, "Conservation of substrate specificities among coronavirus main proteases," *Journal of general virology*, vol. 83, no. 3, pp. 595–599, 2002.

[197] K. Fan, P. Wei, Q. Feng, S. Chen, C. Huang, L. Ma, B. Lai, J. Pei, Y. Liu, J. Chen, *et al.*, "Biosynthesis, purification, and substrate specificity of severe acute respiratory syndrome coronavirus 3c-like proteinase," *Journal of Biological Chemistry*, vol. 279, no. 3, pp. 1637–1642, 2004.

[198] P.-H. Liang, "Characterization and inhibition of sars-coronavirus main protease," *Current topics in medicinal chemistry*, vol. 6, no. 4, pp. 361–376, 2006.

[199] V. Graziano, W. J. McGrath, L. Yang, and W. F. Mangel, "Sars cov main proteinase: The monomer- dimer equilibrium dissociation constant," *Biochemistry*, vol. 45, no. 49, pp. 14632–14641, 2006.

[200] X. Xue, H. Yu, H. Yang, F. Xue, Z. Wu, W. Shen, J. Li, Z. Zhou, Y. Ding, Q. Zhao, *et al.*, "Structures of two coronavirus main proteases: implications for substrate binding and antiviral drug design," *Journal of virology*, vol. 82, no. 5, pp. 2515–2527, 2008.

[201] D. L. Barnard and Y. Kumaki, "Recent developments in anti-severe acute respiratory syndrome coronavirus chemotherapy," *Future virology*, vol. 6, no. 5, pp. 615–631, 2011.

[202] B. L. Haagmans and A. D. Osterhaus, "Coronaviruses and their therapy," *Antiviral research*, vol. 71, no. 2-3, pp. 397–403, 2006.

[203] Y. W. Chen, C.-P. B. Yiu, and K.-Y. Wong, "Prediction of the sars-cov-2 (2019-ncov) 3c-like protease (3cl pro) structure: virtual screening reveals velpatasvir, ledipasvir, and other drug repurposing candidates," *F1000Research*, vol. 9, 2020.

[204] W. Dai, B. Zhang, X.-M. Jiang, H. Su, J. Li, Y. Zhao, X. Xie, Z. Jin, J. Peng, F. Liu, *et al.*, "Structure-based design of antiviral drug candidates targeting the sars-cov-2 main protease," *Science*, vol. 368, no. 6497, pp. 1331–1335, 2020.

[205] C. Ma, M. D. Sacco, B. Hurst, J. A. Townsend, Y. Hu, T. Szeto, X. Zhang, B. Tarbet, M. T. Marty, Y. Chen, *et al.*, "Boceprevir, gc-376, and calpain inhibitors ii, xii inhibit sars-cov-2 viral replication by targeting the viral main protease," *bioRxiv*, 2020.

[206] Z. Jin, X. Du, Y. Xu, Y. Deng, M. Liu, Y. Zhao, B. Zhang, X. Li, L. Zhang, C. Peng, *et al.*, "Structure of m pro from sars-cov-2 and discovery of its inhibitors," *Nature*, pp. 1–5, 2020.

[207] J. J. Irwin and B. K. Shoichet, "Zinc- a free database of commercially available compounds for virtual screening," *Journal of chemical information and modeling*, vol. 45, no. 1, pp. 177–182, 2005.

[208] X. Liu and X.-J. Wang, "Potential inhibitors against 2019-ncov coronavirus m protease from clinically approved medicines," *Journal of Genetics and Genomics*, vol. 47, no. 2, p. 119, 2020.

[209] A.-T. Ton, F. Gentile, M. Hsing, F. Ban, and A. Cherkasov, "Rapid identification of potential inhibitors of sars-cov-2 main protease by deep docking of 1.3 billion compounds," *Molecular informatics*, 2020.

[210] Y. Ge, M. van der Kamp, M. Malaisree, D. Liu, Y. Liu, and A. J. Mulholland, "Identification of the quinolinedione inhibitor binding site in cdc25 phosphatase b through docking and molecular dynamics simulations," *Journal of Computer-Aided Molecular Design*, vol. 31, no. 11, pp. 995–1007, 2017.

[211] K. C. Cassidy, J. Šefčík, Y. Raghav, A. Chang, and J. D. Durrant, "Proteinvr: Web-based molecular visualization in virtual reality," *PLoS computational biology*, vol. 16, no. 3, p. e1007747, 2020.

[212] K. Świderek and V. Moliner, "Revealing the molecular mechanisms of proteolysis of sars-cov-2 mpro by qm/mm computational methods," *Chem. Sci.*, vol. 11, pp. 10626–10630, 2020.

[213] J. A. Maier, C. Martinez, K. Kasavajhala, L. Wickstrom, K. E. Hauser, and C. Simmerling, "ff14sb: improving the accuracy of protein side chain and backbone parameters from ff99sb," *Journal of chemical theory and computation*, vol. 11, no. 8, pp. 3696–3713, 2015.

[214] J. Wang, R. M. Wolf, J. W. Caldwell, P. A. Kollman, and D. A. Case, "Development and testing of a general amber force field," *Journal of computational chemistry*, vol. 25, no. 9, pp. 1157–1174, 2004.

[215] A. Onufriev, D. Bashford, and D. A. Case, "Exploring protein native states and large-scale conformational changes with a modified generalized born model," *Proteins: Structure, Function, and Bioinformatics*, vol. 55, no. 2, pp. 383–394, 2004.

[216] "Interactive molecular dynamics in virtual reality (imd-vr) is an effective tool for flexible substrate and inhibitor docking to the sars-cov-2 main protease: Supporting materials."

[217] A. Paasche, A. Zipper, S. Schafer, J. Ziebuhr, T. Schirmeister, and B. Engels, "Evidence for substrate binding-induced zwitterion formation in the catalytic cys-his dyad of the sars-cov main protease," *Biochemistry*, vol. 53, no. 37, pp. 5930–5946, 2014.

[218] F. Wu, S. Zhao, B. Yu, Y.-M. Chen, W. Wang, Z.-G. Song, Y. Hu, Z.-W. Tao, J.-H. Tian, Y.-Y. Pei, *et al.*, "A new coronavirus associated with human respiratory disease in china," *Nature*, vol. 579, no. 7798, pp. 265–269, 2020.

[219] I. Kufareva and R. Abagyan, "Methods of protein structure comparison," in *Homology Modeling*, pp. 231–257, Springer, 2011.

[220] P. Wernet, D. Nordlund, U. Bergmann, M. Cavalleri, M. Odelius, H. Ogasawara, L. Å. Näslund, T. K. Hirsch, L. Ojamäe, P. Glatzel, L. G. M. Pettersson, and A. Nilsson, "The structure of the first coordination shell in liquid water," *Science*, vol. 304, no. 5673, pp. 995–999, 2004.

[221] L. Simón and J. M. Goodman, "Enzyme catalysis by hydrogen bonds: The balance between transition state binding and substrate binding in oxyanion holes," *The Journal of organic chemistry*, vol. 75, no. 6, pp. 1831–1840, 2010.

[222] K. M. Hart, C. M. Ho, S. Dutta, M. L. Gross, and G. R. Bowman, "Modelling proteins' hidden conformations to predict antibiotic resistance," *Nature communications*, vol. 7, no. 1, pp. 1–10, 2016.

[223] J. Chodera, A. A. Lee, N. London, and F. von Delft, "Crowdsourcing drug discovery for pandemics," *Nature Chemistry*, vol. 12, no. 7, pp. 581–581, 2020.

[224] H. Ballweg, A. K. Bronowska, and P. Vickers, "Interactive sonification for structural biology and structure-based drug design," 2016.

[225] E. Cukuroglu, H. B. Engin, A. Gursoy, and O. Keskin, "Hot spots in protein–protein interfaces: Towards drug discovery," *Progress in Biophysics and Molecular Biology*, vol. 116, no. 2, pp. 165 – 173, 2014.

[226] D. Li, B. Ji, K.-C. Hwang, and Y. Huang, "Strength of hydrogen bond network takes crucial roles in the dissociation process of inhibitors from the hiv-1 protease binding pocket," *PLOS ONE*, vol. 6, pp. 1–13, 04 2011.

[227] S.-C. Cheng, G.-G. Chang, and C.-Y. Chou, "Mutation of glu-166 blocks the substrate-induced dimerization of sars coronavirus main protease," *Biophysical journal*, vol. 98, no. 7, pp. 1327–1336, 2010.

[228] B. N. Walker and G. Kramer, "Mappings and metaphors in auditory displays: An experimental assessment," *ACM Transactions on Applied Perception (TAP)*, vol. 2, no. 4, pp. 407–412, 2005.

[229] D. E. Gordon, G. M. Jang, M. Bouhaddou, J. Xu, K. Obernier, K. M. White, M. J. O'Meara, V. V. Rezelj, J. Z. Guo, D. L. Swaney, *et al.*, "A sars-cov-2 protein interaction map reveals targets for drug repurposing," *Nature*, pp. 1–13, 2020.

[230] I. Dierynck, M. De Wit, E. Gustin, I. Keuleers, J. Vandersmissen, S. Hallenberger, and K. Hertogs, "Binding kinetics of darunavir to human immunodeficiency virus type 1 protease explain the potent antiviral activity and high genetic barrier," *Journal of Virology*, vol. 81, no. 24, pp. 13845–13851, 2007.

[231] F. Noé and C. Clementi, "Collective variables for the study of long-time kinetics from molecular trajectories: theory and methods," *Current Opinion in Structural Biology*, vol. 43, pp. 141–147, 2017.

[232] Y. Shi, D. Jiao, M. J. Schnieders, and P. Ren, "Trypsin-ligand binding free energy calculation with amoeba," in *2009 Annual International Conference of the IEEE Engineering in Medicine and Biology Society*, pp. 2328–2331, IEEE, 2009.

[233] R. Takahashi, V. A. Gil, and V. Guallar, "Monte carlo free ligand diffusion with markov state model analysis and absolute binding free energy calculations," *Journal of chemical theory and computation*, vol. 10, no. 1, pp. 282–288, 2014.

[234] A. Dickson and S. D. Lotz, "Multiple ligand unbinding pathways and ligand-induced destabilization revealed by wexplore," *Biophysical journal*, vol. 112, no. 4, pp. 620–629, 2017.

[235] T. Hüfner-Wulsdorf and G. Klebe, "Role of water molecules in protein–ligand dissociation and selectivity discrimination: Analysis of the mechanisms and kinetics of biomolecular solvation using molecular dynamics," *Journal of Chemical Information and Modeling*, vol. 60, no. 3, pp. 1818–1832, 2020.

[236] P. Tiwary, V. Limongelli, M. Salvalaglio, and M. Parrinello, "Kinetics of protein–ligand unbinding: Predicting pathways, rates, and rate-limiting steps," *Proceedings of the National Academy of Sciences*, vol. 112, no. 5, pp. E386–E391, 2015.

[237] Q. Shao and W. Zhu, "Exploring the ligand binding/unbinding pathway by selectively enhanced sampling of ligand in a protein–ligand complex," *The Journal of Physical Chemistry B*, vol. 123, no. 38, pp. 7974–7983, 2019.

[238] N. Donyapour, N. M. Roussey, and A. Dickson, "Revo: Resampling of ensembles by variation optimization," *The Journal of Chemical Physics*, vol. 150, no. 24, p. 244112, 2019.

[239] K. Zinovjev and I. Tunon, "Adaptive finite temperature string method in collective variables," *The Journal of Physical Chemistry A*, vol. 121, no. 51, pp. 9764–9772, 2017.

[240] M. Souaille and B. Roux, "Extension to the weighted histogram analysis method: combining umbrella sampling with free energy calculations," *Computer physics communications*, vol. 135, no. 1, pp. 40–57, 2001.

[241] J. A. Baker and J. D. Hirst, "Molecular dynamics simulations using graphics processing units," *Molecular Informatics*, vol. 30, no. 6-7, pp. 498–504, 2011.

[242] D. Jiao, J. Zhang, R. E. Duke, G. Li, M. J. Schnieders, and P. Ren, "Trypsin-ligand binding free energies from explicit and implicit solvent simulations with polarizable potential," *Journal of computational chemistry*, vol. 30, no. 11, pp. 1701–1711, 2009.

[243] J. A. Erickson, M. Jalaie, D. H. Robertson, R. A. Lewis, and M. Vieth, "Lessons in molecular recognition: the effects of ligand and protein flexibility on molecular docking accuracy," *Journal of medicinal chemistry*, vol. 47, no. 1, pp. 45–55, 2004.

[244] K. Zinovjev, S. Marti, and I. Tunon, "A collective coordinate to obtain free energy profiles for complex reactions in condensed phases," *Journal of Chemical Theory and Computation*, vol. 8, no. 5, pp. 1795–1801, 2012.

[245] K. Zinovjev and I. Tuñón, "Exploring chemical reactivity of complex systems with path-based coordinates: Role of the distance metric," *Journal of Computational Chemistry*, vol. 35, no. 23, pp. 1672–1681, 2014.

[246] D. Suh, S. Jo, W. Jiang, C. Chipot, and B. Roux, "String method for protein–protein binding free-energy calculations," *Journal of Chemical Theory and Computation*, vol. 15, no. 11, pp. 5829–5844, 2019.